Materials Science and Engineering R 65 (2009) 1–38

Contents lists available at ScienceDirect

Materials Science and Engineering R

journal homepage: www.elsevier.com/locate/mser

Colloidal dispersion of gold nanorods: Historical background, optical properties, seed-mediated synthesis, shape separation and self-assembly

Vivek Sharma [a,1], Kyoungweon Park [a,2], Mohan Srinivasarao [a,b,c,*]

[a] School of Polymer, Textile and Fiber Engineering, Georgia Institute of Technology, Atlanta, GA 30332, United States of America
[b] School of Chemistry and Biochemistry, Georgia Institute of Technology, Atlanta, GA 30332, United States of America
[c] Center for Advanced Research on Optical Microscopy (CAROM), Georgia Institute of Technology, Atlanta, GA 30332, United States of America

ARTICLE INFO

Article history:
Available online 28 April 2009

Keywords:
Gold Nanorods
Plasmon resonance
Self Assembly
Nanocomposites
Seed-mediated synthesis
Evaporative drying

ABSTRACT

The color of colloidal dispersions of gold particles in a fluid, typically water, varies from red to blue, depending upon the shape and size of particles. The color and optical properties of gold nanoparticles originate from localized surface plasmons, and are sensitive to their local dielectric environment. Unlike nanospheres, the optical properties, hydrodynamic behavior as well as phase behavior of nanorods are influenced by their shape anisotropy. Thus, rods have an additional absorption peak, possess very different dynamics (affects sedimentation) and their concentrated dispersions form liquid crystalline phases. In this review, we focus on presenting the essential shape dependent optics, as well as the hydrodynamics and phase behavior of rod-like gold nanoparticles. We reveal our methodology for making less polydisperse nanorods sols by using an optimized seed-mediated synthesis (controlled chemistry), followed by shape separation by centrifugation (based on our hydrodynamics arguments). We elucidate the role of Brownian motion in determining colloidal stability and sedimentation behavior, and describe patterns formed by drying mediated assembly on glass slides and TEM grids. We outline early studies (before 1930) of gold sols that are not only instructive in learning about synthesis and physical properties of gold nanoparticles, but show how the study of colloidal gold established many key principles in colloidal science.

Contents

* Corresponding author at: School of Polymer, Textile and Fiber Engineering, Georgia Institute of Technology, Atlanta, GA 30332, United States of America.
E-mail address: mohan.srinivasarao@ptfe.gatech.edu (M. Srinivasarao).
[1] Current address: Hatsopoulos Microfluids Laboratory, Department of Mechanical Engineering, Massachusetts Institute of Technology, 77 Massachusetts Ave, Bldg 3-249, Cambridge, MA 02139, United States.
[2] Current address: Materials and Manufacturing Directorate, Air Force Research Laboratory, Wright-Patterson AFB, OH 45433-7702, United States.

0927-796X/$ – see front matter © 2009 Elsevier B.V. All rights reserved.
doi:10.1016/j.mser.2009.02.002

1. Introduction

Colloidal gold nanoparticles have received widespread attention in recent years [1–16] both due to their unusual properties, and promising applications. Nanoparticles, typically in the size range of 1–100 nm, possess size and shape dependent properties which differ markedly from their bulk behavior [1,2,16–18]. For example, spherical colloidal gold particles with a diameter around 10 nm make their aqueous dispersions assume a ruby red color, while increase in their size to nearly 100 nm or change in shape to say a rod-like shape, with aspect ratio of say 3 (length 30 nm, diameter 10 nm) makes the colloidal dispersion appear bluish. It must be remarked that bulk gold has unmistakable yellowish color, and the size dependence of the color of colloidal gold is simply a consequence of how light interacts with matter.

Since the recent burst of activity in synthesis of gold nanoparticles [2–7,11,16], optical properties and applications of these nanoparticles has been highlighted in several exhaustive reviews [1–12,16]. Here we focus our attention on aspects related to optical properties, shape separation and self-assembly of gold nanorods that we have uncovered during our research effort. In Section 2, we present a historical background where we point out that the physical properties of gold particles *including rod-like particles* were studied in the early twentieth century and these provided original and ground breaking advances in the field of colloidal matter. The parameters that affect colloidal stability of gold dispersions are outlined in the next section. The physics that determines the optical properties and color of the rod-like nanoparticles will be detailed in Section 4. The subsequent sections will illustrate our seed-mediated synthesis of gold nanorods followed by an elucidation of how they can be shape separated to remove nanospheres (and particles of other shapes) that are the typical byproducts of the synthesis. We will thereafter discuss the self-assembly of colloidal gold nanorods, identifying the means and methodology to study their phase transition to liquid crystallinity.

Colloidal gold sols were produced and used as colorants for centuries, before they attracted Faraday's interest in 1857 [19], in a paper that can be called the most important article in both the history of colloidal science and in the discussion of how light interacts with matter. Unfortunately, Faraday's work was forgotten for nearly forty years, when Zsigmondy, who developed a different synthesis protocol became aware of it [20]. Zsigmondy combined his synthesis technique with Faraday's method, to devise two step "nuclear" method [20]. This method has been rediscovered and is termed as the "seed-mediated" method. Further Zsigmondy managed to design an ultramicroscope to view the size and mobility of nanometer size colloidal particles [20,21]. Like Faraday and Zsigmondy, Svedberg made important contributions in synthesis of colloidal gold [22,23] and used these particles to show how ultracentrifuge designed by him can not only size separate them, but also reveal their size and shape dependent mobility [22–24]. Around the same time, Mie advanced his theory [25] in attempt to explain the color of colloidal gold dispersions. Gans proceeded to discuss the influence of ellipsoidal shape on colloidal gold [26]. Given the fact that the colloidal gold particles played a central role in the development and understanding of the basic colloidal chemistry and physics [19–29], we will draw upon our understanding of colloidal dispersions to cite examples and theoretical insight relevant to our system. The perusal of this classic literature also demonstrates how the pioneers recognized that various observations, for example, color of colloidal gold solutions, could be attributed to the presence of rod-like nanoparticles.

The recent interest in gold nanoparticles is propelled by both the advances in our scientific understanding of their synthesis and physical properties [1–16] as well as the possibility of using them for applications in chemical and biological sensing [2,4,6,10,30–54], cancer treatment [10,48,55–58], catalysis [59,60], as markers for transmission electron microscopy (TEM) and scanning electron microscopy (SEM) [61] and various specialized photonics and electronic applications [30,62–66]. This review is focused at

presenting the essential shape dependent optics, as well as the hydrodynamics and phase behavior of rod-like gold nanoparticles. We discuss the seed-mediated synthesis method useful for making the rod-like particles and illustrate typical examples of the properties of the nanorods from our hitherto unpublished work and review the published research from other groups.

Before we proceed to discuss the current state of the art [1–16], we provide a glimpse of the work of the early pioneers [19–29] especially Faraday, Zsigmondy, Svedberg, Smoluchowski, Mie, Ostwald and Gans. They delved into the synthesis and physical properties of gold sols primarily to establish the existence of particulate nature of colloidal sols and to explore questions related to the reality of atoms and molecules. Apart from providing us with a context for later discussion, their work presents a useful set of experimental and theoretical ideas that can be developed, applied and explored further in modern day research. For example, we elucidate Zsigmondy's method for visualization of gold particles using ultramicroscopy [21] and we show how a modified version of Svedberg's ultracentrifugation analysis and technique [24] can be used for shape separation of nanorods. We hope (and expect!) that our review will project interesting questions, answers and direction to the field of gold nanorods.

2. Historical perspective on colloidal gold sols

The use of colloidal gold as a colorant can be traced back at the least to 5th B.C. for its use in making ruby glass and providing reddish tinge to ceramics. According to Ostwald [27], "This colloidal gold was prepared even in the days of the alchemists by the reduction of gold salts by all kinds of organic substances, including urine." Similar concoctions were used by the Hindu chemists for Ayurveda, the ancient system of Indian medicine [67]. In what follows, we outline the representative significant contributions from the giants of early colloidal chemistry and physics.

2.1. Faraday's experiments on synthesis and color of ruby gold

The definitive study on the nature of gold particles in hydrosols – their synthesis by reduction of dilute gold chloride using phosphorus, size dependent optical properties, coagulation behavior – was carried out by Faraday as presented in his 1857 article titled: "The Bakerian Lecture: Experimental relations of Gold (and other metals) to Light" [19]. He obtained relatively unstable colloidal sols, with colors purple red to sometimes blue, and showed that electrical "collidation" of gold in air or hydrogen gave a precipitate on glass or quartz with the same red or blue color as present in the sols. Faraday determined that the ruby glass was colored so, because of the presence of finely dispersed gold particles, and carried out reactions to ascertain that 'Purple of Cassius' could be obtained by adding tin chloride to gold sol. It must be mentioned here that Purple of Cassius was known for over two centuries as stable colorant for ceramics and glasses.

Apart from use of phosphorus, Faraday showed that the gold chloride can be reduced by heat alone or by reaction with many different reagents including organic matter, phosphorus, tartaric acid, etc. Faraday provided physical and chemical arguments to emphasize that in both ruby fluid and ruby glass, metallic gold was present in finely dispersed state. He states: "I endeavoured to obtain an idea of the quantity of gold in a given ruby fluid, and for this purpose selected a plate of gold ruby glass, of good full color, to serve as a standard, and compared different fluids with it, varying their depth, until the light from white paper, transmitted through them, was apparently equal to that transmitted by the standard glass. Then known quantities of these ruby fluids were evaporated to dryness, the gold converted into chloride, and compared by reduction on glass and otherwise with solutions of gold of known strengths. A portion of chloride of gold, containing 0.7 of a grain of metal, was made up to 70 cubic inches by the addition of distilled water and converted into ruby fluid: on the sixth day it was compared with the ruby glass standard, and with a depth of 1.4 inch was found equal to it;" and he goes on to state: "From these considerations, it would appear that one volume of gold is present in the ruby fluid in about 750,600 volumes of water;"

Faraday also examined other metals (platinum, palladium, rhodium, silver, tin, lead, zinc, iron, mercury, arsenic) in his paper. In the context of his experiments, he attempted to study the optical properties as well as remarked on the aggregation and sedimentation [19]. Apart from reading Faraday's original paper [19], which is a must read for anyone interested in the optical properties of gold sols, we also highly recommend Tweney's perspective [68] on how Faraday discovered gold and other metallic colloids, for it includes replication of Faraday's original experiments as well as observations noted in his laboratory notebook.

2.2. Synthesis of gold sols, including seed-mediated method

For nearly forty years, Faraday's work remained unnoticed [19], and even the scientists who worked on the ruby glass and Purple of Cassius were not aware of it [20]. Thereafter Zsigmondy began his investigations into the color of ruby glass and formulated a method for preparing colloidal gold by reducing dilute, slightly alkaline solution of gold chloride with boiling formaldehyde. After becoming aware of Faraday's methods, especially reduction using phosphorus, he combined both the synthesis techniques to arrive at a two step synthesis method. This method is referred to as the seed-mediated method in the contemporary literature and was called 'nuclear method' in the early days [20]. Also the nanoparticles were typically described as ultramicroscopic particles and the in place of nanometers (nm) as a unit, the equivalent unit used was ultramicrons ($\mu\mu$).

Svedberg played a central role in early studies of gold sols and he pioneered the use of electrochemical methods for the synthesis of gold particles. In his text [22], he reports the use of every conceivable reducing agent of available at his time to produce colloidal gold from hydrochloroauric acid. To quote him, [22] "The best known reduction process is the reduction of chloroauric acid ($HAuCl_4$) to gold. Almost every conceivable reducing agent has been studied, viz., hydrogen, hydrogen peroxide, hydrogen sulphide, carbon monoxide, carbon disulphide, nitric oxide, phosphorus, phosphorus tertoxide, hypophosphoric acid, sulphur disoxide, sodium thiosulphate, sodium bisulphate, ferrous sulphate, tin, stannous chloride, acetylene, terpenes, alcohols, glycerine, aldehydes, acrolein, oxalic acid and oxalates, tartaric acid, sugars, starches, phenols, hydroxide acids, hydrochinones, hydrazines, hydroxylamines, protalbic acid, electric sparks (formation of nitric acid), alpha, beta, gamma-rays, etc., etc." Faraday [19] had likewise used many of the reducing agents of his time to produce gold sols.

Ostwald's remarkable text on colloids which presents key experimental and theoretical principles through a series of demonstrations must be mentioned at this juncture for it embodies several principles useful for the synthesis of gold sols [27]. "In order to obtain it (colloidal gold) by condensation, I begin with a molecularly or ionically dispersed solution of gold chloride to which sodium bicarbonate has been added until neutral to litmus. I need now to reduce the gold chloride to metallic gold, but this must be done in such a way that metallic gold remains so highly dispersed as not to exceed colloidal dimensions. As you know, gold chloride can be reduced by many different kind of substances, especially organic ones. You need but dip your finger into the solution when it becomes stained with bluish violet by the colloid

gold produced through the reducing action of the organic substances contained in the skin." The complete demonstration is a must read for everyone working on colloidal gold as well as on synthesis and characterization of any colloidal particles. In our context, we will note that Ostwald's remark shows the importance of size in keeping particles dispersed, and we shall return to this discussion in detail when we deal with the role of Brownian motion. Further Ostwald points out the importance of pH in the synthesis, and in demonstration, he expounds how this is useful in changing the final product from being a red to blue dispersion (of course, he never uses the word pH). As an aside, we must add that in this text Ostwald, winner of the Nobel Prize in Chemistry in 1909 for catalysis, presents endless examples of experiments that may be carried out in a classroom to demonstrate nearly every aspect of physics and chemistry of gold sols and other colloids.

Ostwald also advanced an explanation for formation of Liesegang rings which are bands or rings formed in a reaction-diffusion system [69], where typically precipitation reaction is introduced into a homogeneous solution or gel, by diffusion of a second species. According to Ostwald, the phenomenon is a result of interplay of discontinuous nucleation and supersaturation affected by local concentration gradients. We will look at the formation of Liesegang-like patterns in evaporating drops of colloidal gold rods in Section 7.

The role of supersaturation in determining the nucleation and growth of gold particles, both in condensation growth from solution and in vapor deposition, was also discussed by Svedberg [22,23] and Zsigmondy [20,21] in their pioneering studies. In his 1921 text [22], Svedberg contends: "The degree of dispersion of gold colloids formed by reduction of $HAuCl_4$ without adding of condensation nuclei is, according to Zsigmondy (Kolloidchemie, p. 143 (1918)) dependent on two factors, viz.: (1) The spontaneous production of nuclei (s.p.n.) and (2) The velocity of the growth of the particles (v.g.p.)." He continues: "The spontaneous production of gold nuclei is a kind of coagulation and is therefore accelerated by coagulating electrolytes in small quantities. Higher concentrations drive the coagulation of the particles too far. Weak reducing agents, e.g. potassium thiocyanate, potassium citrate, congo red, etc., added before the reduction give rise to small gold particles that act as nuclei. Protective electrolytes, e.g. NH_3, $K_4Fe(CN)_6$, $K_3Fe(CN)_6$, retard production of nuclei. Protective colloids do not retard the s.p.n., their particles being too coarse for these very small gold particles. The growth of the particles is also a kind of coagulation. It is retarded by protective colloids and accelerated by coagulating colloids." We will point out how the critical dependence of nucleation and growth on supersaturation can be used in the so-called seed-mediated method to generate particles with lower polydispersity.

2.3. Size and shape dependent color of gold sols

In his text [20], Zsigmondy notes: "The color of colloidal gold solutions in transmitted light may be red, violet, or blue, and occasionally yellowish brown, or brown. The ultramicrons of red solutions are green; those of blue solutions are yellow to reddish brown; violet solutions contain both. We have to do with green, yellow, or brown ultramicrons." He also points out: "With regard to the brown color of very small particles a large number of experimental facts point to the assumption that the ultramicrons are not composed of massive gold. The assumption that the particles are spherical in form is made solely for the purposes of calculation, and a number of facts would seem to discredit the hypothesis. The very great independence of the color on the diameter makes it seem plausible that ultramicrons in red hydrosols are not necessarily spherical when the size is 40 μμ and under."

The dependence of optical properties on their shape was thus apparent to researchers including Zsigmondy whose text describes difference in color observed by using polarized light parallel and perpendicular to the anisotropic particles oriented by spreading out on a gelatin film [20]. "It must be noted that gold often crystallizes in a leaf-like form having six sides and that Ambronn has observed dichromatic microscopic rods. If the light vibrations from the polarizer are parallel to the shorter diameter of the particles, that is right angles to the flat side, then the transmitted light is red and diffracted green. If, on the contrary, the vibrations are parallel to the larger surface and at right angles to the shorter, then the transmitted light is blue and the diffracted light yellow or brown." Similar concepts can be utilized in making the composite films of gold nanorods with polymers and polymer films can then be stretched to create color filters [62]. This approach will be discussed in the section on polymer–nanorod composites (in Section 4).

Zsigmondy invented the ultramicroscope [21] which allowed Siedentopf and Zsigmondy to visualize the colloidal gold particles (i.e. nanoparticles), showing that colloidal matter consisted of dispersion of particles of measurable size. Zsigmondy was able to make some of the first particle tracking studies to determine the diffusion behavior of the nanoparticles. Zsigmondy was awarded Nobel Prize in 1925 "for his demonstration of the heterogeneous nature of colloidal solutions and for the methods he used, which have since become fundamental in modern colloid chemistry." His texts are a remarkable testimony to the central role played by colloidal particles in his discoveries and inventions. While transmission electron microscopy can be employed to determine the size and shape of the nanoparticles, typically dried onto a substrate, ultramicroscopy presents the option of looking at the particles in their dispersed state. The advances in optical techniques that have taken place in the past decades and the expertise developed in the theoretical and experimental aspects of quantum dot based or single molecule imaging [70–76], make ultramicroscopy an ideal candidate for revisiting colloidal dispersions of metallic nanoparticles. For example, in principle one can follow the growth kinetics of particles in situ by visualization through the ultramicroscope. In this respect we will describe the concept in effort to demonstrate its overlooked utility.

In this respect, the text by Svedberg [23] also describes few other experiments used to determine size and size or shape dependent properties, including Scherrer's determination of particle size using X-ray scattering, and Svedberg's attempts to determine particle size using particle tracking and Brownian motion as well as measurement of size using osmotic pressure and ultrafiltration. His text [23] mentions that Scherrer and Björnståhl demonstrated that the gold sols have same X-ray diagram as gold wires. Björnståhl (see Svedberg's text [23]) also measured the double refraction of gold sols in presence of external electric, magnetic and flow fields, and found that shape anisotropy as well as coagulation of particles can be studied using these. Though most of these techniques have not been fashionable for the studies on gold nanoparticles, they incorporate concepts and applications that must be reassessed.

2.4. Scattering and absorption: Mie theory for spherical, and Gans theory for ellipsoidal particles

Exactly hundred years back (in 1908), Mie wrote a seminal paper [25] to theoretically describe the absorption and scattering by metal particles, and his motivation was to explain the color of gold sols. His classic paper "Beiterage zur Optik truber Medien, speziell kolloidaler Metallosungen" which translates to "Contributions on the optics of turbid media, particularly colloidal metal solutions" include calculation of absorption spectrum for gold sols

in water, and he plots the absorption and scattering spectra as a function of particle size for spherical gold particles. Mie's theory is applicable to only spherical particles. So when Mie compared his theoretical predictions to the experiments results of his student, (Walter Steubing), Mie attributed the deviation to non-spherical particles in certain cases. Mie closed his seminal paper with a statement: "*To complete the theory it is absolutely necessary to study the behavior of ellipsoidal particles*." Gans [26] extended the theory to consider the spheroid particles, showing how smaller aspherical particles can show absorbance at longer wavelengths than spherical particles of comparable size. We will discuss how the electron cloud of the nanoparticles interacts with electromagnetic radiation and determine the physical basis for the size and shape dependent absorbance of colloidal gold sols.

2.5. Shape effects on Brownian motion: sedimentation, diffusion and viscosity

The properties of colloids depend, to a large extent, on the movement of particles and this movement consists of translational and rotational Brownian motion. The advances in theoretical understanding of Brownian motion brought about by Einstein [77–79], Smoluchowski [80–82] and Langevin [83] (also see Chandrasekhar's review [84] and recent perspectives [85–88]) in the beginning of twentieth century provided the requisite understanding to describe the continuous motion of particles observed in ultramicroscope as well to understand the size dependence of their stability and sedimentation behavior.

Einstein (1905) [77,78] reasoned that suspended particles behave quite like solute molecules and therefore an osmotic pressure should be ascribed to the suspended particles. By applying van't Hoff's law to suspensions and by assuming that dissipative force described by Stokes law balances the force due to osmotic pressure, Einstein was able to describe Brownian motion as a diffusion process. Further by formulating the statistical analysis for Brownian motion, he laid a basis for testing the reality of 'molecular kinetic theory' of matter which became accepted only after Perrin's experiments [89–91]. Einstein showed that mean squared displacement of particles scales linearly with time and postulated that these results could be used to determine molecular dimensions [77–79].

Meanwhile, Smoluchowski (1906) [80] who independently derived the time dependence of distance covered by a Brownian particle, determined that the number of suspended particles as a function of height shows exponential dependence in sedimentation equilibrium, which is akin to variation of atmospheric pressure with height. This sedimentation equilibrium can be reached between osmotic pressure or diffusion and an effective gravitational force [23], such that the number density of particles, $\rho(h)$ at height, h is given by the Boltzmann distribution and follow the barometric profile, i.e. $\rho(h) \sim \exp(-mgh/k_BT)$, where m is the mass of particle, g is the gravitational constant, T is the temperature and k_B is the Boltzmann's constant. Smoluchowski's studies on Brownian motion led him to develop theory of kinetics of coagulation [82,84] as well as to explanation of how fluctuations lead to critical opalescence [90,92]. Finally Langevin [83] outlined a simpler derivation for the time dependence of the displacement of Brownian particles by introducing a fluctuating random force and counteracting it with Stokesian drag, and the modern treatment of Brownian motion is typically based on it [84].

Perrin [23,90,91] carried out meticulous experiments to count the number of particles as the function of height present in the sedimentation equilibrium. Further he used the distribution function thus obtained to calculate Avogadro's number and establish the equivalence between a colloidal particle and a molecule as required by the molecular kinetic theory. His experiments [90,91] were done using a microscope with water immersion, large numerical aperture objective that gave him depth of focus of about 1 μm, and allowed him to image and count gamboge particles dispersed in water placed at a certain height. Perrin chose these particles in part because all the theories assumed hard-core repulsion, and hence he needed particles that would behave as such. Perrin observed [85,91] that these gamboge particles (a resin derived from the sap of a particular tree) were easily dispersed in water, and form very stable suspensions of spherical particles that displayed all the characteristics of particles interacting via hard-core repulsion. Perrin painstakingly fractionated these particles so that he could have a very narrow size distribution of particles for his experiments.

Svedberg's texts [22–24] contain reference to similar initial experiments on gold sols [23,24]. He notes [23]: "Westgern in his studies of the sedimentation equilibrium of gold and selenium sols also determined the Avogadro constant and actually obtained lower values than Perrin." Perrin's experiments in 1909 gave a value of 6.8×10^{23}, while Westgern got 6.05×10^{23} [23]. Further, Perrin determined that the displacements or velocities of the Brownian particles show a Maxwellian distribution and these calculations, as well as experiments on Brownian motion, were inspired partly by his friend, Langevin [90]. Perrin's careful experiments on translational and rotational Brownian motion not only led support to the theories of Brownian motion but also established the reality of molecules and established the statistical nature of thermodynamics. Brownian motion and thermal forces set the rules for structure, dynamics and function of soft matter [93–96] (polymers, liquid crystals, emulsions, and colloidal dispersions), and the analysis or theories of Brownian motion apply to stochastic problems in systems ranging from single cells to financial markets to galaxies [84,97].

We will discuss the role of Brownian motion in determining colloidal stability, together with the role of interaction forces in the next section of this review. We will also discuss the how the diffusion, aggregation and sedimentation behavior of rod-like particles is qualitatively and quantitatively very different from that of spherical nanoparticles. For example, rods experience difference in mobility parallel and perpendicular to their major axis, and their aggregation can result in the formation of a liquid crystalline phase. Since high purity, nearly monodisperse gold (and other inorganic) nanorods have been synthesized only recently, several predictions regarding their behavior remain untested.

Svedberg invented the ultracentrifuge, allowing Rinde and Svedberg [22–24] to size separate particles and to investigate the role of shape and size on the sedimentation equilibria. The basis of the size separation in the spherical particles is simply understood in terms of the Brownian motion of colloidal particle under an external field, where the equilibrium sedimentation velocity is related to the size dependent drag that opposes the centrifugal force. The synthesis and physical behavior, including hydrodynamics of gold particles, was central to the studies of Svedberg, who later earned the Nobel Prize for "his work on disperse systems." We have extended and developed the theoretical and experimental protocol to show how shape dependent drag or hydrodynamics during centrifugation leads to shape separation of particles [98]. The sedimentation velocity normalized by the centrifugal acceleration is called Svedberg's coefficient and commonly used unit for comparing it is called Svedberg. The details of this mechanism and its usefulness for separating gold nanorods from a collection of particles of other shapes will be discussed in Section 6.

Einstein's viscosity relation for dilute suspensions captures the experimentally observed fact that the addition of spherical colloidal particles to a solvent results in an increase in viscosity of the solution. This increase is directly proportional to the size and

number of particles, and can be used to determine the hydrodynamic volume of these particles. The relationships derived for non-spherical shapes are not used as extensively in the studies of effect of rod-like colloidal particles on solution viscosity. Onsager remarked [99] on "Viscosity and particle shape in colloid solutions" as follows: "Einstein has shown that spherical particles in solution will increase the viscosity by a factor $\Delta\eta/\eta = 1 + 2.5\phi$, where ϕ is the fraction of total volume occupied by the solute. For an extension to ellipsoidal particles, the necessary hydrodynamic calculations have been made by Jeffery (Proc. Roy. Soc. A102, 161 (1922)). Presently, the Brownian motion is taken into account. For ellipsoids of rotation, with semi-major axes $a \gg b = c$, the factor 2.5 in Einstein's formula is replaced by $(4a^2/15b^2)\log(a/b)$. The time of relaxation for rotation is $\tau = \rho/6kT$, where $\rho = \eta \times (8\pi a^3/3)\log(a/b)$, e.g. for $\eta = 0.01$ and $a = 100b = 5 \times 10^{-5}$ cm. The calculated viscosities are much greater than those measured by Staudinger for solutions of paraffins in tetralin, etc., which indicates that such molecules do not retain a straight linear shape in solution. In addition, it seems necessary to assume slip at the surface of hydrocarbon molecule." Rod-like metal nanoparticles can be synthesized to rigorously examine their effect on viscosity of dispersions.

2.6. Colloidal stability, 'gold number' and protective action of macromolecules

Zsigmondy drew the attention of von Smoluchowski to the problem of colloidal coagulation of gold particles, asking him to derive an experimentally verifiable formula (Nobel Lecture [100]). Smoluchowski's theories for diffusion and coagulation [80,82,84,101] are central to our understanding of collision and coalescence issues in both colloidal sols and other such systems including the stability of fog. Smoluchowski computed the rate at which a diffusing particle arrives in a 'sphere of influence' of another particle. The assumption is that if the diffusing particle moves about in the region outside this sphere of influence, it moves unaffected, but if it enters the region, it sticks to the other particle [84]. Thus Brownian motion, together with the interparticle attractive and repulsive forces that form the physico-chemical basis for the sphere of influence, determines the phase behavior and stability of colloids.

Zsigmondy investigated the stability of colloidal gold in the presence of ions, biomolecules, gums and gelatin, etc., and noted that certain proteins and substances displayed a "protective action" [20]. The color of a red gold sol when coagulated with NaCl, changes to blue. Zsigmondy used this property to define the so-called gold number [20] as number of milligrams of the hydrophile colloid per 10 cm^3 of gold sol that is sufficient to prevent the coagulation and hence color change to occur when 1 cm^3 of 10 per cent NaCl solution is added. The studies were used in characterizing different proteins as well as in detecting changes in the composition of liquids containing different proteins. We will discuss the role of Brownian motion in determining colloidal stability, together with interaction forces and problem of aggregation in Section 3.

2.7. Other metal nanoparticles and inorganic lyotropic liquid crystals

We must remark here that the treatises by Zsigmondy [20,21], Svedberg [22–24] and several texts on colloidal matter written in early twentieth century [27,29,102] contain some very illustrative experiments and theoretical insight not only about the behavior of gold sols but other metal nanoparticles and organic colloids as well. Silver, platinum, mercury, bismuth, copper, tellurium, etc. were some of the other metal hydrosols studied as a natural extension of studies on gold sols [19,20,23]. The experiments devised contain some of the first investigations into the characteristic properties displayed by nanoparticles and colloidal matter. The liquid crystalline properties of rod-like colloidal suspensions of vanadium pentoxide, V_2O_5, dispersed in water, were first studied by Zocher in 1925 [103], who also later (1929) discovered anisotropic phase in β-FeOOH. Later, in 1938, Langmuir reported the phase separation of suspensions of bentonite clay platelets showing an isotropic phase (I) in equilibrium with a nematic liquid crystal phase (N) [104]. Bawden et al. [105] found the nematic ordering of suspensions of tobacco mosaic virus (TMV), a rod-like virus, and Onsager [99,106] laid out a theory for describing phase behavior of hard rods. The reader may refer to recent reviews by Davidson and Gabriel [107,108] that summarize the advances and history of lyotropic liquid crystals based on inorganic nanoparticles and mineral moieties. We will discuss liquid crystalline behavior of rod-like nanoparticles in the context of gold nanorods, and introduce aspects of self-assembly in Section 7 of the review.

2.8. Recent interest in colloidal gold

The revival of interest in gold sols has occurred after innumerable advances in our understanding of various concepts in physics and chemistry. To list a few: (1) the quantum mechanics and the effects associated with nanoscopic systems; (2) the nature of interaction between colloidal particles and the dependence of colloidal stability on presence of surfactants, charge, polymer chains, among others; (3) the statistical mechanics or thermodynamic behavior of aggregates, crystals and liquid crystals, that can be formed by colloidal particles; (4) the mathematics and physics associated with pattern formation, pattern characterization and how interplay of kinetic and thermodynamic effects creates assemblies; (5) the mechanism of micelle formation, role of depletion attraction and phase behavior of surfactants and polymers; (6) biological physics, and (7) numerical methods and simulation protocols. The corresponding advances in technology related to optical and electron microscopy, optics, lasers, computing facilities for data acquisition and data analysis as well as simulations, and instruments designed with better precision and options imply that the corresponding research for colloidal metal particles can really become useful for applications to lab on a chip devices, electronic, photonic and sensing applications based on plasmonics, cancer treatment, etc.

Since most of the researchers mentioned in this section, flourished (early twentieth century) before they had access to the theoretical insight, technological advancement and computer based simulation facilities available to us now, there is an endless wealth of questions left unanswered or incompletely understood by these pioneers that can be explored now. Their papers are representative of how efforts of zealous experimentalists and theoreticians can resolve problems in spite of lack of so many facilities that we take for granted!

The latest gold rush is likely to revolutionize the field of biosensing and chemical sensing by allowing development of technologies that help in identification of chemical or biological strains with high accuracy, by using highly environmentally sensitive nature of plasmon resonance as well as other optical effects (say surface-enhanced Raman or fluorescence) associated with the gold and other noble metal particles.

3. Colloidal nature of gold

Typically, a substance is called a colloidal dispersion if it consists of particles within a typical size range of 1 nm–10 μm [94,95]. The dispersion may consist of inorganic particles (say gold or silver nanoparticles), emulsions (milk, mayonnaise), macro-

molecules (in jellies, gels, bio-fluids), micelles (of surfactant) or clay slurries (mud or toothpaste) or drops (fog, mist). The most distinguishing feature of colloidal dispersions is their ability to keep the dispersed phase suspended by virtue of thermal motion or Brownian motion. In equilibrium, colloidal suspensions occur in the phase with the lowest free energy, and their behavior is governed by the laws of statistical physics. We noted earlier how Perrin and Westgern had looked at the barometric height distribution of particles in gravitation [23,84]:

$$\rho(h) \sim \exp\left(-\frac{mgh}{kT}\right)$$

They counted the number of particles distributed due to the diffusion–sedimentation equilibrium for calculating Avogadro's number and verifying the statistical predictions of the theory of Einstein [77–79] and Smoluchowski [80,84].

From this relation, it follows that the average height of a colloidal particle above the surface is equal to

$$\langle h \rangle = \frac{k_B T}{mg}$$

The colloidal regime is best delimited by requiring that the average height, $\langle h \rangle$ is greater than the particle size, which is indeed saying that to be colloidal, a dispersion must display characteristics of Brownian dynamics [95]. For a spherical particle of dimension "a", and effective mass density, ρ_{eff} (after subtracting of density of the fluid displaced by the particle, to account for buoyancy), the criteria yields

$$a = \left(\frac{6k_B T}{\pi g \rho_{eff}}\right)^{1/4}$$

For a particle with ρ_{eff} of 1 g/cm^3, the above criteria is satisfied for $a \sim 1$ μm, whereas for metallic nanoparticles, say gold, where the ρ_{eff} is nearly an order of magnitude larger (ρ is 19.3 g/cm^3 for gold), the corresponding estimate tells us that particles above diameter of 0.5 μm cannot be kept dispersed as Brownian particles in a solvent with density comparable with water, under the influence of earth's gravitational field. Further, even though a particle could be stabilized or kept afloat by either using a density matched fluid or by placing it in low gravity environment, the particles can display the characteristics of a colloidal particle only if it observes Brownian motion.

As Frenkel notes in his lecture on colloidal systems [95], both the length scale and time scale of this motion are important. To move a distance comparable to its size, a, the time scale required for a Brownian particles is

$$\tau = \frac{a^2}{D}$$

where the diffusion coefficient D, of the particle is given by Stokes–Einstein relation:

$$D = \frac{k_B T}{\zeta}$$

For spherically symmetric or spherically isotropic bodies, the friction coefficient, $\zeta \sim \eta a$ where η is the viscosity of the solvent or the medium. For the sphere, the exact relation as derived by Stokes is $\zeta = 3\pi\eta a$. While a brick could be kept afloat for example, the time required for it to diffuse a distance comparable to its size is of the order of million years [90,95], where the timescale for a typical colloidal particle turns out to be a second or less. The understanding of Brownian motion is key to appreciating the sedimentation behavior of gold sols, and is essential for designing separation techniques that can exploit the difference in hydrodynamics of rods and spheres, as will be discussed in Section 6.

It has been remarked in literature that in the seed-mediated method, "for reasons not presently understood" [3], the gold nanorods can grow no more than length of 600 nm, diameter 20–30 nm. We contend that this is probably due to the fact that these particles are no longer Brownian. Depending upon the effective density of the particles, beyond a certain physical size, particles cease to display the characteristic physical properties of colloids. Simple, back-of-the-envelope estimate based on argument outlined in this section shows gold particles would behave as colloids in all respects as long as their size is below a few hundred nanometers. While we have already noted the role of thermal motion in determining the colloidal behavior, the overall stability and phase behavior of the sub-micron particles depends upon the interplay of the attractive or repulsive interparticle forces with the random Brownian forces. These interparticle forces include electrostatic repulsion, attraction due to dispersion forces, attraction and repulsion caused by soluble polymers, and hydrodynamic effects that arise due to relative motion between particles and the liquid [94,95,109].

In Table 1, we provide an order of magnitude estimate of the relative importance of forces relevant for gold nanospheres of diameter, a, dispersed in medium with dielectric constant, ε. The contribution of Brownian forces is of the order of $O(k_B T/a)$; with k_B being the Boltzmann's constant, and T is the temperature. The dispersion force, which has the contribution from London–van der Waals interaction, is $O(A_{eff}/a)$, where A_{eff} is the Hamaker constant, that depends upon the nature of the particles and the intervening fluid, and the value used (~1.9 eV) here is for gold–gold attractions through dodecane [110]. Coulomb's law, $\varepsilon\varepsilon_0\zeta^2$, gives an estimate of electrostatic forces between two particles (though they are actually moderated by ions in the intervening fluid); here ε_0 is the permittivity of free space (8.85×10^{-12} C/V m), and ζ is the electrostatic potential of the particles. The viscous forces for particles moving with velocity U can be estimated by Stokes law to be $O(\eta a U)$, which depends upon viscosity of the material, η, while the inertial forces are $O(a^2 \rho U^2)$. For a typical particle dispersed in a medium, with density difference $\Delta\rho$ between the particle and the medium, the effective gravitational force (taking buoyancy into account) is $O(a^3 \Delta\rho g)$. While the estimates are made for spherical particles, the corresponding values for rod-like nanoparticles would not be too different.

The absolute magnitude of the interparticle forces depends upon the distance between them. While the screened electrostatic repulsion between two flat surfaces decays exponentially with distance, the dispersion forces scales as $1/r^3$. The attractive dispersion forces might dominate the repulsion forces when particles are separated by shorter distances. But as particles try to move into a closer contact, they encounter separation dependent viscous forces, that are required to drain away the intervening fluid layer, and this force diverges as the distance goes to zero. The sedimentation or gravitational force is insignificant as compared to

Table 1
Magnitude of the characteristic forces: $a = 20$ nm, $\mu = 10^{-3}$ kg/(m s), $U = 1$ μm/s, $\rho = 20 \times 10^3$ kg/m^3, $\Delta\rho/\rho = 20$, $g = 10$ m s^{-2}, $A_{eff} = 10^{-20}$ Nm, $\zeta = 47$ mV and $\varepsilon = 10^2$.

$\frac{Electric\ force}{Brownian\ force} = \frac{a\varepsilon\varepsilon_0\zeta^2}{kT} \approx 10$	
$\frac{Attracti\ force}{Brownian\ force} = \frac{A_{eff}}{kT} \approx 10$	
$\frac{Viscous\ force}{Brownian\ force} = \frac{\eta U a^2}{kT} \approx 0.01$	
$\frac{Gra\ force}{Brownian\ force} = \frac{a^3\,\Delta\rho g}{kT} \approx 0.001$	
$\frac{Gra\ force}{Viscous\ force} = \frac{a^3\,\Delta\rho g}{\eta U a} \approx 0.1$	
$\frac{Inertial\ force}{Viscous\ force} = \frac{\rho a^2 U^2}{\eta U a} \approx 10^{-4}$	

Brownian forces (0.001 in Table 1), though as particle size grows the gravitational forces start to dominate behavior as discussed before. If the particles are placed in a centrifugal field, where effective gravitation is two to three orders of magnitudes higher, the gravitational forces become comparable or larger than Brownian forces (a g_{eff} of 10,000 makes the forces comparable). Change in solvent implies a different viscosity, which affects viscous forces and also a different dielectric constant, which changes the magnitude of repulsive electrostatic and attractive dispersion forces, as can be seen from the formulae listed in Table 1. Adding a salt or an electrolyte can promote particle aggregation precisely because it changes the magnitude of the dispersion force. Lastly, the presence of soluble polymers or polymers adsorbed to particles or proteins or surfactant molecules also affects the interparticle forces, and the contributions typically arise from the strong dependence of local osmotic pressure on concentration and distribution of adsorbed or attached species. A comprehensive list of these (and other) forces and their origin can be found in the text by Evans and Wennerstrom [109].

We will mention the role of some of these interparticle forces in the course of our discussion on sedimentation behavior during gravitation and centrifugation and in context of self-assembly. In the historical perspective, we had noted how Faraday, Svedberg, Zsigmondy and others observed the coagulation of gold sols using salts and increase in stability of colloidal particles in presence of gelatin for example. The exact nature of interparticle forces relevant for gold sols depends upon the solvent used, surfactant and salts present, particle shape and so on. While interparticle forces capture the contributions to thermodynamic stability of the colloidal dispersions, their overall stability depends kinetic considerations as well, for the interparticle dynamics is modulated by hydrodynamic interactions which become important during the study of dynamic properties of the colloids. Several colloidal textbooks [94,95,109] can be consulted for detailed discussion on the nature and aspects of the interaction forces and hydrodynamic interaction. At the same time, we must emphasize that while we focus on the behavior of gold nanorods, these are mostly stabilized by the use of amphiphilic surfactant molecules, that can aggregate to form micelles spontaneously, and their aggregate size and shape influences growth and stability behavior of particles. The aggregate size and shape of micelles depends upon the solution conditions, including pH, temperature, salt, etc. [109], and in studying any effect of these on stability or response of dispersed gold nanoparticles, one must bear the response of surfactants in mind.

4. Optical properties of gold nanoparticles

4.1. Genesis of extinction spectrum

The interaction of light with matter containing particles invariably involves scattering and absorption, both of which cause attenuation in the intensity of beam passing through the medium [111,112]. Scattering is caused by heterogeneity in the system, which could be caused simply by density or concentration fluctuations, or by presence of particles or drops as dispersed phase. When we are dealing with particles dispersed in a fluid or a gas, typically the scattering by fluctuations in the media is much lower than by the particles and can be neglected for practical purposes. The blue color of sky is a result of scattering [113], and the attenuation of light passing through turbid media like fog is also due to scattering. Scattering is often accompanied by absorption, whereby depending upon the material in question, certain frequencies are absorbed and dissipated either as heat or for other internal processes in the molecules or particles. The color of black smoke or of Indian ink dispersed in water is due to absorption.

A light beam passing through a colloidal dispersion of metal nanoparticles gets attenuated by the combined contribution of absorption and scattering, as given by

$$I(z) = I_0 \exp(-n_0 C_{ext} z)$$

Here I_0 is the intensity of the incident beam, $I(z)$ is the intensity of the beam after travelling path length, z within the sample, n_0 is the number density of particles and C_{ext} ($=C_{abs} + C_{sca}$) is the extinction cross section of a single particle; and is the sum total of the absorption and scattering cross sections respectively. The product $n_0 C_{ext}$ is often termed as the extinction coefficient, γ and it has units of reciprocal length. The absorption spectrum determined by UV–vis spectroscopy is in fact a measure of attenuation caused by a dispersion of gold nanoparticles, and is thus related to the absorption cross section. In what follows, we will elucidate the relationship of the size and shape of gold nanoparticles to extinction cross sections, thus establishing the physical basis for their optical response. In the process, we will also determine the local electric fields associated with nanoparticles are important for their applications.

The optical properties of noble metal particles originate from localized surface plasmons. These phenomena occur when electromagnetic field interacts with conduction band electrons and induces the coherent oscillation of electrons. As a result, a strong absorption band appears in some region of the electromagnetic spectrum depending on the size of the particle (described in more detail in the next sub-section). This plasmon absorption is a small particle effect. It is absent in the individual atoms as well as in the bulk. Even for thin films, at the interface between a metal and a dielectric, the electromagnetic field can couple to the oscillations of conduction electron plasma creating surface plasmon polaritons. These surface plasmon polaritons are *dispersive*, *propagating* electromagnetic excitations on the interface that are evanescently confined in perpendicular direction. The detailed derivation and discussion of applications of surface plasmon polaritons is presented in texts like Maier [66], and is outside the scope of this article.

But when a metal nanoparticle is exposed to such a field, *non-propagating* excitations of conduction electrons create size dependent localized surface plasmons that arise simply when we consider the absorption and scattering by gold (or other metallic) nanoparticles. When a conductor or metal is placed in an oscillating field of incoming radiation, the electrons cloud is driven into oscillations (Fig. 1). In the case of a sub-wavelength conductive nanoparticle, the curved surface of the particle exerts an effective restoring force on these driven electrons (analogy with a damped, driven harmonic oscillator). Like any driven oscillator system, in nanoparticle case, a resonance can arise leading to the field amplification both inside and outside the particle. This resonance for gold and silver particles lies in the visible region of the electromagnetic radiation which is responsible for their bright

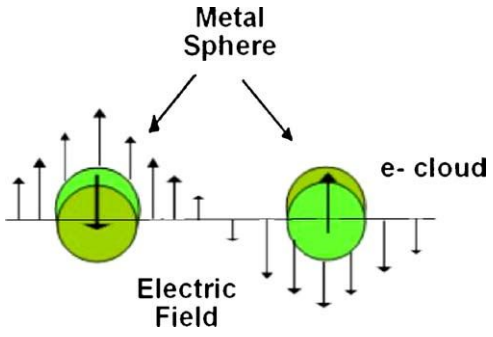

Fig. 1. Size dependent localized plasmon resonance in metal spheres.

colors in both transmitted and reflected light. The reason for field amplification as well as optical response of gold nanoparticles will perhaps more clear when we approach this problem using electrostatics.

Mie [25] first explained this phenomenon theoretically by solving Maxwell's equations for a radiation field interacting with a spherical metal particle under the appropriate boundary conditions. He applied an exact electromagnetic theory for spherical particles using electrodynamics, and this describes the extinction (absorption + scattering) of spherical particles of any given size. In this section, we will first describe the basis for plasmon resonance, illustrating the underlying quantum effect by discussing the basis for the absorbance by spherical and non-spherical metal particles. The theoretical background presented is essential for understanding the color of gold sols as well as for appreciating how and why localized field enhancements can occur for these particles, leading to their utility as sensors. The reader may wish to refer to textbooks by Bohren and Huffman [111], van de Hulst [112], Kerker [114] and Jackson [115] for more detailed derivations of absorption and scattering. We must suggest the excellent, recent text by Maier [66] for it focuses on fundamentals and applications of plasmonics, and indispensible articles [1–15,49,116–123] that focus on optical properties of gold nanoparticles.

4.2. Localized surface plasmon resonance for spherical particles

In the plasma model, the free electrons in a metal can be considered to be like a gas of number density 'n_0' moving against the fixed background of positive ion cores. The dielectric function of the metal, $\varepsilon(\omega)$ is related to the refractive index, n and the absorption coefficient, k by the following relations:

$$\varepsilon(\omega) = \varepsilon_1(\omega) + i\varepsilon_2(\omega)$$

$$\varepsilon_1 = n^2 - k^2 \quad \text{and} \quad \varepsilon_2 = 2nk$$

$$n^2 = \frac{1}{2}\varepsilon_1 + \frac{1}{2}\sqrt{\varepsilon_1^2 + \varepsilon_2^2}; \qquad k = \frac{\varepsilon_2}{2n}$$

In what follows, we proceed from Maxwell's equations to describe a much simpler electrostatics computation of interaction of a nanoparticle of size with an electromagnetic radiation of wavelength λ such that $a \ll \lambda$. Let us first consider a homogeneous, isotropic sphere with dielectric function $\varepsilon(\omega)$, radius a placed in the electric field E placed in a medium with the dielectric constant of the medium as ε_m. In the case, the solution to the Laplace equation

$$\nabla^2 \Phi = 0$$

can be written as

$$\Phi(r,\theta) = \sum_{l=0}^{\infty} [A_l r^l + B_l r^{-(l+1)}] P_l(\cos\theta)$$

where $P_l(\cos\theta)$ is the Legendre polynomial of order l. Now by solving for the potential inside and outside the sphere, and by using the boundary condition at the sphere to be the equality of the tangential and normal component of the electric field (gradient of potential), we can arrive at the resulting electric field as described in textbook examples in say Jackson [115]. This leads to a polarization of the sphere given by

$$\vec{P} = 4\pi\varepsilon_0\varepsilon_m a^3 \left[\frac{\varepsilon - \varepsilon_m}{\varepsilon + 2\varepsilon_m}\right]\vec{E}_0$$

implying simply that the applied field introduces a dipole moment inside the sphere. We can rewrite the expression in terms of the polarizability, α as

$$\vec{P} = 4\pi\varepsilon_0\varepsilon_m\alpha\vec{E}_0$$

implying therefore that polarizability is

$$\alpha = 4\pi a^3 \left[\frac{\varepsilon - \varepsilon_m}{\varepsilon + 2\varepsilon_m}\right]$$

Since the dielectric function of the gold is frequency dependent, we can arrive at the resonant condition when the extrema of the polarizability is reached. This occurs when the denominator is a minimum, i.e. $|\varepsilon + 2\varepsilon_m|$ is a minimum, which for the case of small or slowly varying Im[ε] around the resonance condition simplifies to Re[$\varepsilon(\omega)$] = $-2\varepsilon_m$ called the Fröhlich condition. The associated mode is called the dipole surface plasmon of the nanoparticle, and for a given metal, depends on the dielectric constant of the medium. This implies that the change in the absorption peak of a given metal nanoparticle can sense the local changes in refractive field, and can be used as a marker for following the changes in refractive index [45]. It would perhaps be most useful for systems where such a change can be brought about by a chemical reaction that could be marked in terms of localized change in the environment of the nanoparticle. We note here that the magnitude of the polarizability at the resonance condition is well-defined, because even though the Fröhlich condition is satisfied, the Im[ε] is non-vanishing.

In the plasma model, when the electrons oscillate in response to the applied electromagnetic field, their motion is damped via collisions that occur with the frequency of $1/\gamma_d$. The dielectric function for free electrons of metal, can be written using Drude model as

$$\varepsilon_D(\omega) = 1 - \frac{\omega_p^2}{\omega^2 + i\gamma_d\omega}$$

Here the $\omega_p^2 (= n_0 e^2/\varepsilon_0 m_{eff})$ is the plasmon frequency of free electron gas, and m_{eff} is effective mass of the electrons. Since electron–electron, electron–phonon and electron-defect scattering processes determine the value of γ_d, which is a phenomenological damping constant of the bulk material, it is constant for bulk material, implying that the dielectric function is constant. As we approach particle sizes comparable to the mean free path of the electrons, collisions of conduction electrons with particle surface contributes to the damping constant, as described by

$$\gamma_d(r) = \gamma_{d0} + \frac{A\nu_F}{r}$$

Here γ_{d0} is the bulk damping constant, ν_F is the velocity of the conduction electrons at Fermi energy and A includes the details of scattering process. The size dependence of damping constant makes dielectric constant and hence the resonance condition function of radius r of the particles. It may be remarked here that the consequence of this resonantly enhanced polarization is an enhancement in the efficiency of scattering and absorption of light by metal nanoparticles. This is evident if one examines the corresponding cross sections for scattering and absorption [111]:

$$C_{sca} = \frac{k^4\alpha^2}{6\pi} = \frac{8\pi}{3}k^4a^6\left[\frac{\varepsilon - \varepsilon_m}{\varepsilon + 2\varepsilon_m}\right]^2$$

$$C_{abs} = k\,\mathrm{Im}[\alpha] = 4\pi k a^3\,\mathrm{Im}\left[\frac{\varepsilon - \varepsilon_m}{\varepsilon + 2\varepsilon_m}\right]$$

It is very difficult to distinguish smaller particles from the background of large scatterers because of the a^6 dependence of scattering cross section. But for small particles with $a \ll \lambda$, absorbance scales with Volume and the scattering with (Volume)^2 so absorbance dominates over scattering. Hence when we refer to the extinction measured experimentally, we are typically seeing absorbance spectrum, and the expression for extinction for spherical particles can be written as:

$$\frac{\gamma}{N_p V} = \frac{18\pi\varepsilon_m^{3/2}}{\lambda}\frac{\varepsilon_2}{(\varepsilon_1 + 2\varepsilon_m)^2 + \varepsilon_2^2}$$

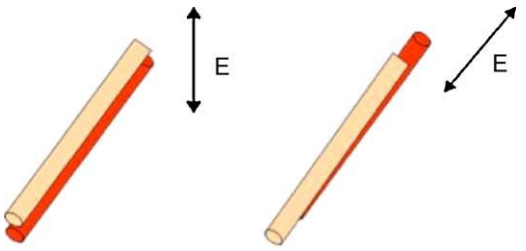

Fig. 2. Transverse and longitudnal modes of plasmon resonance in rod-like particles.

4.3. Plasmon resonance for ellipsoidal nanoparticles

For gold nanorods, the plasmon absorption splits into two bands (Fig. 2) corresponding to the oscillation of the free electrons along and perpendicular to the long axis of the rods [14]. The transverse mode (transverse surface plasmon peak: TSP) shows a resonance at around 520 nm, while the resonance of the longitudinal mode (longitudinal surface plasmon peak: LSP) occurs at higher wavelength and strongly depends on the aspect ratio of nanorods. As aspect ratio is increased, the longitudinal peak is red-shifted. To account for the optical properties of NRs, it has been common to treat them as ellipsoids, which allows the Gans formula (extension of Mie theory) to be applied. Gans' formula [26] for randomly oriented elongated ellipsoids in the dipole approximation can be written as

$$\frac{\gamma}{N_p V} = \frac{2\pi\varepsilon_m^{3/2}}{3\lambda}\sum_{j=A}^{C}\frac{(1/P_j^2)\varepsilon^2}{[\varepsilon_1 + ((1-P_j)/P_j)\varepsilon_m]^2 + \varepsilon_2^2}$$

where N_p represents the number concentration of particles, V the single particle volume, λ the wavelength of light in vacuum, and ε_m the dielectric constant of the surrounding medium and ε_1 and ε_2 are the real $(n^2 - k^2)$ and imaginary $(2nk)$ parts of the complex dielectric function of the particles. The geometrical factors P_j for elongated ellipsoids along the A and B/C axes are respectively given by

$$P_A = \frac{1-e^2}{e^2}\left[\frac{1}{2e}\ln\left(\frac{1+e}{1-e}\right) - 1\right]$$

$$P_B = P_C = \frac{1-P_A}{2} \quad \text{and} \quad e = \left(\frac{L^2 - d^2}{L^2}\right)^{1/2}$$

Fig. 3 shows the absorbance spectra for gold nanorods with varied aspect ratio calculated using the Gans expressions. The dielectric constants used for bulk gold are taken from the measurements done Johnson and Christy [124], while the refractive index of the medium was assumed to be constant and same as for H_2O (1.333). The maximum of the longitudinal absorbance band shifts to longer wavelengths with increasing aspect ratio. There is the small shift of the transverse resonance maximum to shorter wavelengths with increasing aspect ratio. Electron microscopy reveals that most nanorods are more like cylinders or sphero-capped cylinders than ellipsoids. However, an analytical solution for such shapes is not derived yet, and so while the results are compared to the formula given by ellipsoids, we must remember that such comparisons are somewhat approximate.

4.4. Beyond dipole resonance and beyond electrostatics

In the so-called Rayleigh limit, i.e. when the size of the particle, a, is much smaller than the wavelength of light, λ, i.e. satisfies $|m|x \ll 1$, where $x = ka$, (and $k = 4\pi/\lambda$) the first term of the expansion or dipole term, is enough to provide a reasonable estimate of the scattering coefficient [25]. In this limit, where both

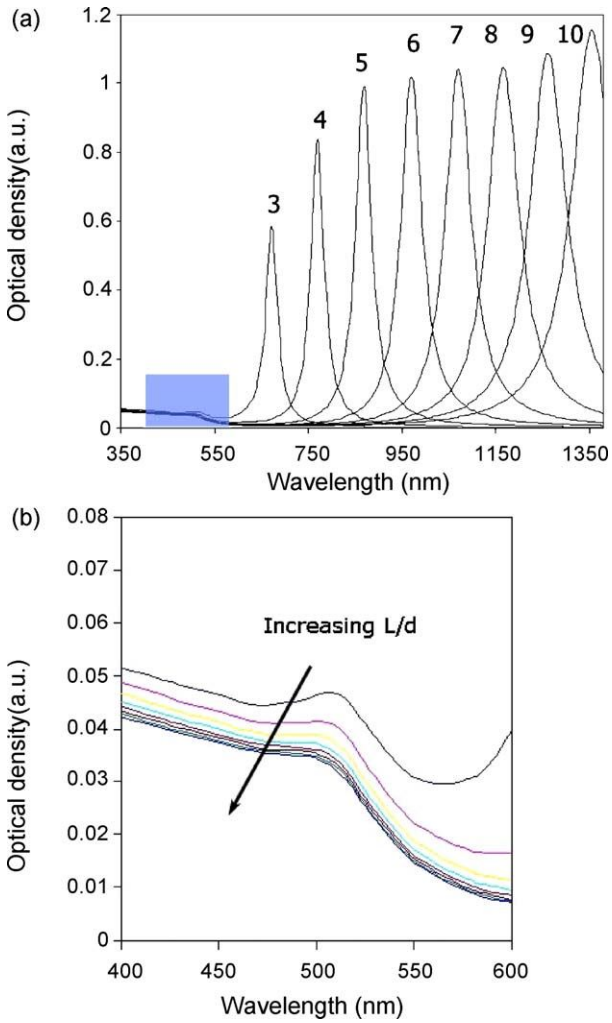

Fig. 3. Absorbance spectra calculated with the expressions of Gans for elongated ellipsoids using the bulk optical data for gold. (a) The numbers on the spectral curves indicate the aspect ratio (L/d). (b) Enlargement of the shaded area of (a) showing slight blue shift of transverse plasmon resonance peak on increasing aspect ratio [125].

$x \ll 1$ and $|m|x \ll 1$, a spherical particle experiences a fairly uniform field and we can derive the extinction cross section by evaluating field scattered or radiated by a dipole. This simply follows from electrostatics as the sphere gets polarized due to external field and emits as a dipole. As the size parameter increases towards one, higher order, multipole contributions, become important. For example, the quadrupole contribution, computed easily for spheres, leads to spreading of the expected resonance peak. For example, if we consider the expansion based on Mie theory for polarizability of the sphere of Volume, V [66,126]:

$$\alpha_{sph} = \frac{1 - (1/10)(\varepsilon + \varepsilon_m)x^2 + O(x^4)}{((1/3) + \varepsilon/(\varepsilon - \varepsilon_m)) + (1/30)(\varepsilon + 10\varepsilon_m)x^2 - i(4\pi 2\varepsilon_m^{1.5}/3)(V/\lambda_0^3) + O(x^4)}$$

where $x = \pi a/\lambda_0$ relates size to the free space wavelength.

As we can see, a number of additional terms appear in both numerator and denominator. The quadratic term in the numerator includes the retardation effect of the exciting field over the volume of the sphere leading to shift in plasmon resonance. Similarly a shift in plasmon resonance is affected by the quadratic term that appears in the denominator, representing the retardation of polarization field inside the particles. For gold (and other noble metals) the overall shift is towards lower energies and hence the

spectral position of the dipole resonance shifts towards longer wavelengths. This means that there is a red-shift due to increase in particle size. Intuitively, we can say that the distance between the charges at the opposite interfaces of the particle increase with increase in size, thus leading to a smaller restoring force and hence a smaller resonance frequency. The red-shift underscores the fact that effects of the interband transitions (which increase Im[ε]) not captured by Drude model decrease as the plasmon resonance moves away from the interband transition edge [66].

The quadratic term in the denominator increases the magnitude of polarization as well as leads to a decrease in the influence of absorption (from Im[ε]). However, the completely imaginary term present in the denominator, which accounts for radiation damping, counteracts this effect. Radiation damping [15] is caused by the direct radiative decay of the coherent electron oscillations into photons. It is the main cause for weakening of the dipole plasmon resonance for particles with increase in size, and as a result, despite of the decrease in absorption, a significant broadening of plasmon sets in. More detailed discussion of radiation damping and non-radiative decay can be found in the work of Link and El-Sayed [15]. The multipole plasmon resonances in colloidal gold nanorods [127]. were reported recently for rods that are few hundred nanometers in length, and the experimental results were captured by Discrete Dipole Approximation (DDA) simulations, described in the next sub-section.

4.5. Computational methods

While analytical solutions are hard to come by, various numerical methods and techniques have been applied to solve Maxwell's equations for non-spherical particles. In case of metal nanoparticles, these allow us to compute both the plasmon resonance as well as local electric fields, and hence the local enhancement of fields and effects resulting from them. The most commonly used numerically exact methods are DDA and T-matrix methods, though multiple multipole methods (MMP) and finite difference time domain (FDTD) methods have been utilized as well [128].

The DDA method is a numerical method first introduced by Purcell and Pennypacker [129] in which an object of arbitrary shape is represented on a cubic lattice of N polarizable point dipoles localized at r_i, $i = 1, 2, \ldots, N$, each one characterized by a polarizability α_i. The induced dipole polarizations at each point in the lattice are determined self-consistently, where local field at each dipole includes the effect of the polarization at other dipole fields. This makes for computationally intensive procedure, leading to $N \log(N)$ dependence of the computational time on the number of cubes. For particles with dimensions of tens of nanometers, it involves coarse graining, which perhaps limits the accuracy of the simulated values quoted for field enhancement and extinction coefficients. Schatz and co-workers [12,117–120,127,128,130] have demonstrated the use of DDA for optical calculations of metallic systems with different geometries and environments. While the DDA is a useful technique for yielding extinction, absorption and scattering cross sections for particles of complex shapes, one must remember that: (1) the assumption on size of dipole and refractive index mean the results are at best approximate, and (2) the coarse graining required to evaluate the resonance and absorbance limits the accuracy to which local fields and field enhancements can be determined for complex particle shapes and for interacting or coupled particles.

4.6. Absorption spectrum of colloidal dispersions of gold nanorods

It is made evident in previous sections that the longitudinal and transverse plasmon resonance can be computed as a function of aspect ratio either by using analytical expression put forth by Gans in 1912 [26] or by using one of numerical techniques [111,128]. We now describe the how the absorption spectrum measured experimentally compares to the results from Gans theory [26] and DDA simulations [128]. The gold nanorods cited from our research were synthesized using a seed-mediated method based on use of binary surfactant, as described in the next section and all UV–vis–NIR spectra were acquired with a Cary 5G UV-visible-near-IR spectrophotometer. Even though optical properties of pure water were used for calculating the spectrum, the peak resonance measured experimentally show a remarkable agreement with theoretical and simulation results (Fig. 4). Several groups have observed similar trends [3,14]. Though we assert that the best comparisons can be made only with samples with lowest possible polydispersity. It must be pointed out here that the nanorods used in our research were not only synthesized in a controlled manner to produce lower size dispersity, but they were also separated more efficiently from nanospheres using our understanding of what controls shape separation during centrifugation. The methodology for controlled synthesis and the theoretical and experimental aspects of shape separation are summarized in next two sections of this review.

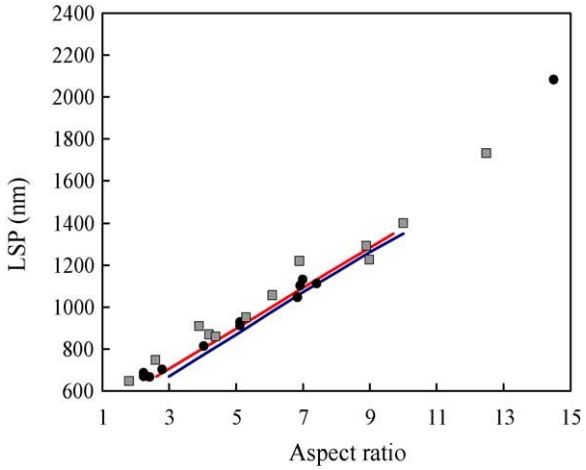

Fig. 4. Longitudinal surface plasmon peak (nm) versus the aspect ratio of nanorods. Simulation results using the DDA method [12] and the corresponding fit (red straight line) and Gans' calculation (blue straight line). Experimental data from the work (gray squares). Experimental data from our study (black circles) [125].

It is well known though that the plasmon resonance is very sensitive to change in the dielectric constant of the medium, and in case of mixed solvents or in sensing applications, we must take this effect into consideration. Theoretically predicted change in optical properties of colloidal gold suspensions expected upon changing medium has been observed experimentally by several groups [46,131]. For the gold nanorods, the computed longitudinal plasmon peak increases with an increase in the dielectric constant of medium, as shown in Fig. 5. The effect of medium seems more pronounced for longer nanorods, as is evident from the increase in slope observed for higher aspect ratios.

4.7. Local field enhancements and sensing applications

Let us remind ourselves that the electric field is the gradient of potential, and hence using the expression for potential derived earlier, we note that the electric fields inside and outside the sphere are:

$$E_{in} = \frac{3\varepsilon_m}{\varepsilon + 2\varepsilon_m} E_0$$

$$E_{out} = E_0 + \frac{3\vec{n}(\vec{n}\cdot\vec{p}) - \vec{p}}{4\pi\varepsilon_0\varepsilon_m}\frac{1}{r^3}$$

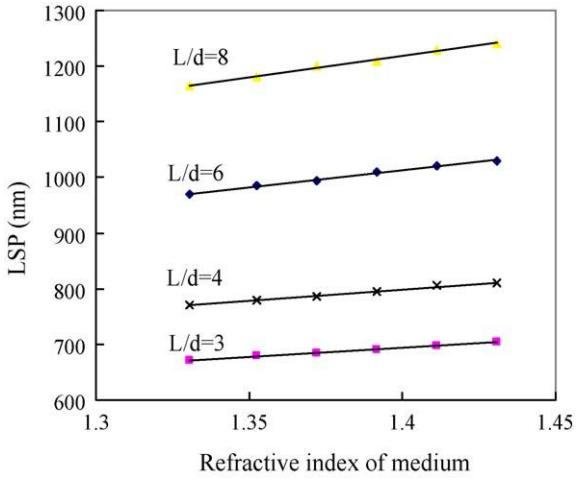

Fig. 5. Calculated LSP as a function of refractive index of medium [125].

Resonance in polarizability leads to the resonant enhancement of both the internal and the external dipolar fields. The wavelength at which this resonance occurs depends upon the dielectric function of the metal as well as the medium around it. Since the resonance condition and resulting enhancements of the fields are directly correlated with the shape and size of particle, the basic understanding of this relationship is crucial for their widespread use. The sensitivity of plasmon resonance to the local dielectric environment, implies that any changes within a few nanometers of the particles can be used in say biological or chemical sensing applications [1–10,12,16,17,30–47,66,132–137]. Non-linear applications as well as surface-enhanced Raman sensing are dependent on our ability to maximize the local fields and generate electro-optical effects that can be monitored easily. For the perfectly spherical particles that can be described by electrostatic approach (Rayleigh limit), only the dipole surface plasmon contributes to the localized enhancement, limiting the overall enhancement achieved. In rod-like particles, highly localized fields can be generated at the tips, providing a much stronger response function for sensing applications. The theoretical and experimental aspects of SERS and plasmonics based sensing are widely discussed and debated in literature [31,66] and it forms one of the most anticipated applications of non-spherical gold and noble metal particles. For now, we will focus on color of colloidal dispersions of rod-like gold particles, and polarization dependence color and absorption that can be used and illustrated using polymer nanocomposites.

4.8. Color of colloidal dispersions of gold nanorods

Since the color of colloidal gold depends on both the size and shape of the particles, as well as the refractive index of the surrounding medium, it is important to independently account for the color change of gold nanorod suspension due to presence of either nanospheres or any substance that affects the refractive index of the solvent. Since color of the gold sols is traditionally linked to their shape or size, we decided to characterize the dependence of perceived color on shape and dimensions of the nanoparticles using color science.

Color science or science of colorimetry is standardized in terms of CIE color space [138,139], based on 2° observer data, which essentially describes the response of "average" observer to a color stimulus on which perception is based. To simulate the color of gold nanorods from the calculated absorption spectra and experimental spectra, CIE XYZ tristimulus values was calculated. The absorbance (A) was converted to transmittance (T) according to the following equation:

$$A = \log_{10}\frac{1}{T}$$

Following the standard procedure from the color science, we calculated CIE XYZ tristimulus values by integrating the relative spectral transmittance $T(\lambda)$ together with the relative spectral energy distributions of the illuminant, $E(\lambda)$, and by using the standard observer functions $x(\lambda)$, $y(\lambda)$, and $z(\lambda)$. We used the spectral distribution power function of daylight D_{65}. The integration is approximated by summation, thus:

$$X = \frac{1}{k}\sum T(\lambda)E(\lambda)x(\lambda), \qquad Y = \frac{1}{k}\sum T(\lambda)E(\lambda)y(\lambda),$$
$$Z = \frac{1}{k}\sum T(\lambda)E(\lambda)z(\lambda)$$

where $k = \sum E(\lambda)y(\lambda)$ and λ = wavelength.

The amounts of red, green, and blue needed to form any particular color are called the tristimulus values and are denoted X, Y, and Z, respectively. A color is then specified by its trichromatic coefficients, defined as

$$x = \frac{X}{X+Y+Z}, \quad y = \frac{Y}{X+Y+Z}, \quad z = \frac{Z}{X+Y+Z}, \quad x+y+z = 1.$$

The color was identified by positioning x and y values in the CIE chromaticity diagram.

This visible light region consists of a spectrum of wavelengths, which range from approximately 700 to 400 nm. For the nanorods, the transverse plasmon resonance peak is not quite as sensitive to the change of aspect ratio, as the longitudinal peak, which shows noticeable shifts in the aspect ratio as seen in Fig. 6 which shows the UV–vis–NIR spectrum of gold nanorods dispersions. The relatively intensity of transverse peaks shows that mostly nanorods are present, which were obtained by optimizing synthesis and separation techniques described in subsequent sections. As predicted by theory, the transverse peak blue shifts with an increasing aspect ratio. The blue shift is not typically seen in experimental results and its presence here shows that the synthesis and separation methodology developed by us leads to relatively monodisperse samples.

Fig. 7 shows the photograph of the colloidal dispersions of gold nanorods and the color patches simulated using theoretical absorbance data equivalent to the aspect ratio of gold nanorods. The color of solution is basically the same beyond an aspect ratio of around 4. Also the color of the hydrosols of gold nanorods we made is identical to the simulated color. Therefore in a visible region, the dramatic color change cannot be achieved by only changing aspect ratio. But once the longitudinal peak goes beyond 700 nm, (for aspect ratio ~3) the change in peak absorption cannot be detected by the human eye and color of gold nanorod dispersion does not change with further increase in aspect ratio. Therefore the color change could be only observed for relatively short range of aspect ratios. But the tunability of optical properties gold nanorods as a function of aspect ratio provides potentials to use gold nanorods as an optical filter in near infrared region. We demonstrate this aspect using polymer nanocomposites in a later section.

We found that the color in a visible region is rather sensitive to the amount of spherical particles included as byproducts since surface plasmon peak of sphere positions between 500 and 550 nm. Fig. 8 shows the color of colloidal dispersion of gold nanorods containing different amount spheres as byproducts. The color changes from purple to brown as the amount of byproducts decreases.

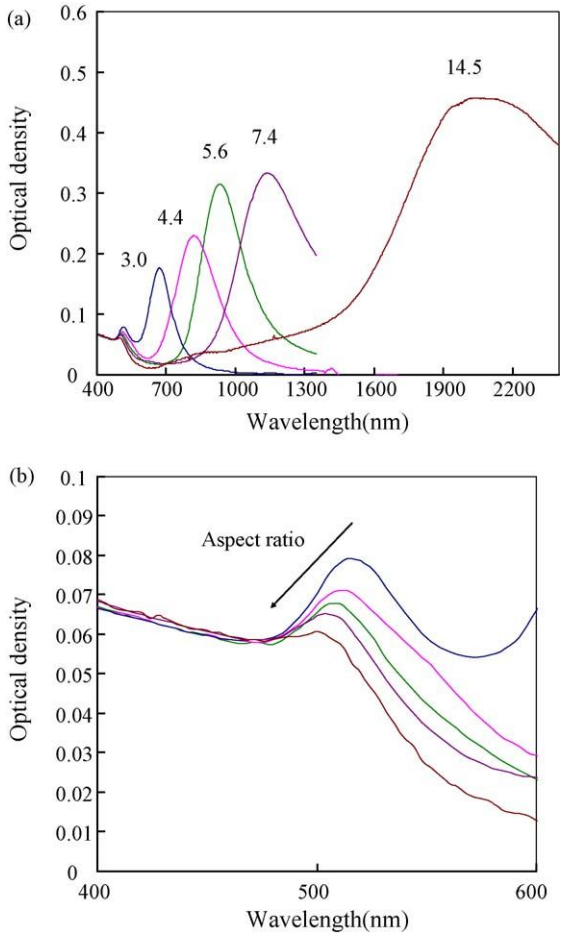

Fig. 6. (a) UV–vis–NIR spectra of dispersions containing gold nanorods with different aspect ratios and (b) transverse peak, showing the blue shift with increase in aspect ratio [125].

4.9. Polarization dependent color and absorption in polymer–gold nanocomposite films

We have noted both in the historical section (Section 2) and in discussion of the localized surface plasmon of rod-like particles that optical properties are dependent on the state of polarization of incident light, on size and aspect ratio of the particles, and the dielectric properties of the medium. The optical response of a colloidal dispersion of nanorods, as revealed by UV–vis spectroscopy can be thought of as the response from randomly oriented rods. The polarization dependent response of nanorods can be observed by dispersing them in a gel or polymer matrix, and then stretching the matrix uniaxially, thus aligning the dispersed rods. When the incident light is polarized in the direction of stretching or in the direction coinciding with the average orientation of long axis of nanorods, absorbance is dominated by the response due to the longitudinal resonance. As the angle between the stretching direction and polarization of incoming light is increased, the absorbance shows a marked blue shift. Thus the composite films show a marked polarization dependent color and absorption, making them suitable for use as polarization dependent color filters and for other optical applications [62,63].

Caseri [62] presented a very comprehensive historical perspective and discussion of optical properties of polymer/nanoparticle composites. Caseri and co-workers [62,140,141] found that spherical gold nanoparticles can form 'pearl necklace type arrays' by aggregating along the stretching direction and produce dichroic filters that have potential application in creating bicolored displays as illustrated in Fig. 9. Al-Rawashdeh and Foss [63] studied the linear dichroic properties of polyethylene/gold rods composites and studied how the local field enhancement could make these composite films impacts the infrared absorption of probe molecules attached to the surface of nanorods. Like several other researchers [142–144], we used water soluble polymer, polyvinyl alcohol (PVA) to make the polymer/nanorod nanocomposites. We mixed the gold nanorod dispersions into an aqueous solution with ~10% PVA of Mw 95,000 (98–99% hydrolyzed, Aldrich), and studied the optical properties of casted films. Uniaxial drawing was carried out on a hot plate at 60 °C.

The absorbance spectra of randomly oriented gold rods in water and in PVA films is shown in Fig. 10. The shift in the longitudinal plasmon peak visible here is accounted for by the change in dielectric medium for the refractive index of PVA is 1.521 as compared to 1.333 for H_2O. Though the calculation using Gans theory does not capture the shift quantitatively, we observe the expected red-shift. Also, the absorbance peak of the nanocomposite with longer aspect ratio (~6.3) lies in near infrared region, and so the appearance of the films shows contribution only from the transverse peak that lies in the visible region.

The polarization dependent absorption of the films was characterized using the experimental set-up (see Fig. 11). We found that by increasing the draw ratio from 2 to 4, as shown in Fig. 12, the intensity of longitudinal plasmon peak is highly diminished when illuminated by light polarized perpendicular to the stretch direction. The result clearly shows that the particle orientation increases with increase in draw ratio, and draw ratio of 4 is sufficient to produce a polarization color filter.

The transmittance spectra as a function of polarizer angle are shown in Fig. 13 for a nanocomposite with gold nanorods of aspect ratio 2.8, and draw ratio of 4 was used for this study. The longitudinal plasmon resonance blue shifts as polarization angle is increased, and the intensity of the peak drops, in accordance with the observations by other groups [62] (Fig. 14).

We obtained transmittance spectra at different polarizer angles and calculated extinction ratio, E.R. = 10 $\log_{10}(T_\perp/T_\parallel)$ [dB] where $T_\perp$ and $T_\parallel$ are the transmittance perpendicular and parallel to the stretching direction, respectively. Maximum extinction ratio [125] is 18 dB at $\lambda = \lambda_{LSP}$ and is comparable to those previously reported in the literature [145]. The thickness of the film is 50 μm and it has good flexibility. When the aspect ratio of nanorods is sufficiently large, the LSP shifts to the near-IR region. This indicates that the wavelength region displaying optical dichroism can be shifted from the visible to the near-IR. This enables the fabrication of thin-film optical filter that respond to the wavelengths in the near-IR region (Fig. 15).

4.10. The ultramicroscope

In recent literature, we find that size and shape of gold particles is often characterized by TEM and such measurements allow direct visualization of nanoparticles deposited and dried onto a copper grid. In the context of our studies too, morphology and mean size of nanoparticles were examined by TEM (JEOL100 at 100 kV). It is widely recognized that broad plasmon resonance peaks observed in UV–vis absorption spectroscopy can arise due to either polydispersity or difference in shape and size of constituent particles and hence a directly visualization provides necessary and complimentary information. We note however that while TEM images are almost indispensible sources of size and shape, a simpler technique for direct visualization of particles exists in ultramicroscopy and has been completely ignored by the community. In what follows, we expound on the basis of ultramicroscopy and its demonstrated ability to show size and optical response of nanometer size particles. We will discuss how particles

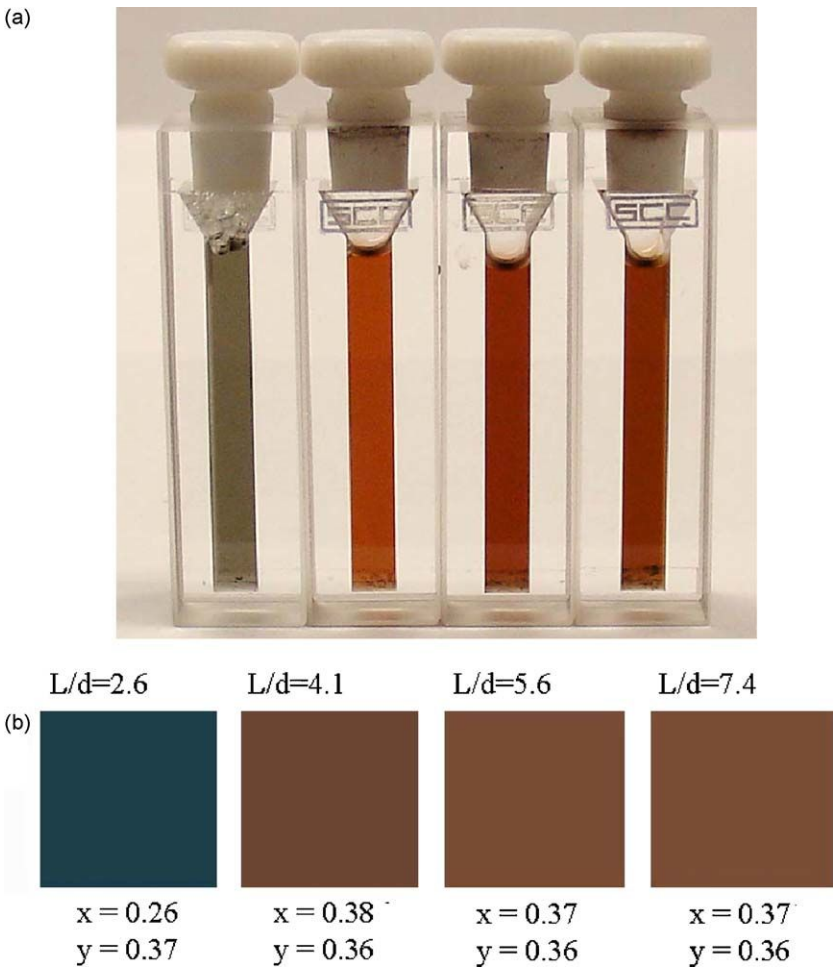

Fig. 7. (a) Photograph of 4 sols of colloidal gold prepared in water. Aspect ratios are 2.6, 4.1, 5.6 and 7.4 (from the left), respectively. (b) The simulated color of dispersion of gold nanorods of different aspect ratio [125].

can self-assemble, size or shape separate on TEM grids in the last section of assembly and liquid crystallinity of rods. There is a merit in looking at particles in their dispersed phase, and hence we describe ultramicroscopy for stressing why it could be revived for studies on colloidal dispersions of gold and other noble metal particles.

When a narrow beam of sunlight enters a dark room, the scattering from dust particles makes them visible. If there were no dust particles, the medium will behave as optically void, and if the particles are decidedly small in size, the beam of light acquires a bluish tinge. This phenomenon is called Tyndall effect and is indicative of presence of suspended particles. Hence all colloidal suspensions exhibit this phenomenon in proper illumination. In his seminal paper [19], Faraday looked at gold sols under such illumination and noted that the gold particles scatter light. Zsigmondy placed a microscope to visualize the Faraday–Tyndall cone of light, and was able to establish that gold sols consist of nanometer size particles [21] (Fig. 16). (Of course, as we remarked before, he never called the particles nanoparticles and never referred to the dimensions in nm units, rather used the term ultramicrons and called particles ultramicroscopic.)

Abbe's diffraction theory tells us that the resolution of the microscope depends upon the wavelength λ of light, and the numerical aperture, NA ($n \sin \alpha$), of the objective of the microscope, where n is the refractive index of the immersion medium. This implies that we can distinguish points that are at a distance larger than $d \sim \lambda/\mathrm{NA}$. Under the best conditions, by using highest numerical aperture objective and by using oil immersion to extend the resolution, we see that the minimum distances resolved by an optical microscope tend to be $\sim$0.2 μm. The reader can refer to any standard text [146–149] for more detailed discussion on image formation and resolution of microscopes. While it is commonly believed that particles smaller than this size cannot be resolved by a microscope, the real limit is set by our ability to detect the light reflected or emitted by particles of sub-microscopic or as Zsigmondy called them ultramicroscopic size. Any particle that can be made to emit enough light can be seen if it is not too close to another particle, and this condition can be satisfied by taking a

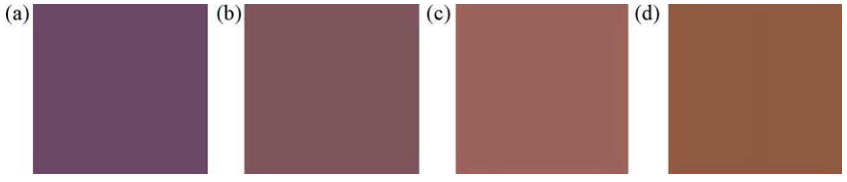

Fig. 8. The color of dispersion of gold nanorods containing different amount of spheres as byproducts: (a) 50%, (b) 30%, (c) 10% and (d) 0% [125].

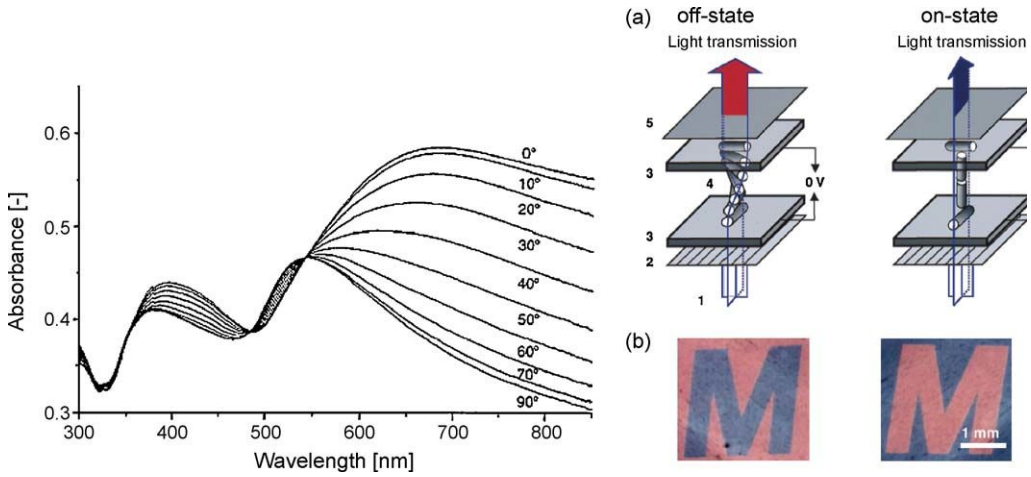

Fig. 9. (a) UV–vis spectra of uniaxially stretched films of high-density polyethylene/gold composites. The angle on spectra indicates the angle between the polarization direction of the incident light and the drawing direction. (b) Color display made possible by using a drawn polyethylene–silver nanocomposite with Twisted-nematic liquid crystal displays (LCD) [62].

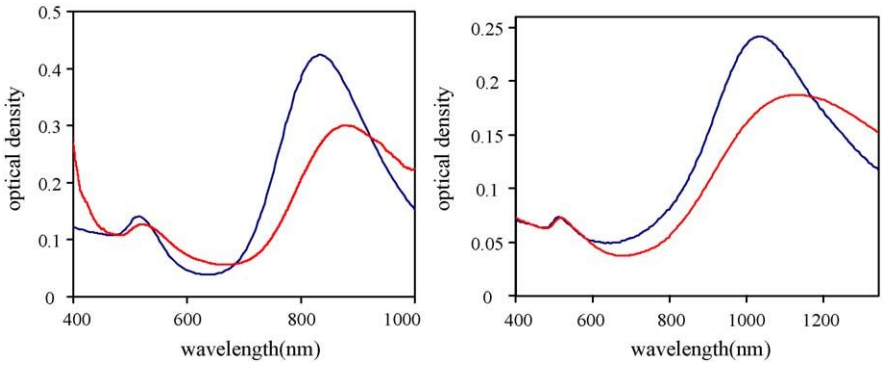

Fig. 10. The absorbance spectra of randomly oriented gold rod dispersions. (a) Aspect ratio 4.3 and (b) aspect ratio 6.3. The blue line is the absorbance spectra of aqueous solution. The red line is the absorbance spectra of PVA film [125].

dilute colloidal suspension. The next step is to illuminate the particles with a strong source of light and to observe them with an optical system that collects maximum possible light emitted by the particles. The smallest size reported to be seen by Zsigmondy was 1.7 nm! [29]. Colloidal solutions of gold and other metals are particularly conducive for ultramicroscopy due to the marked difference between the optical constants of the dispersed phase and the disperse media.

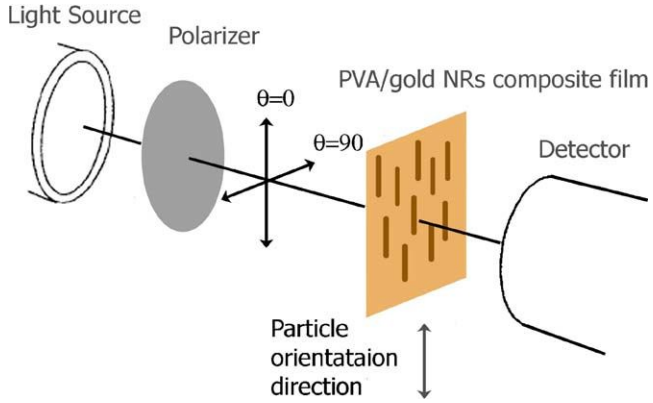

Fig. 11. The experimental set-up of the polarization spectroscopy studies. At a polarization angle $\theta = 0^{\circ}$ the electric field of the light is polarized parallel to the stretch direction, whereas at a polarization angle $\theta = 90^{\circ}$ the electric field of the light is polarized perpendicular to the stretch direction [125].

5. Synthesis of gold nanorods

The wet chemical methods typically involve reduction of an aqueous solution of Au(III) derivatives–chloroaurate ($AuCl_4^-$) where reduced Au atoms initially can form a sub-nanometer cluster particle in the first nucleation stage. Later, the reduced Au atoms stick to these existing particles, leading to growth. Particle aggregation is prevented through vigorous stirring and by adding stabilizing agents. Since the difference between the redox potentials (ΔE) of the two half cell reactions (reduction of Au ion and oxidation of reducing agent) [150] drives the reaction, higher ΔE translates into a more spontaneous reaction. The concentration of reactants, temperature and pH influence the kinetics of nucleation and growth, and therefore control on the size, shape and structure of the colloidal gold nanoparticles [19–23,27,29,150–154]. For example, strong reducing agent such as $NaBH_4$ or phosphorus produces small gold particles while mild ascorbic acid produces larger gold particle due to the smaller ΔE. Ever since aspherical Au particles were observed as a byproduct of the synthesis of colloidal sols, researchers have focussed on developing recipes that make particles of desired shapes and size. The revival of interest in gold nanoparticles in past two decades [1–10,16,17] has been accompanied by increasing research effort in designing processes where nanorods are the main or only product. In our brief survey of synthesis methods, we will outline some important results relevant to nanorod synthesis and then describe our own findings.

Yu et al. [155] used electrochemical reduction in the presence of cetyltrimethylammonium bromide (CTAB) in solution to make

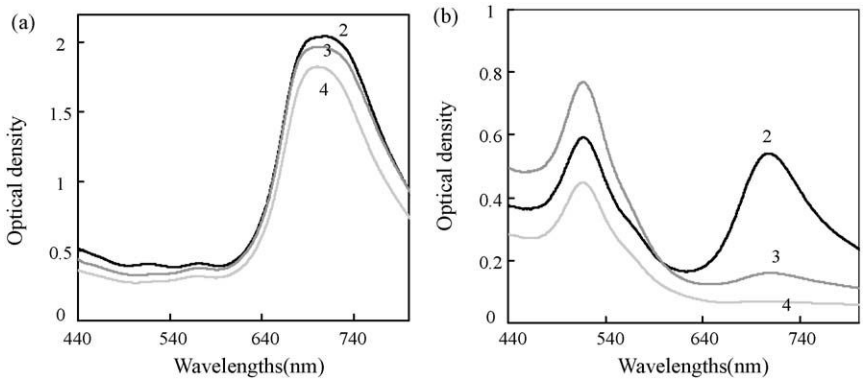

Fig. 12. The polarization spectra of the gold nanorods with L/d = 2.8 dispersed in PVA for various draw ratios indicated on the spectral curves. (a) $\theta = 0^\circ$ and (b) $\theta = 90^\circ$. The numbers on the spectral curves represent the elongation with respect to the original film [125].

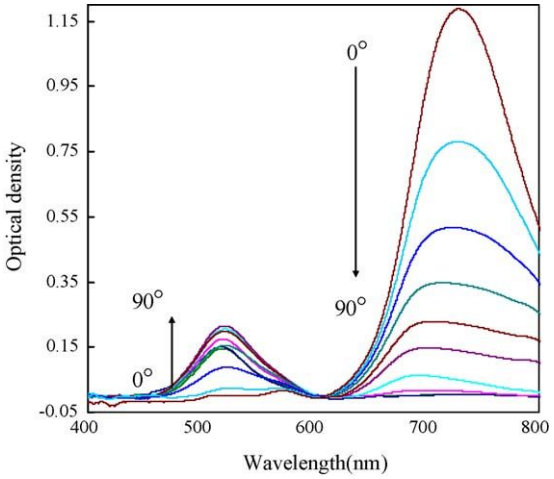

Fig. 13. UV–vis–NIR spectra of PVA/gold nanorods nanocomposites for varying polarization angles. L/d of gold NRs is 2.8 [125].

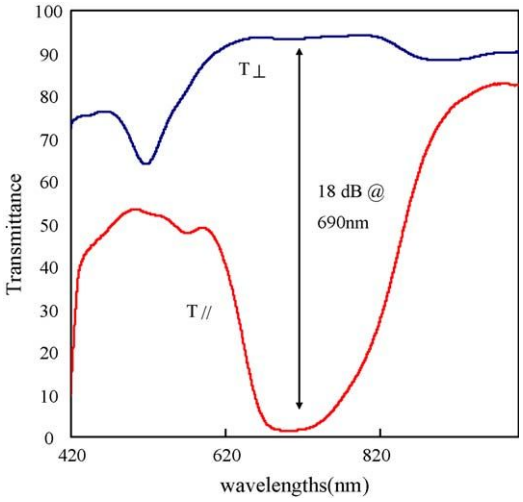

Fig. 15. UV–vis–NIR spectra of PVA/gold nanorods nanocomposites for varying polarization angles. L/d of gold NRs is 2.8 [125].

colloidal sols with nanorods as the major product. Thereafter Jana et al. [156] produced nanorods using seed-mediated method by changing the concentration of surfactant used and by adding $AgNO_3$ to the recipe used for synthesis of nanospheres [157]. The several growth mechanisms [158–161] proposed for single surfactant system concur in stating that CTAB confines the growth direction of gold nanoparticles by adsorbing preferentially on to the specific crystal facet of the growing particle.

Nikoobakht and El-Sayed [162] further modified the seed-mediated method by using a cosurfactant mixture of CTAB and benzyldimethylhexadecylammonium chloride (BDAC) and reported that the use of binary surfactant results in nanorods of fairly good uniformity, higher yield, and yet fewer byproducts. Many researchers have focussed on various aspects of synthesis of gold nanorods [2–7,11,16,163], especially through seed-mediated method [7,156,160–162,164–169]. So we will restrict the remaining discussion to our studies on making gold nanorods and our studies aimed at establishing the growth mechanism in the presence of binary surfactant mixtures.

5.1. Recipe for nanorod synthesis using seed-mediated method with binary surfactant

We modified the seed-mediated method of Nikoobakht and El-Sayed [162] for this study. First the seed solution was prepared by mixing CTAB solution (5.0 ml, 0.20 M) with 5.0 ml of 0.00050 M $HAuCl_4$. 0.60 ml of ice-cold 0.010 M $NaBH_4$ was added to the stirred solution, and this resulted in the formation of a brownish yellow solution. Vigorous stirring of the seed solution was continued for 2 min. After the solution was stirred, it was kept at 25 °C. Thereafter, the growth solution was prepared by mixing 5 ml of the solution at a known concentration of surfactant (CTAB, hexadecyltrimethylammonium chloride (CTAC), BDAC to 5 ml of 0.001 M $HAuCl_4$ solution. 200 μl of 0.0040 M $AgNO_3$ solution was

Fig. 14. Optical micrographs of drawn PVA–gold nanocomposites (4% w/w gold, draw ratio 4): (a) unpolarized, polarization direction, (b) parallel and (c) perpendicular to the drawing direction. Scale bar is 50 μm [125].

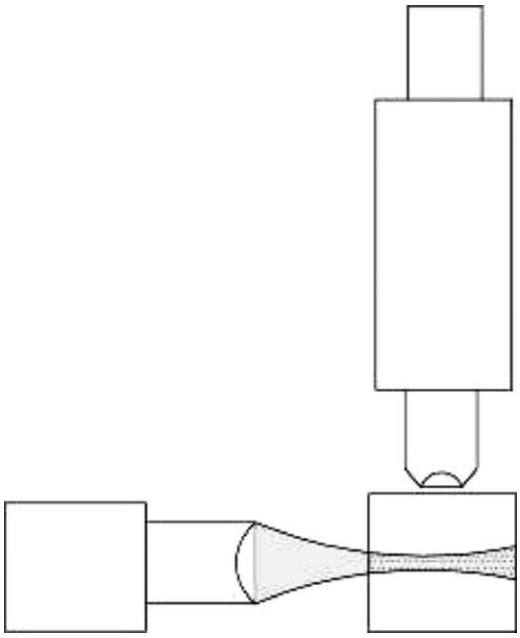

Fig. 16. A simple schematic of Siedentopf–Zsigmondy ultramicroscope, where particle in Faraday–Tyndall cone are visualized using a microscope.

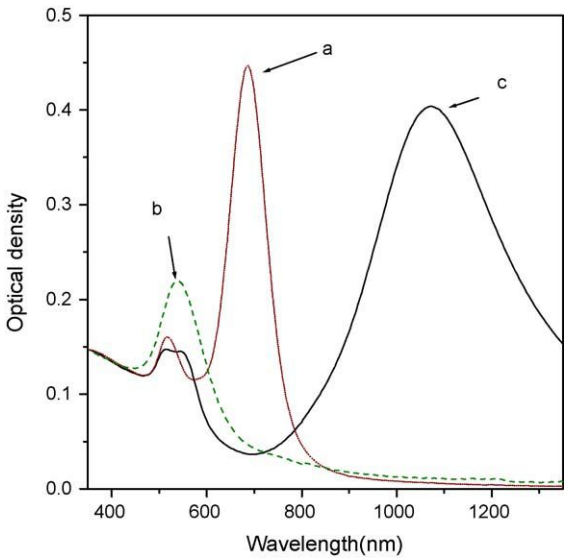

Fig. 18. Influence of the type of surfactant used in growth solution on the aspect ratio of the gold NRs. (a) CTAB (0.1 M), (b) CTAC (0.1 M) and (c) CTAB/BDAC (mixing molar ratio is 1 to 1 and [total surfactant] = 0.2 M) [125].

added to the solution at 25 °C. After gentle mixing of the solution, a known amount of 0.10 M ascorbic acid was added to the test tube. The color of the growth solution changed from dark yellow to colorless (Fig. 17). The final step was the addition of 10 μl of the seed solution to the growth solution. The color of the solution changed over the period of time depending on the final size of the nanorods. The surfactants, CTAB and BDAC, were purchased from TCI America and all the other chemicals ($HAuCl_4$, $AgNO_3$, $NaBH_4$, potassium bromide, hexadecyltrimethylammonium chloride, and L-(+)-ascorbic acid) were purchased from Sigma–Aldrich. All chemicals were of analytical grade (purity > 98%) and were used without further purification. Deionized water (18 MΩ) was used in all the experiments.

5.2. Effect of surfactant 'counter-ion' on morphology of nanoparticles

We first assessed the role of surfactant by synthesizing rods in the presence of CTAB, CTAC and BDAC. In this case, CTAB and CTAC have the same hydrophobic group but different counter ion, Br^- and Cl^- respectively. When CTAB was used, short nanorods (aspect ratio less than 4, Figs. 18a and 19d) were obtained with higher yield. When CTAC was used, only spherical particles were obtained (Figs. 18b and 19a). When CTAB was used with BDAC, larger aspect ratio nanorods were obtained in high yield (Figs. 18c and 19e) However, the spherical nanoparticles that are formed as a byproduct had diameter that is greater than the diameter of the rods, thus resulting in a shallower transverse plasmon peak. It is

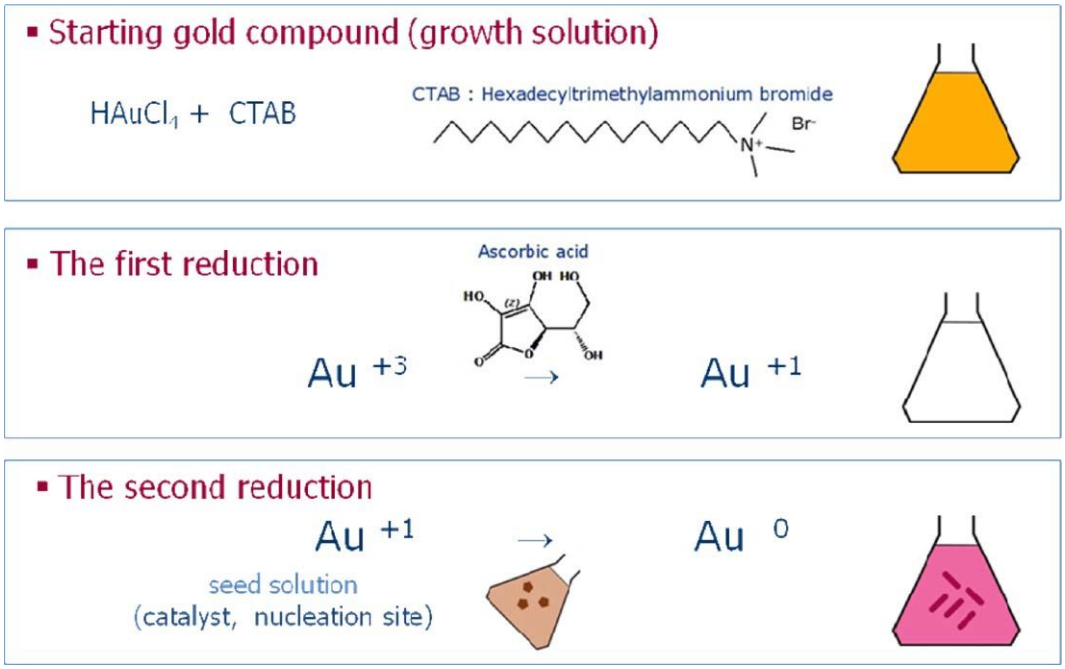

Fig. 17. Schematic of seed-mediated method with CTAB as surfactant and ascorbic acid as the reducing agent.

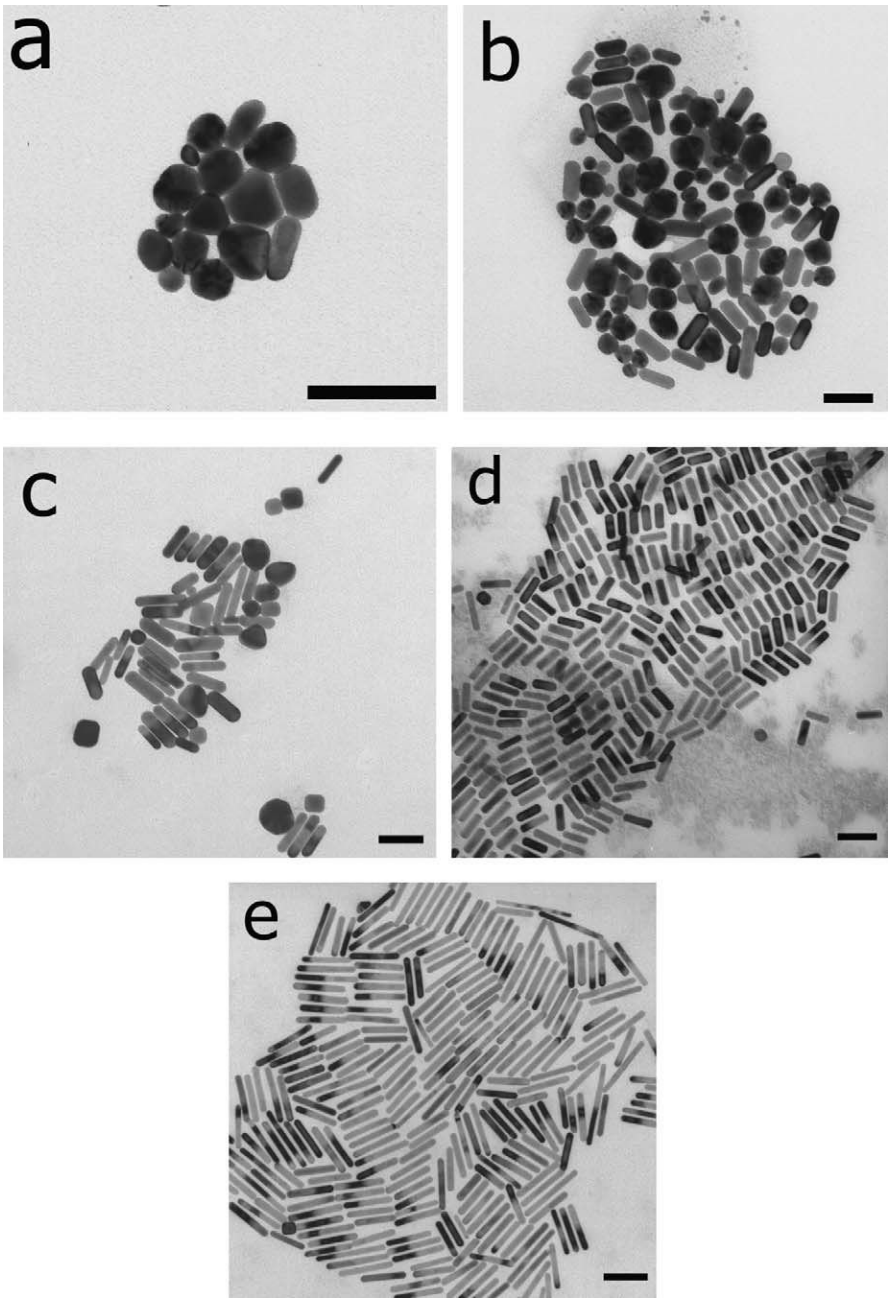

Fig. 19. Influence of the type of surfactant used in growth solution on the morphology of the gold nanorods. (a) CTAC, (b) CTAC + KBr, (c) CTAC + BDAC + KBr, (d) CTAB and (e) CTAB + BDAC. The scale bar is 50 nm [125].

believed that bromide ion forms a complex with other reactants, resulting in change in the size and reactivity of the CTAB on the gold surface, which affects the adsorption of CTAB on the gold surface and hence affects the growth process [162].

Our results underline the importance of Br^-, since CTAC lacks only Br^- compared to the CTAB, and BDAC by itself cannot produce nanorods. The difference in CTAB and CTAC may result from difference in their adsorption behavior. This depends upon attractive electrostatic interactions between the cationic head-group and the anionic surface of growing gold nanoparticles, and bromide ions have a 5-fold greater binding affinity for CTA^+ than that of chloride ions [170–172]. The adsorbed CTAB forms a bilayer on the surface of gold nanorods [173]. Compared to CTAB, the head group of BDAC is bulkier and the counter ion, Cl^- is different. While BDAC by itself cannot produce nanorods, it is believed to facilitate the adsorption of CTAB on the specific surface of gold [162]. We will examine the effect of counter ion in greater detail in the next sub-section, where we remark on our studies on the role of precursor complex.

5.3. The role of binary surfactant and precursor complexes

The color of $HAuCl_4$ solution changes immediately upon adding surfactant solution. Since the resulting color depends on the type of surfactant, we used UV–vis–NIR spectroscopy to examine the characteristics of precursors which form before the reduction begins. Transition metal complexes such as $[PdCl_4]^{2-}$ and $[AuCl_4]^-$ are known to show specific interactions with oppositely charged surfactants [174]. The complex of $[AuCl_4]^-$ and CTAC is reported to form 1:1 stoichiometry complex [175]. Upon mixing $HAuCl_4$ solution to CTAC solution, brilliant yellow-white fine crystals of gold–surfactant complex were produced. Above the critical micelle

concentration (CMC) of CTAC, the complex was solubilized and the solution became clear. Our visual observations indicate that $[AuCl_4]^-$ also interacts with CTAB and the change of color is more pronounced than that of CTAC and $[AuCl_4]^-$ mixture. Upon addition of CTAB to the pale-yellow solution of $HAuCl_4$, orange color precipitate forms. As the concentration of CTAB increases, the precipitate disappears. But in this case the color of the solution becomes orange indicating water-insoluble Au–surfactant complex is solubilized into micelles.

The UV–vis spectrum of $HAuCl_4$ solution shows two peaks at 220 and 300 nm due to the ligand metal charge transfer [176]. When $HAuCl_4$ solution is mixed with CTAB solution, the peaks are shifted to 260 and 380 nm which are very close to the peaks of $[AuBr_4]^-$ as compared in Fig. 20. The change is caused by the change of ligand X in $[AuX_4]^-$ from Cl to Br, since it is easier to oxidize Br than Cl [176]. When we examined the spectral changes that take place on increasing the amount of KBr added to the $HAuCl_4$ solution, the characteristic peaks at 220 and 300 nm shifted gradually to 260 and 380 nm. Thus the net interaction between CTAB and $HAuCl_4$ in aqueous solution results in the formation of [CTA]–$[AuBr_4]$, while CTAC and $[AuCl_4]^-$ form a complex without changing ligand. This organic salt is solubilized by the surfactant micelles to produce "metallomicelles".

$$[AuCl_4]^- + 4CTAB \leftrightarrow CTA{-}[AuBr_4] + 4Cl^- + 3CTA^+$$

So, we are lead to the conclusion that having $[AuBr_4]^-$, instead of $[AuCl_4]^-$ is beneficial to form longer NRs. If metallic species are involved in the formation of solute complexes or compounds, the standard redox potential will be lower since the complex is more stable than the Au ion (Table 2).

Thus, the potential of Au complex is lower than that of Au ion. Furthermore, $[AuBr_4]^-$ has a lower potential compared to $[AuCl_4]^-$ as does $[AuBr_2]^-$ in comparison to $[AuCl_2]^-$. It can be deduced that reduction is harder for the Br complex than Cl complex. In the growth solution, $[AuBr_4]^-$ exists as CTA–$[AuBr_4]^-$ which is expected to be even more stable. This is why a weak reducing agent such as ascorbic acid (AA) cannot reduce the complex to Au atom while AA easily reduces the $[AuCl_4]^-$ to Au atom to produce spherical particles. AA can only reduce $[AuBr_4]^-$ in the metallomicelles to $[AuBr_2]^-$. So the nucleation can be withheld until the seed solution is added. With the catalytic action of the seeds, Au^{1+} ion in the metallomicelle is reduced to Au atom. Therefore the effectiveness of CTAB comes from the formation of Au–Br complex with low redox potential. To demonstrate the effect of Br substitution, KBr was added to the growth solution prepared with CTAC. When KBr was added to CTAC, short rods are obtained in significant fraction (Fig. 19b), confirming that the form of precursor is important in determining the morphology of the particle. Further the binary surfactant system of BDAC/CTAC produces nanorods only if KBr was added. When KBr was added to the system, BDAC was effective to yield longer NRs in higher fraction (Fig. 19c), implying that BDAC as a cosurfactant works well only if the precursor is [CTA]–$[AuBr_4]$ (Fig. 21).

Fig. 19e shows that when BDAC was used along with CTAB it leads to formation of longer nanorods. In earlier studies, this was attributed to a more flexible template made by surfactant mixture and the different affinity of CTAB and BDAC on the facet of growing gold NRs [162]. We decided to see if BDAC has some role even at the precursor stage of growth solution. The precursor in the growth solution of CTAB and BDAC shows the characteristic peaks of $[AuBr_4]^-$ instead of $[AuCl_4]^-$, indicating that CTAB is used for forming precursor (Fig. 22).

As we mentioned before, the addition of surfactant to the $HAuCl_4$ solution produces a visible color change. For a quantitative comparison, we prepared a series of vials containing $HAuCl_4$ at constant concentration and increased the concentration of surfactant successively until the turbidity disappeared. The solutions were sonicated for an hour after which the UV–vis spectra were taken for the change in turbidity monitored by the change of absorbance. The absorbance at 600 nm was chosen because this peak is not related to any of the characteristic peaks of the solution [178]. When the absorbance is plotted as a function of the concentration of surfactant (Fig. 23), it is apparent that the complex is solubilized at a much lower concentration in binary surfactant than in CTAB alone. This result is consistent with the report that in a mixed surfactant system of BDAC and CTAB, the first CMC decreases from 0.001 to 0.0005 M and the second CMC is also dramatically lowered from 0.28 to 0.0014 M over all mixing ratios [170].

Since second CMC is lowered by BDAC, the size of micelle is expected to become even bigger through structural transitions from spherical micelle to rod shaped micelle. Therefore, we reasoned that the bigger micelles accommodate the precursor

Table 2
Standard potentials in aqueous solutions [177].

Half reaction	Standard potential (V)
Au(III)/Au(I)	
$Au^{3+} + 2e^- \rightarrow Au^{1+}$	+1.40
$AuCl_4^- + 2e^- \rightarrow AuCl_2^- + 2Cl^-$	+0.926
$AuBr_4^- + 2e^- \rightarrow AuBr_2^- + 2Br^-$	+0.805
Au(I)/Au(0)	
$Au^+ + e^- \rightarrow Au$	+1.71
$AuCl_2^- + e^- \rightarrow Au + 2Cl^-$	+1.154
$AuBr_2^- + e^- \rightarrow Au + 2Br^-$	+0.962
Ascorbic acid	
$C_6H_6O_6 + 2H^+ + 2e^- \rightarrow C_6H_8O_6$	+0.13

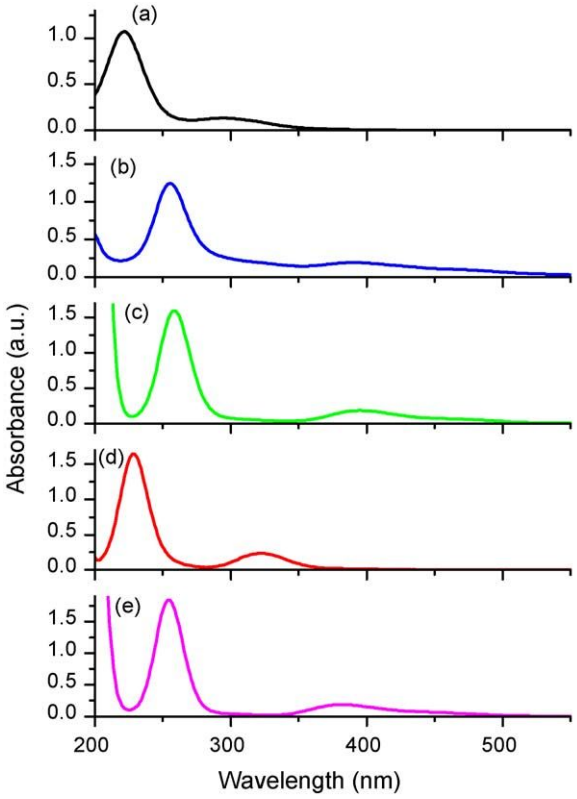

Fig. 20. The spectral change in aqueous solutions of $HAuCl_4$ upon adding different surfactants. $[HAuCl_4] = 5 \times 10^{-4}$ M for all solutions and $[surfactant] = 5 \times 10^{-2}$ M if added (a) $HAuCl_4$, (b) $HAuBr_4$, (c) $HAuCl_4$/CTAB, (d) $HAuCl_4$/CTAC and (e) $HAuCl_4$/KBr (0.05 M) mixture [125].

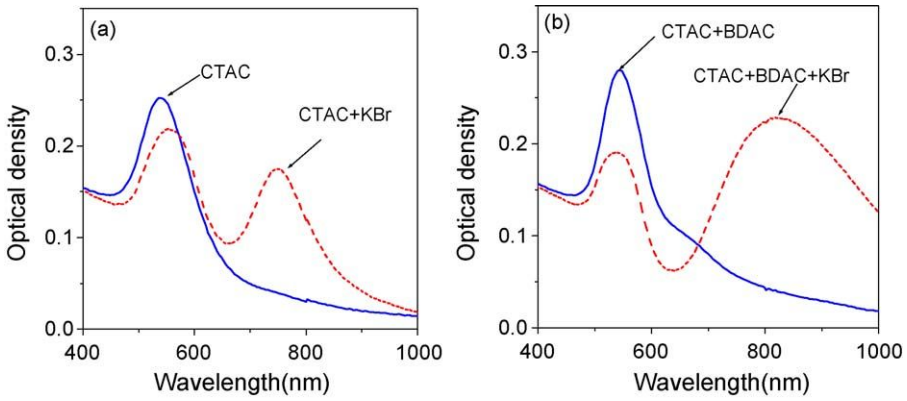

Fig. 21. Influence of the type of surfactant and additive used in growth solution on the aspect ratio and yield of the gold nanorods [125]. The appearance of longitudnal plasmon resonance indicates that gold nanorods are formed.

facilely preventing immediate reduction which may lead to the growth of gold NRs. Thus the role of CTAB in the formation of gold NRs is summarized as follows: (1) it forms a stronger complex with gold salt and slows down the reduction, (2) it protects the Au ion from being instantly reduced by capturing the complex inside the micelle, (3) it adsorbs on the surface of growing nanorods and thus confines the direction of growth, and (4) it acts together with BDAC (for binary mixture has lower first and second CMC) to promote effective formation of metallomicelle.

5.4. Role of ascorbic acid (AA) as a reducing agent

The seed-mediated method helps to separate the nucleation stage from the growth, and thus enables a better control over the final shape and size of the particles. In our method, the growth solution involved the use of ascorbic acid, which is a mild reducing agent. The reduction process of the Au ion by AA can be described as:

First reduction: $Au^{3+} \rightarrow Au^{1+}$

$$CTA{-}AuBr_4 + C_6H_8O_6 \rightarrow CTA{-}AuBr_2 + C_6H_6O_6 + 2H^+ + 2Br^-$$

Second reduction: $Au^{1+} \rightarrow Au^0$

$$2CTA{-}AuBr_2 + C_6H_8O_6 \rightarrow 2Au + C_6H_6O_6 + 2CTA^+ + 2H^+ + 4Br^-$$

The first reduction is confined in the metallomicelles. The second reduction only begins after the seed solution is added. The overall reaction is

$$2CTA{-}AuBr_4 + 3C_6H_8O_6 \rightarrow 2Au + 3C_6H_6O_6 + 2CTA^+ + 6H^+ + 8Br^-$$

The stoichiometry of this reduction reaction can be calculated by considering the ionization of ascorbic acid and pH of the growth solution (p*Ka* of ascorbic acid = 4.17, pH of the growth solution during the synthesis = 3.15–3.3). That turns out to be 1.6. So for complete reduction, molar ratio should be greater than 1.6. We studied the effect of the concentration of AA on the growth of nanorods. In particular, we investigated how the reduction rate affects the morphology of nanorods. In a related study, the length of the rod (and aspect ratio) was found to be larger when the molar ratio was smaller [167] but to draw any general conclusions, we must keep the other reaction conditions (such as the addition of $AgNO_3$) the same. The molar ratio of AA to Au ion was changed from 1 (which is the ratio required to reduce Au^{3+} to Au^{1+}) to 1.9.

When the molar ratio of AA to Au was 1, no NPs were obtained. As the molar ratio increased from 1.1 to 1.9, the absorbance at the peaks increased indicating higher yield of particles. As the molar ratio

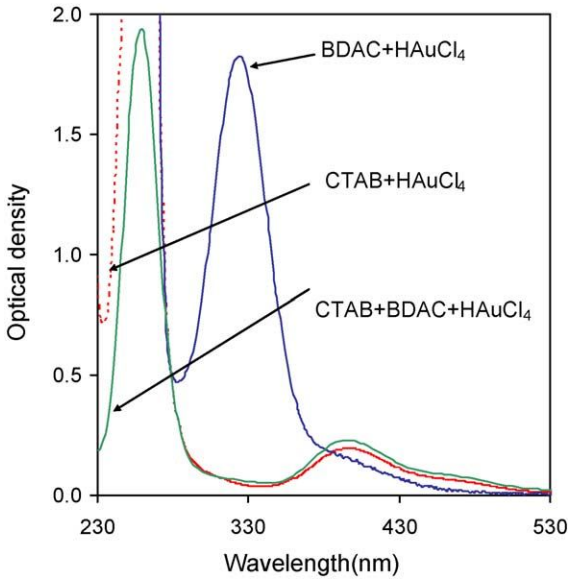

Fig. 22. The spectral change in aqueous solutions of $HAuCl_4$ upon adding different surfactant. $[HAuCl_4] = 5 \times 10^{-4}$ M for all solutions and [surfactant] = 5×10^{-2} M [125].

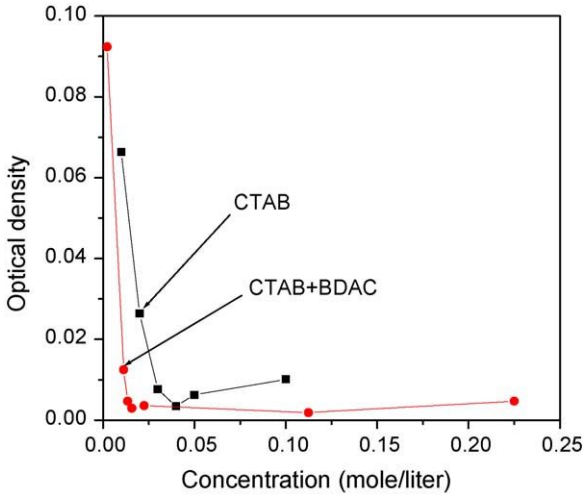

Fig. 23. Change of the absorbance of the surfactant–$HAuCl_4$ mixture solution at 600 nm as a function of total surfactant concentration. The concentration of $HAuCl_4$ was fixed at 5×10^{-4} M [125].

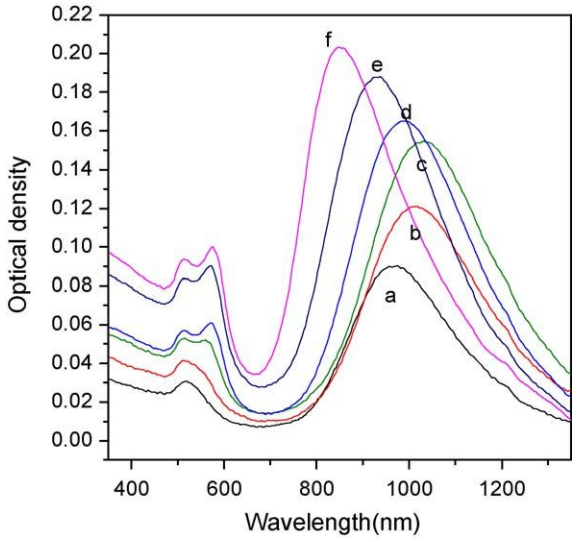

Fig. 24. UV–vis–NIR spectra of 6 identical growth solutions in which the ascorbic acid contents increased from (a) to (f). The ratio of AA:Au ion was (a) 1.1, (b) 1.2, (c) 1.3, (d) 1.4, (e) 1.5 and (f) 1.6. The spectra were taken from the as-made solutions after the growth was ended (measured in 1 mm path quartz cell) [125].

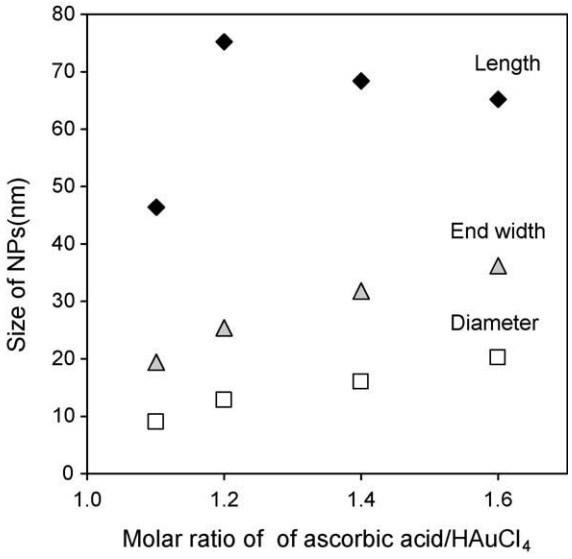

Fig. 26. The change in size of gold NR by varying the molar ratio of AA to Au ion [125].

increased from 1.1 to 1.3, longitudinal plasmon peak shifts to longer wavelength but upon further increasing the molar ratio, LSP shifted back to shorter wavelength (Fig. 24). As it can be seen in the TEM images (Fig. 25), the initial red-shift can be related to the apparent increase in the length of NR, thus resulting in an apparent increase in the aspect ratio. When the growth rate of the diameter is faster than the growth rate along the long axis, the apparent aspect ratio is lower. When the molar ratio was greater than 1.6, the shape of nanorods was no longer a spherocylinder. The growth in diameter direction was greatest at the ends and progressively slower towards the center, giving a taper shape as shown in Fig. 25c.

The reduction rate depends on the concentration of the reducing agent. As the amount of AA increases, the reduction becomes faster. As a result, the reduction takes place before the surfactants confine the growth direction (Fig. 26). The formation of taper shaped nanorods implies that the adsorption of surfactant competes against the reduction of gold precursor on the same surface of nanorods.

5.5. Effect of temperature on growth

Since temperature affects the reduction rate, and hence the morphology of gold nanorods, we varied the temperature of the reaction bath while all other experimental conditions were kept the same. TEM images of gold nanorods grown at different temperatures between 20 and 50 °C are shown in Fig. 27. The aspect ratio increased from 3 to 6 as temperature was decreased. It is worth noting that this increasing aspect ratio is due to decreasing diameter of the nanorods as shown in Table 3. The decreasing diameter of the nanorods can be ascribed to the effective confinement of the growth in diameter direction at low temperature which renders low reduction rate.

5.6. The role of supersaturation in producing monodisperse sols

We have shown that the morphology of gold nanorods can be controlled by manipulating the reduction rate and the adsorption kinetics of the surfactant in binary surfactant system. The choice of

Table 3
Longitudinal plasmon resonance peak maximum (λ_{max}) as a function of length, diameter and aspect ratio of gold NRs synthesized at different temperature.

Temperature (°C)	λ_{max} (nm)	Average length (nm)	Average diameter (nm)	Aspect ratio
20	954	46.8	7.9	6.0
30	732	53.4	10.0	5.6
50	1020	40.7	12.6	3.3

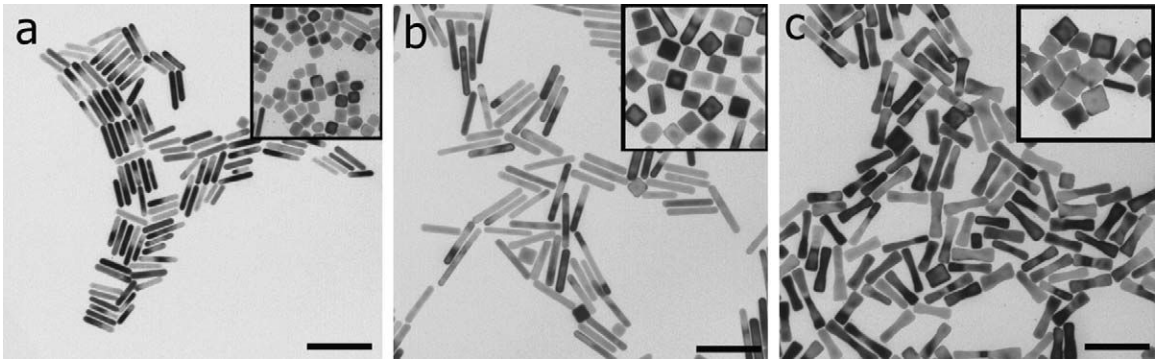

Fig. 25. Changing morphology of NRs by varying the molar ratio of AA to Au ion: (a) 1.1, (b) 1.3 and (c) 1.6 (Insets show the NCs as a byproduct from the same solution.). Scale bar is 100 nm [125].

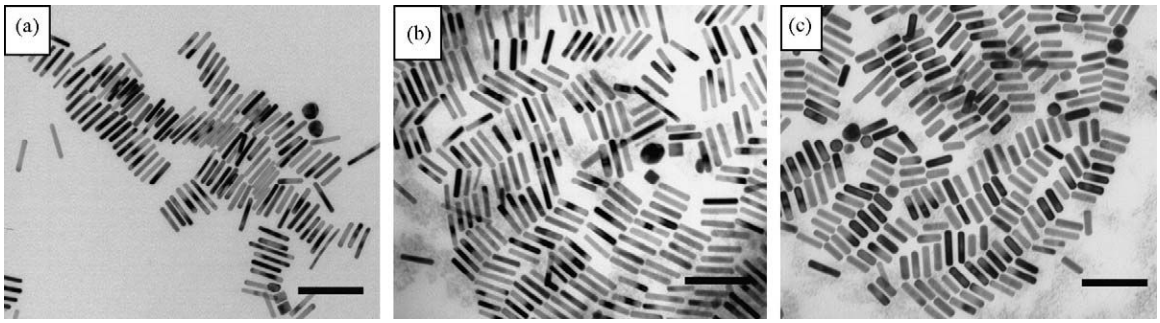

Fig. 27. Changing morphology of nanorods by varying the temperature of reaction bath: (a) 20 °C, (b) 30 °C and (c) 50 °C. All other experimental parameters are the same. The scale bar is 100 nm [125].

surfactant is important not only because of its adsorption on the surface of growing particles but also because the precursor of gold–surfactant complex has significant influence on determining ΔE of reduction reaction. Our results show that the adsorption competes against the reduction of Au ion on the same surface of nanorods and when the reduction rate is slowed down say by decreasing temperature of the reaction bath, nanorods with higher aspect ratio and smaller diameter are obtained. Before we end our discussion of seed-mediated synthesis, we must remark on how and why the control of supersaturation, through control of reactant concentrations, can not only separate the nucleation and growth steps, but thereby provide us with means of controlling size dispersity in the as-made nanoparticle dispersion. The argument at present is qualitative, but is known to produce monodisperse sols in a variety of colloidal dispersions [109] and in other condensation growth processes, such as formation of drops in the atmosphere [179].

The nucleation of particles in a solution requires a certain critical concentration or solubility product to be exceeded, before it becomes thermodynamically favorable for the nuclei to appear. In the seed-mediated method, this is accomplished in the first bath, where the addition of reactants creates the required concentration, such that nuclei are formed in a single burst, and this causes the concentration to drop below the critical value. In the second bath, the growth of nanoparticles can be accomplished by providing just enough reactants such that growth of existing particles is favored, where new nuclei cannot be formed (Fig. 28). As long as concentration is kept within these limits, and Ostwald ripening and coalescence are ruled out, the condensation growth can proceed to give monodisperse sols. The determination of solubility product in a reaction bath consisting of seed solution, binary surfactant, reducing agents, and other additives is thus the crucial ingredient in progressing towards controlled synthesis. The parameters including pH, temperature and ionic content affect colloidal stability and phase behavior of surfactants as well, and thus their role in controlling morphology and polydispersity of as-produced particles is a realm of endless possibilities. Since current methods produce dispersions that are relatively polydisperse in shape and size, we will discuss the use of centrifugation assisted separation in next section of the review.

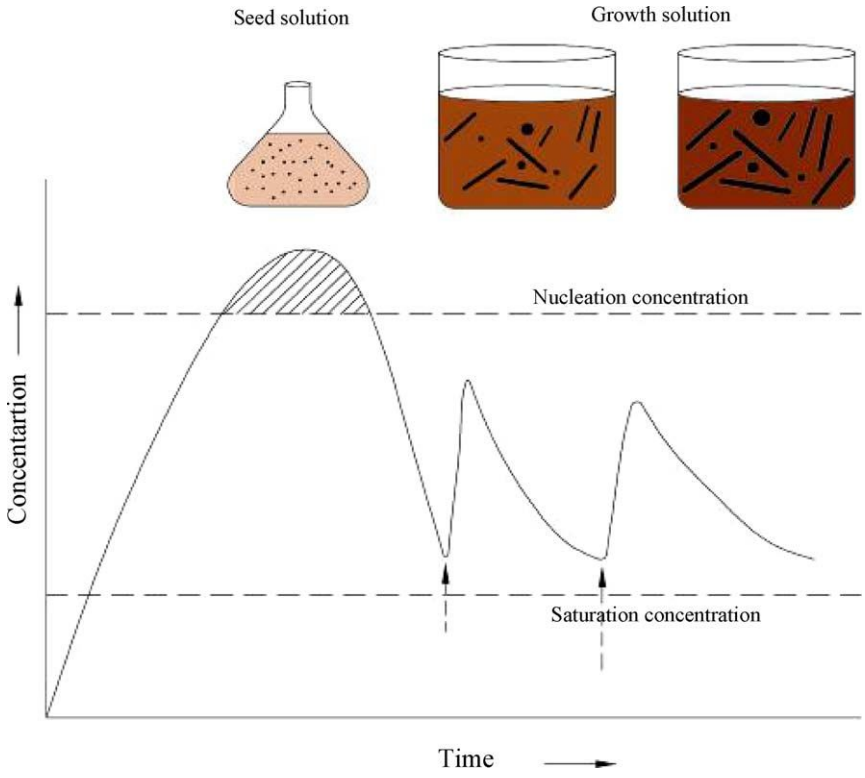

Fig. 28. Nucleation and growth during seed-mediated method. The threshold concentrations for nucleation and saturation are shown with dotted lines. Nucleation (dashed region) creates seed solution. Growth is carried out in separate steps by controlled addition of reactants.

6. Shape separation of colloidal gold nanorods

In the previous section, we mentioned that nanoparticle synthesis by typical condensation from solution methods is characterized by a polydispersity in shape and size. As we know, the physical and chemical properties as well as the applications of nanoparticles are controlled and limited by their dimensions and shape, which implies that it is highly desirable to produce nanoparticles with well-defined and controlled size and shape. While great strides have been made in optimizing conditions and parameters during synthesis, there is a definite need for shape and size selective separation methods. Conventionally spherical colloidal particles have been separated based on their hydrodynamic behavior using sedimentation, flocculation, electrophoresis or centrifugation [24,94,180]. We have demonstrated how shape dependent hydrodynamics can be used to predict the centrifugation assisted sedimentation behavior of rods and spheres, and used it successfully to shape separate rods and spheres as well as rod-like nanoparticles with different aspect ratio [98]. In what follows, we will present a short summary of theoretical arguments advanced by us and related experiments elucidating how this shape separation is accomplished.

6.1. Theoretical aspects of sedimentation of rods and spheres

First we consider a simple phenomenological analysis of forces acting on a Brownian particle placed in a centrifuge. The forces acting on the particle include centrifugal force, $F_c = \omega^2 rm$, buoyant force, $F_b = -\omega^2 rm_0$, Brownian fluctuating force, F_f and viscous drag force, $F_d = -\zeta v$, where ω is the rpm, m the mass of the particle, m_0 the mass displaced by the particle, r the distance from the center to the location of particle, v the sedimentation velocity and ζ is the friction or drag coefficient. The balance of these forces leads to the Langevin equation of a particle undergoing Brownian motion under the influence of an external force. At equilibrium, $F_{total} = F_d + F_b + F_c + F_f = 0$ implies $\omega^2 r(m - m_0) - \zeta v = 0$. This yields the Svedberg coefficient, $S = v/\omega^2 r = (m - m_o)/\zeta$, which expresses the sedimentation velocity normalized by the applied angular acceleration. Svedberg coefficient is a measure of sedimentation rate and depends upon the ratio of effective mass, and friction factor [22,24].

The relative importance of thermal diffusion and flow is judged by a dimensionless number called the Peclet number, *Pe* which for typical Brownian nanosphere is $Pe = /D = (m - m_0)\omega^2 ra/k_B T < 1$, where a is the radius of the sphere and D is the thermal diffusivity, implying that the thermal fluctuations are non-negligible. This distinguishes nanoparticle sedimentation theories from the theories applied to macroscopic falling objects [181].

In the context of our earlier description of the barometric number distribution of colloidal particles with height, we note here that qualitatively the only thing different in our case is the presence of centrifugal field, which essentially acts like a much stronger gravitational field. So the expression for Svedberg coefficient can also be written as $S = v/g_{eff} = m_{eff}/\zeta$, emphasizing that essentially we are still dealing with sedimentation behavior, and the use of centrifugation allows us to overcome the $k_B T$ forces and distribute particles of effective mass according to effectively a greater "gravitational" force. Since $g_{eff} \gg g$, the centrifugation-assisted sedimentation is much faster, and when the sedimentation–diffusion equilibrium is reached, the average height $\langle h_{eff} \rangle$ for colloidal particles is of course diminished (see Section 3). Let us for now focus on the determination of Svedberg coefficient (which is simply renormalized sedimentation velocity).

We basically need a shape dependent computation of the effective mass, and of friction factor, ζ so that a comparison of sedimentation rates of rods to that for spheres can be made. The expression for friction coefficient depends upon another dimensionless number, the Reynolds number, *Re* and $Re \ll 1$ for the typical sedimentation problems in nanoscale. Reynolds number, $Re = \rho UL/\eta$ where η represents the viscosity, ρ represents the density of the fluid, U represents the characteristic speed and L the characteristic length, represents the ratio of characteristic magnitudes of inertial and viscous forces. Being in low Reynolds number regime implies that the inertial effects are negligible and the Stokes or creeping flow equations apply. Drag on a Stokesian sphere is $6\pi\eta aU$, implying a friction coefficient, $\zeta = 6\pi\eta a$ and this yields us with a Svedberg coefficient of $S^{sph} = 2(\rho - \rho_0)a^2/9\eta$. In fact, the friction coefficients are similar for spherically isotropic objects, i.e. all regular polyhedra and bodies derived from them by symmetrically cutting or rounding off the corners, edges and/or faces [182].

On the other hand, for anisotropic bodies both force and torque balance is required, and coupling of translation and rotation needs to be considered. Translational friction coefficient of a falling single rod depends on the orientation of rod, and friction felt parallel to the rod is 1/2 that of the transverse falling rods, i.e. $\zeta_\perp = 2\zeta_{||}$ [93,180,182]. Using the expressions of friction coefficient, and mass of the rods, we derive the Svedberg coefficient for rods to be $S_0^{rod} = (\rho - \rho_0)D^2[2\ln(L/D) - (\upsilon_\perp + \upsilon_{//})]/24\eta_0$, where $\upsilon_\perp$ and $\upsilon_{||}$ are the correction factors of the rod perpendicular or parallel to the rods orientation, respectively. Relative sedimentation behavior of colloidal rods and spheres can be described by the ratio of the sedimentation coefficients between rods and spheres. The ratio $s_0^{rod}/s_0^{sph} = v_0^{rod}/v_0^{sph} = \lambda_0 = 6(d/2a)^2[\ln(L/d) + (\upsilon_\perp + \upsilon_{//})]$ for single rod and single sphere allows us to see that for this case *the central role in separation is played by the ratio of the squares of diameters of the rod and sphere* [98]. For a given L/d, whether the rods or spheres sediment faster is mainly controlled by the relative diameters of the particles, and since the aspect ratio dependence enters through the logarithmic term, the effect is much less dramatic than the effect of the diameters. While the effective weight of the rod might be more than that of sphere, the overall sedimentation velocity could still be lower.

The physics and use of centrifugation for separating spherical colloidal particles is well documented [20,22–24,29,94,180,182,183] and it is easy to see that relative sedimentation velocity of spheres of same material (effective density) is simply equal to the square of ratio of their diameters. Also we note that for two rods, with different aspect ratios, again the critical parameter will be the ratio of their diameters, for effect of length or aspect ratio is again in logarithmic term.

$$\frac{S_{0(1)}^{rod}}{S_{0(2)}^{rod}} = \left(\frac{d_{(1)}^2}{d_{(2)}^2}\right) \times \frac{2\ln(L/d)_{(1)} - (\upsilon_\perp + \upsilon_{//})}{2\ln(L/d)_{(2)} - (\upsilon_\perp + \upsilon_{//})}$$

The above relationships are derived using single rod and single sphere sedimentation behavior. As the concentration of the particles increase, their hydrodynamic behavior starts to get affected by the flow field of each other, and the correction for this appears in form of "hydrodynamic interaction" term [94,184–186]. The detailed analysis which includes effect of hydrodynamic interaction as well as the concentration profile expected for centrifugation-assisted sedimentation is discussed in our paper about shape separation of gold nanorods using centrifugation [98]. It must be mentioned however that the sedimentation diffusion equilibrium was used by early practitioners of ultracentrifugation (Rinde, Westgern, and Svedberg) to determine the size and size distribution of gold sols [23], which typically comprised of spherical nanoparticles. We expect that a similar determination for rod-like gold particles will be equally useful. In what follows, we will limit the discussion to the examples from our research, where we show how our hydrodynamic arguments about relative

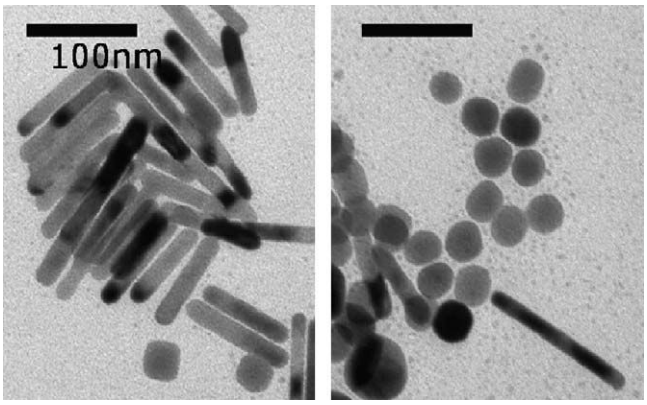

Fig. 29. TEM image of mother colloidal sol. L/d of gold NRs is 7.3 [125].

sedimentation velocity can be employed to obtain nanorods of greater purity, viz. lower size and shape dispersity.

6.2. Separation of nanorods from spherical nanoparticles using centrifugation

As-made dispersions of nanorods were centrifuged at 5600 G for 20–40 min (Jouan centrifuge MR23i, fixed angle rotor). After centrifugation was stopped, the tube was taken and visibly inspected. Fig. 29 shows the TEM image taken from the mother dispersion showing the mixture of rods and spherical particles. The average diameter of the spherical particles is 16.59 nm while the average diameter of NRs is 8.06 nm. The average length of NR is 58.54 nm. Hence, the aspect ratio is 7.3. The fraction of spherical particles is less than 10% (counting 700 particles). Fig. 30 shows the UV–vis–NIR spectrum of the as-made mother solution.

The centrifuge tube upon centrifugation is schematically illustrated in Fig. 31. The color of sols taken from the bottom and the side wall of the centrifuge tube is distinctively different indicating that the particles deposited in different sites have different optical properties, and hence are different in the size or shape or both.

The UV–vis–NIR spectrum of the sol of the side wall shows intense longitudinal surface plasmon peak red-shifted from the mother sol and very tiny transverse plasmon peak indicating that it contains mostly nanorods and the aspect ratio is larger than that of the mother sol. The spectrum of the sol prepared by redipersing particles from the bottom shows broad transverse plasmon resonance peak with high intensity indicating that it contains spherical particles and nanorods. The longitudinal plasmon peak of this sol is blue shifted from the mother sol indicating that the

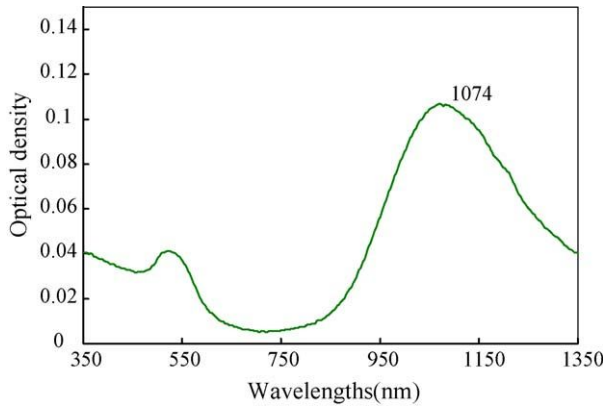

Fig. 30. UV–vis–NIR spectrum of mother colloidal sol. L/d of the gold NRs is 7.3 [98].

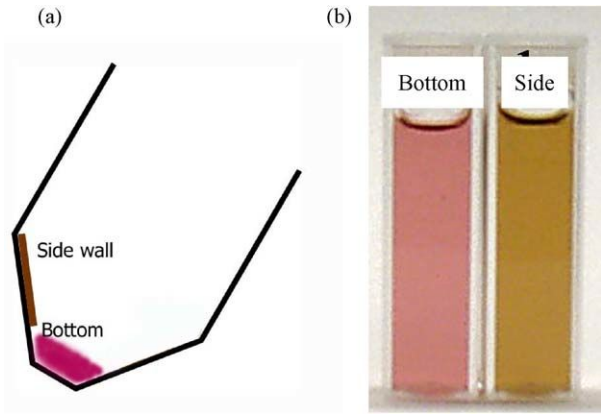

Fig. 31. (a) Schematic drawing of the centrifuge tube after the centrifugation and the color of resulting sols. (b) The color of the sols taken from two different locations shown in (a) [98].

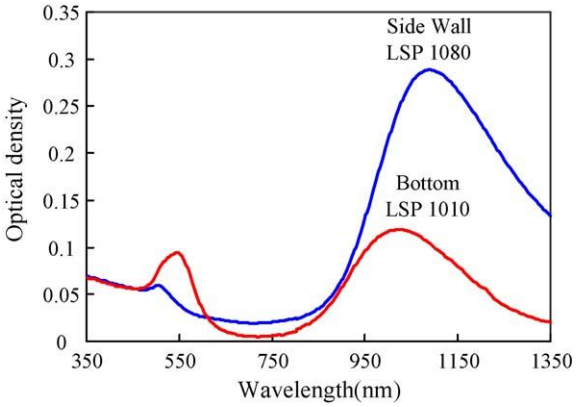

Fig. 32. UV–vis–NIR spectrum of separated sols of deposit on the side of the tube and deposit at the bottom [98].

aspect ratio of nanorods is smaller than those of mother sol (Fig. 32).

The size of the particles in these two sols was measured by TEM (counting 500 particles from each sol). TEM images (Fig. 33) show that the separation of nanorods was successfully accomplished using the described centrifugation conditions. The dispersion made from the bottom deposit contains lots of spherical particles, while the dispersion from the side wall contains mostly NRs. In the as-made dispersion of colloidal gold, the average diameter of spherical particles was almost twice as large as of the diameter of NRs, implying that the ratio $s_0^{rod}/s_0^{sph} = v_0^{rod}/v_0^{sph} = \lambda_o << 1$ (average diameter of sphere is 16.6 nm) and therefore, in this case the spherical particles sediment faster than the nanorods. The nanorods that segregated to the side wall have longer length and smaller diameter (higher aspect ratio) than the mother dispersion. Shorter and fatter NRs were found to dominate the dispersion made from nanoparticles deposited at the bottom (Table 4).

Yield of nanorods can be calculated based on the amount of sol and the intensity of the UV–vis–NIR absorption peak. Through a single centrifugation, the yield was 20–60% depending on the

Table 4
The size of nanorods before and after the separation (unit: nm).

	L	D	L/D
Mother	58.54	8.06	7.30
Separated	65.73	7.87	8.35

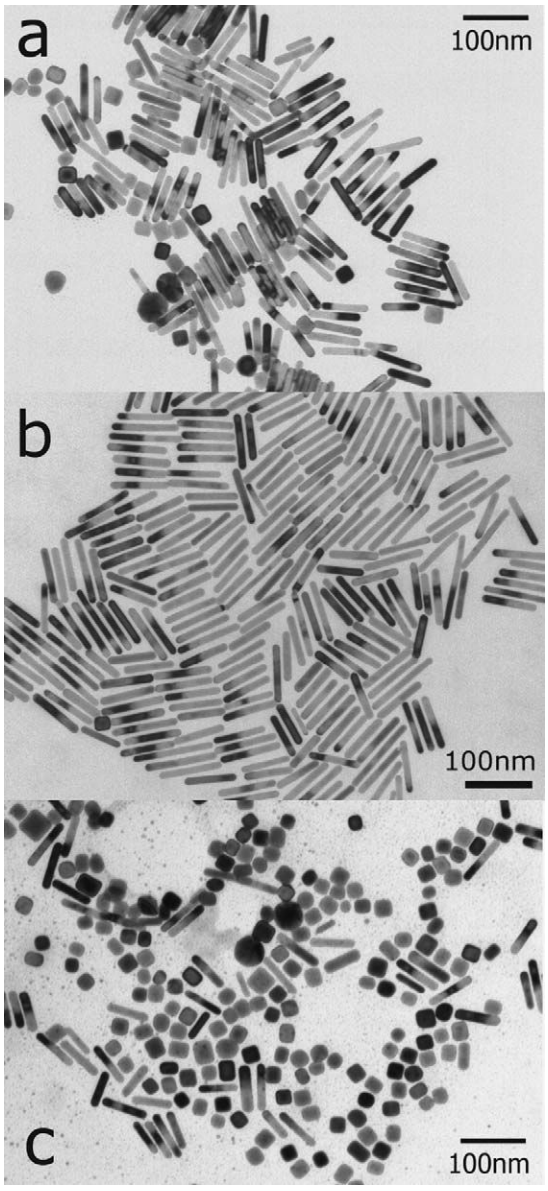

Fig. 33. TEM images of gold nanoparticles: (a) mother sol, (b) after centrifugation, nanorods deposited on the side of the tube and (c) after centrifugation, sedimented at the bottom; nanocubes, spheres and nanorods with larger diameter [98].

property of as-made sol such as the fraction of nanospheres and the relative dimensions of the dispersed particles. The yield can be increased up to 70–80% by repeated centrifugation of the supernatant sol. But if centrifugation is repeated more than 3 times irreversible precipitation of nanorods occurs.

6.3. Separation of nanorods with different aspect ratio

Dispersion of nearly pure nanorods was centrifuged. The centrifuge was stopped every 10 min and the deposit at the bottom was taken. Fig. 34 shows the UV–vis–NIR spectra of the centrifuged sample as a function of time. By the red-shift of longitudinal plasmon peak (as well as blue-shift of the transverse peak), it is apparent that the aspect ratio of the nanorods obtained at different times becomes longer as a function of time indicating longer nanorods sediment later then the shorter nanorods. Also the shape of peak due to transverse plasmon resonance changes as a function of time. The sol obtained earlier has a broad shoulder and it become suppressed towards the later stage.

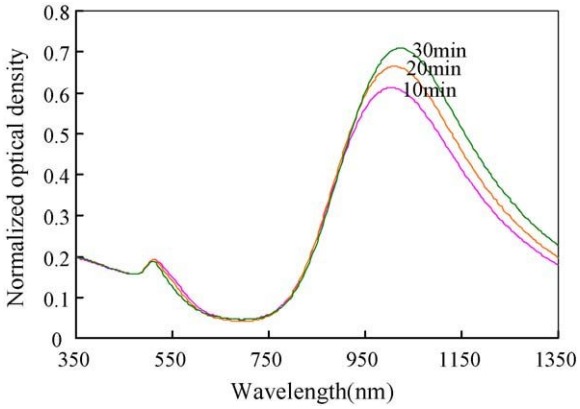

Fig. 34. The UV–vis–NIR spectra of the centrifuged sample as a function of time [125].

In our synthesis, generally longer nanorods have smaller diameter, as shown in Fig. 35. The result that nanorods having larger diameter, sediment faster than nanorods with thinner diameter (albeit a large aspect ratio) agrees with the theoretical prediction that the sedimentation behavior of nanorods depends more strongly on the diameter of nanorods than on their total weight or aspect ratio. Again the key factor for the sedimentation is the ratio of Svedberg coefficients of the nanorods.

In this context, we tried to repeat the protocol reported by Jana [187] as "surfactant assisted separation of nanorods" from a concentrated dispersion, where he emphasizes that nanorods preferentially precipitated by the formation of liquid crystalline phase. While it is plausible that increasing surfactant concentration can induce phase separation in a mixture of rods and spheres, the typical as-made dispersions, as well as the denser dispersions obtained after centrifugation have extremely low volume fraction of rods, thus precluding the formation of liquid crystalline phase. The increase in surfactant concentration was found to increase the yield of nanorods in the shape separation affected by centrifugation [125]. This is perhaps related to the effect of changing ionic content that is known to affect the sedimentation behavior of colloidal dispersions containing charged or interacting particles [188–191]. The effect of dissolved surfactant and of particle shape and size can be critically examined only by conducting a thorough study of how interparticle forces act together with Brownian motion in determining sedimentation equilibrium, electrophoretic mobility and coagulation behavior. The phase behavior of nanorods is richer than spherical particles and the concentrated dispersions of rods can transition to liquid crystalline phases. The

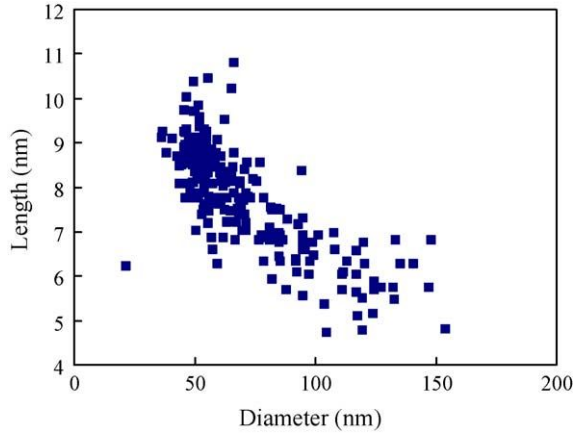

Fig. 35. The plot of diameter and length of the nanorods [125].

theoretical and experimental aspects of the formation of liquid crystalline phase will be discussed in the next section.

7. Self-assembly of rod-like nanoparticles

Self-assembly has emerged as one of the most significant paradigms for fabricating devices for applications in nanotechnology [192–196]. The possible sub-micron structures encompasses the whole spectrum of possible morphologies emerging from drying mediated aggregation [197–200] or crystallization of colloids [201–215], microphase separation of block copolymers [216–218], self-assembled monolayers [219–221], phase behavior of amphiphilic molecules [222–224], breath figure templated assembly to make holey films [225–228] among others. Additionally rich complexity of non-equilibrium patterns can be derived by interplay of different external fields and inherent phase possibilities [196,229]. Qualitative understanding of these structures can be guided by our understanding of the analogies derived from various realms of condensed matter physics [96,196,229–231]. The process and outcome of self-assembly is controlled by the size and shape of the moieties, their interaction and packing behavior, and surface and hydrodynamic forces they encounter. While self-assembly provides a way of bottom up fabrication, it also presents a range of fundamental scientific problems. Various researchers have explored the realm of self-assembly of spherical or spherically isotropic nanoparticles as a viable means of organizing them into useful lattice structure [2,136,200–213,232–237].

In the present section, we explore the exciting opportunities present in the self-assembly of rod-like nanoparticles, where self-assembled patterns contain treasures of knowledge about their drying mediated aggregation and as well as their liquid crystalline behavior prior to drying. We have looked at pattern formation during drying of colloidal dispersions of gold nanoparticles on glass substrate using optical microscopy, and on assemblies formed on a TEM grid, and we will discuss the consequences of shape anisotropy and influence on other factors that control the observed behavior.

7.1. Lyotropic liquid crystals from inorganic colloidal particles

Rod-like nanoparticles are particularly interesting because anisotropy in shape provides them access to order at lower concentrations. Just like spherical colloids are considered good model systems for comparison with hard sphere fluids [95,238,239], rod-like nanoparticles can be thought of model systems for comparison with hard rod fluids [240–242]. The rods are randomly aligned in an isotropic phase, on increasing concentration they demonstrate an increasing amount of long range orientation order, forming a nematic phase. This long range order of the nematic is described by a unit vector **n**, known as the director. Assuming that the liquid crystal consists of a distribution of cylindrically symmetric rods oriented preferentially along the director, the scalar order parameter, S for a three-dimensional system is given by $S = (1/2)\langle 3\cos^2\theta - 1\rangle$. Here θ is the angle between the long axis of rods and the director, **n**. The angular brackets show that the order parameter is a statistical or ensemble average quantity. The order parameter is 0 for random orientation, and equals 1 for a perfectly parallel alignment and typically has a value between these limits. The distribution function that represents the orientation of the rods in the system and the corresponding order parameter can be measured using various experimental techniques and the related anisotropic physical response measured or calculated using theory and experiments [243–245]. At still higher densities, sometimes rods organize themselves into smectic order, such that rods lie in layers, though layers themselves are no thicker than the rods, and this stratified structure possesses both higher positional and orientational order. The rods can also form a crystalline structure, and the transition from one phase to another is characterized by differences in their physical properties (manifested in textures in microscope, flow viscosity and difference in X-ray scattering, etc.) [243–245]. Our approach to understand their self-assembly stems from the marriage of two exciting fields: the assembly of colloidal (spherical) particles [2,136,200–213,232–237] and the physics of lyotropic liquid crystals [108,240–247] (Fig. 36).

While the first lyotropic liquid crystals based on V_2O_5 were reported by Zocher in 1925 [248], synthesis and assembly of inorganic nanoparticle based liquid crystal assemblies has seen resurgent interest in last few years, mainly through seminal work by Davidson and co-workers [107,108,248–258] and from Lekkerkerker and collaborators [259–271]. Ever since the first report about lyotropic phases formed by tobacco mosaic virus (TMV) appeared in 1936 [105], the major experimental studies on lyotropic liquid crystals have relied on studies with TMV and fd-virus. Much of the recent work on phase behavior of viruses and mixtures of rods of different dimension or mixtures of spheres and rods has come from Fraden and co-workers [272–279]. Interestingly, Onsager [106] was trying to explain the formation of anisotropic phases by TMV when he pointed out that beyond a certain concentration of rods, there is a net increase in entropy on transition from isotropic to nematic phase. While the rotational entropy is maximized by having random orientation distribution of rods, the translational entropy is maximized by having smallest free volume or largest translational motion per unit rod. At high enough concentrations, the loss in rotational entropy is more than compensated by a gain in translational entropy, due to the lower excluded volume required in a nematic phase (Fig. 37).

Since Onsager's theory [99,106] is based only on two particle interaction, it is exact only for aspect ratios of hundred or higher.

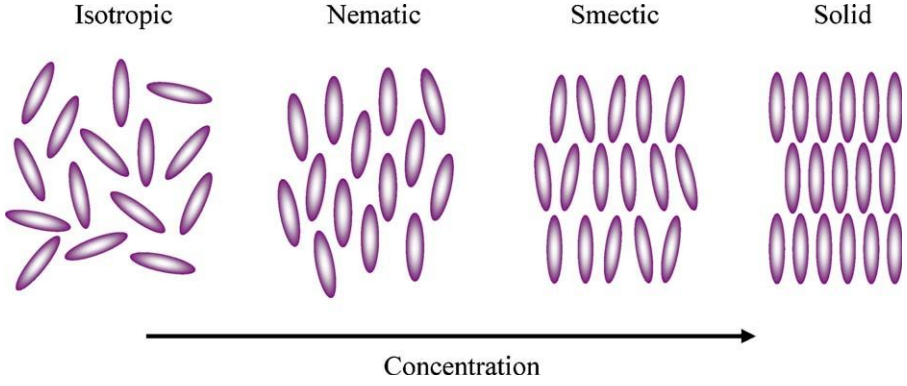

Fig. 36. Phase transition of lyotropic liquid crystals.

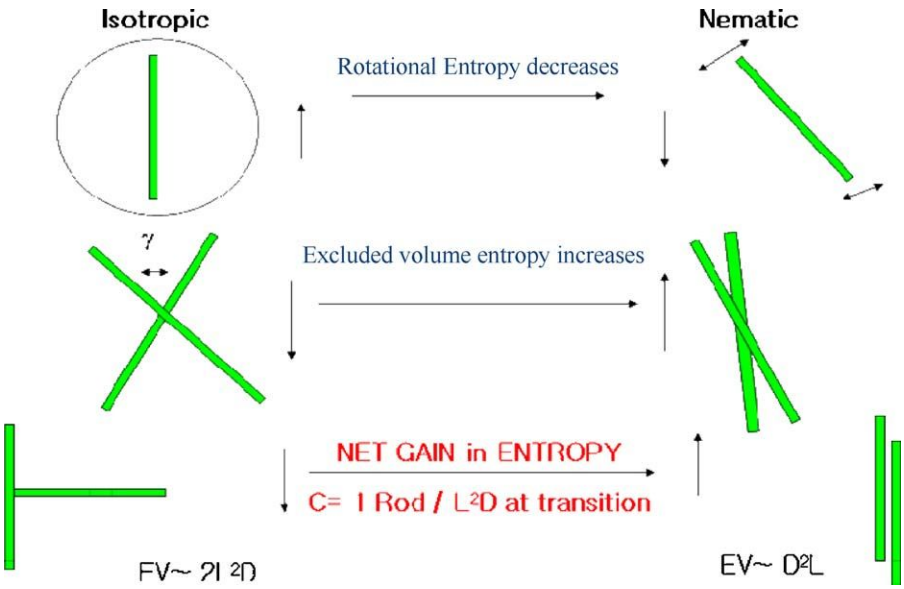

Fig. 37. Onsager theory [106]: How phase transition is driven by a net gain in entropy.

For lower aspect ratios generally found in rod-like nanoparticles, one must account for multi-particle interactions, and this requires extension of theory as done by Lee and Meyer [280,281] or by the use of excellent simulations from Frenkel and co-workers [240,241,282–290]. The relevant extensions to Onsager's theory as applied to theoretical and experimental studies on lyotropic phases formed by colloidal particles and rod-like polymers are summarized in several reviews [247] and books [243–245]. We will incorporate suitable theoretical predictions and examples from viruses to outline aspects of self-assembly we understand and anticipate for rod-like nanoparticles.

7.2. Liquid crystalline behavior of spherocylinders

In the present article, only the rod-like nanoparticles that can be approximated as spherocylinders are considered. The aspect ratio of spherocylinders is described in terms of L/D, implying a sphere has $L/D = 1$. Further the examples considered are limited to particles with $L/D < 20$ and $L \sim 100$ nm, ensuring that even for metallic particles, the particles considered are Brownian (see Section 3 for discussion). Most of the nanoparticles are stabilized by the presence of charge or steric hindrance. Presence of charge results in an extra interaction term, which can be accounted for by using an effective diameter, D_{eff}, where D_{eff} is dependent on the Debye screening length, κ^{-1} [106,247]. Additionally the presence of charge leads to an orientation dependent potential, which acts to misalign the particles and its magnitude is characterized by a twist parameter [247], $h = \kappa^{-1}/D_{eff}$. If $h > 1.33$, the nematic phase ceases to exist, or in other words, the behavior of charged rods is richer than that of hard rods, and this must be born in mind, when we compare experimental results from dispersed gold nanorods to the theoretical results.

For the lower aspect ratios that concern us here, the phase diagram for spherocylinders was obtained by Frenkel and co-workers [240,285–290] for both two-dimensional and three-dimensional systems for hard spherocylinders. In the phase diagram shown, Bolhuis and Frenkel [288] have mapped out the phase diagram for the spherocylinders in three dimensions, showing how it depends on the density as well as the aspect ratio of the constituent particles, as shown in Fig. 38. The density

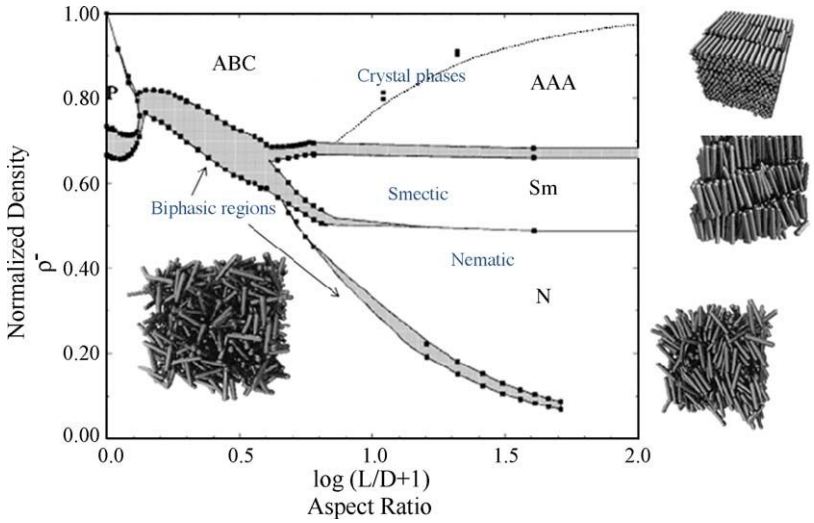

Fig. 38. Phase diagram for spherocylinders, as computed by Bolhuis and Frenkel [288].

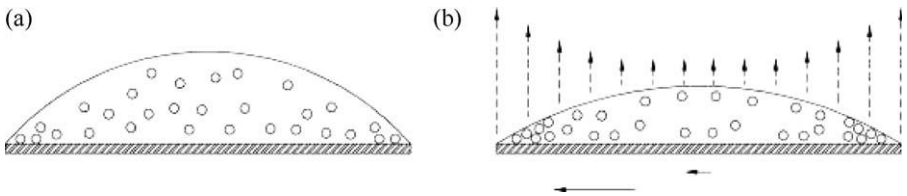

Fig. 39. Mechanism of coffee ring formation: (a) sessile drop containing homogeneous dispersion of nanoparticles. (b) The evaporating drop, with pinned contact line, i.e. same drop radius, though height decreases. The evaporation flux (vertical arrows) is maximum at the edges; this drives the flow of particles towards the edge. The flow becomes stronger radially outwards (horizontal arrows). (The particles and drops are not to scale.)

here is normalized in terms of the close packed density, which is given by $\rho_{cp} = 2/(\sqrt{2} + (L/D)\sqrt{3})$ and depends upon the aspect ratio of the rods. Their computation indicates that while hard ellipsoidal particles do not form a smectic phase, the spherocylinders can form a stable smectic phase for $L/D \sim 3.1$. The subtle difference in particle shape, dimensions and concentrations, apparently translate to different phases, making phase behavior of rods quite different from that of ellipsoids [284,291] or platelets [259–263].

Further Bates and Frenkel [286] used Monte Carlo simulations to show that the increasing polydispersity in length of particles destabilizes the smectic phase, making it almost non-existent beyond a polydispersity of 0.18 (as measured by standard deviation in length). Purdy et al. [276] have shown that a mixture of thick and thin colloidal rods has a rich phase behavior, and Fraden and co-workers [272,279] have studied how addition of spheres can alter both the concentration at which liquid crystalline phase occurs and how also create a layered smectic like phase. In any observations made on the TEM, as will be emphasized again later, the observation of low polydispersity in the size and "shape" of as-made nanoparticles can sometimes be an effect or artifact of phase separation, rather than due to efficient synthesis method. If we are aware of the phase diagram, we can relate observed patterns to the nanoparticle dimensions, or at least ensure that we are not misguided from observations from one region of the TEM grid.

7.3. Coffee ring-like pattern formation with rod-like particles

The as-made dispersion of gold nanorod produced by seed-mediated method is extremely dilute and must be concentrated to observe the liquid crystal phase. We rationalized that the concentrated phase can be reached by evaporating a drop of aqueous dispersion or by emulating the process by which drop of coffee dries to form a ring-like deposit of the dried powder. The mechanism by which coffee ring forms is as an example of colloidal self-assembly and has been studied extensively [197–199,292,293], According to Deegan et al. [197–199], when a drop of coffee starts to evaporate on a solid substrate, the presence of spherical coffee powder particles pins the contact line, and for this geometry, the evaporative flux is highest at the edge as shown in Fig. 39. Due to evaporation, the particles in the edge become depleted of the fluid, and their interstices act as capillaries that drive a strong outward, radial flow that carries nearly all the solute to the edge. The velocity of the flow is dictated by evaporation rate, which is diffusion limited, as the evaporated vapor must be removed from the top of the fluid.

In analogy with the studies by Deegan [197–199] and Popov [292,293] we observed that similar ring forms when a dispersion of gold nanorods is dried over a glass substrate, as observed in Fig. 40. The flow within the drying drop of coffee is a result of the capillary pressure which depends upon the packing fraction (Darcy's law), and hence the shape of the particles. While the qualitative features of ring formation in rods will be similar to coffee stain, since the maximum packing fraction, ρ_{cp} is different for the rods, the capillary pressure and the flux inside the drop will be different. In principle, by using Darcy's law, one can compute the capillary pressure and by computing the diffusion limited evaporation, determine corresponding flow field within the drop, as well as how the concentration of rods at any location changes as a function of time. Since the concentration increases as particles approach the edge, and liquid crystal phase forms beyond a certain concentration (that depends upon aspect ratio, among other things), we determined that the ring formation will be accompanied by formation of liquid crystalline phase. The liquid crystalline phase can be simply observed by using polarized light microscopy, for the liquid crystalline phases are birefringent and exhibit characteristic textures that are used for identifying them (in conjunction with other techniques). The quantitative theory or simulation based on these ideas remains an open question, and for the present, we will describe the experimental results.

As the drop of colloidal gold nanorods is dried, formation of a highly birefringent deposit is observed under crossed polarizers on a polarized optical microscope. For a dispersion containing mainly nanorods with the aspect ratio larger than 4, the formation of rings is preceded by appearance of highly birefringent domains that are

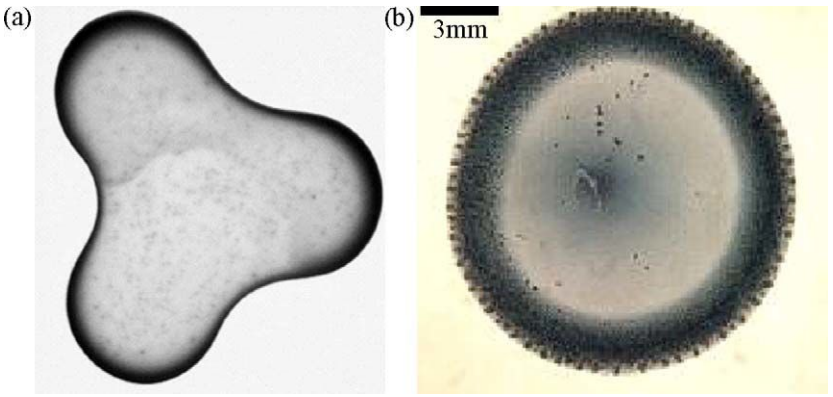

Fig. 40. (a) Coffee stain (2 mm in diameter) and (b) dried colloidal gold NRs [125].

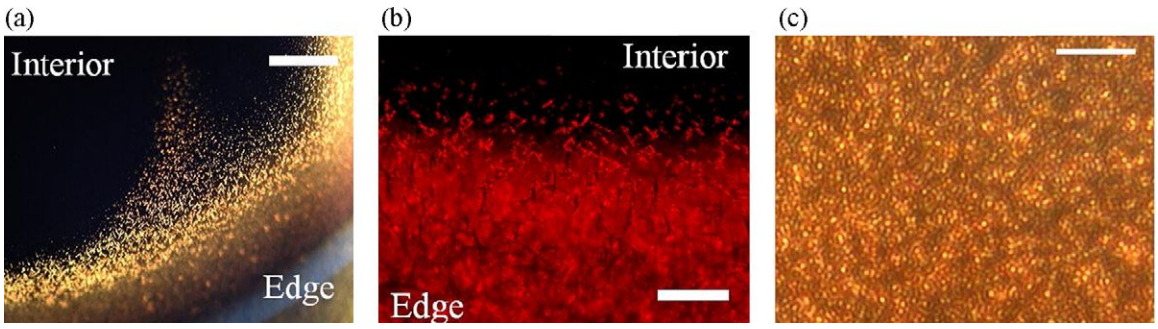

Fig. 41. The images of the drop of colloidal dispersion of gold nanorods during evaporation under optical microscope with cross polarizers, as described in the text. (a) Emerging liquid crystal domain from the interior and moving toward the edge. (b) Magnified image showing the individual domain joins the existing structure. (c) The assembly of liquid crystal domains. The scale bar is 200 μm for (a) and 20 μm for (b) and (c) [125].

about 3–4 μm in size, that appear to move towards the edge as shown in Fig. 41. Certainly, the drying and densification drives the system into the bistable region and the spontaneous phase separation creates these domains of liquid crystals. We see that these domains exhibit the characteristic birefringence and fluidity of liquid crystals drops, and keep sparkling until the drying is completed. The sparkling is a consequence of fluctuations in the director field that are caused simply by the thermal fluctuation within these drops or domains. The domain size can be determined by minimization of free energy, where the surface tension term tries to minimize the surface area while the confinement of rods is opposed by an elastic term (estimated from Frank's constants, using theory of Lee and Meyer [280,281,294]). The minimization for the typical values of Frank's constants and surface tensions for these gold nanorods gives a domain size of few microns, as observed. The domains in this case are non-spherical, called tactoids, and their specific size and shape depends upon the aspect ratio of the constituent nanorods.

The width of this highly birefringent increases inwards as a function of time, as shown in Fig. 42. A drop of 2 μl takes 11 min to evaporate completely. The highly birefringent edge only appears after 3 min. The evaporation at the edge drive flow within the drops carrying more and more solute towards the edge. While these processes continue, the supply of fluid to the outer limits of the birefringent band becomes insignificant, and a distinct color change distinguishes the outer, drier part from the inner region where presence of fluid lends different optical path to the observed radiation.

When a drop containing gold nanorods with aspect ratio less than 4 is evaporated, the ring depositing near the contact line is not birefringent, though the birefringence from the surfactant crystal appears after water evaporates completely, as shown in Fig. 43. As predicted by the simulations of Bolhuis and Frenkel [288], the liquid crystalline phase is expected to form only beyond a certain aspect ratio (∼3 from their simulations on hard rods).

7.4. Concentric birefringent bands on glass slide: Liesegang ring like patterns

Apart from the single birefringent band that appears in certain cases, as described above, we find that certain drops form multiple bands or rings on evaporation. We varied the evaporation conditions and the concentration and aspect ratio of nanorods dispersed in the droplets to determine the conditions that lead to the formation of these multiple rings. Fig. 44 shows the deposits resulting from dried drops of different initial volume fraction of

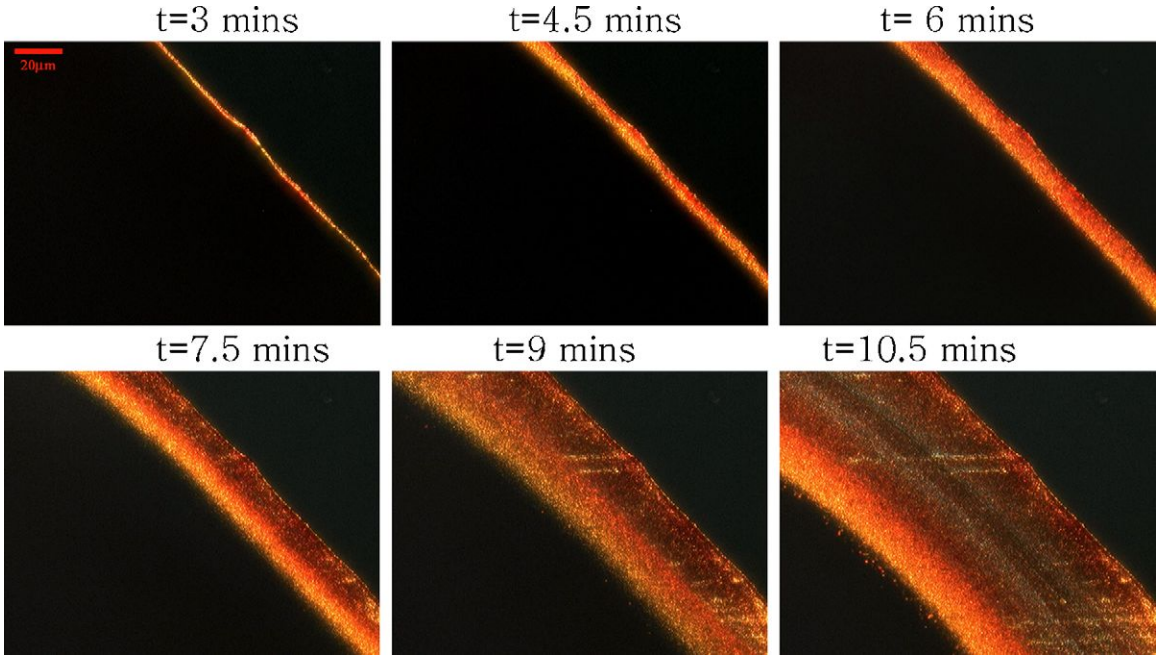

Fig. 42. In this series of images the center of the drop is in the bottom left corner. The images of the drop of gold NRs sol during evaporation under optical microscope with cross polarizers, as described in the text [125].

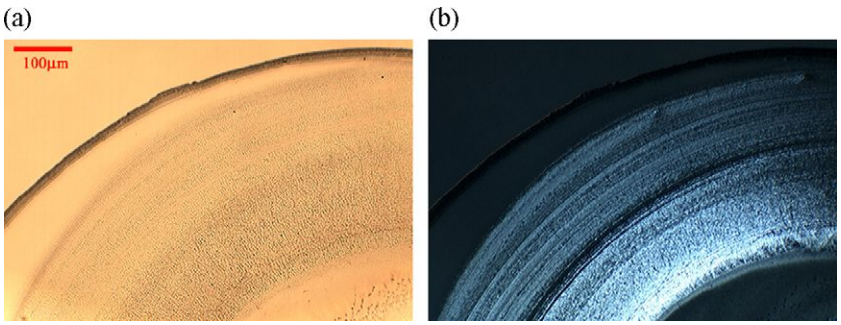

Fig. 43. (a) Bright field image of the drop of gold NR; aspect ratio of 3. Ring formed at the edge of (b) image with crossed polarizers. Birefringence from the surfactant crystals, observed after evaporation is completed [125].

gold NRs (aspect ratio 6). For each image, a drop of 2 μl gold NR sol was deposited on the glass slide. Drops of size ~ 3 mm in diameter is formed on the substrate.

The upper row in Fig. 44 shows the images of dried deposits formed from the slow evaporation, accomplished by keeping the evaporating drop in a closed environment. Under these conditions, it takes 1 h for the drop to be completely dried. Regardless of the volume fraction of the solute in the drop, a single ring/band forms at the contact line, though the width of the band decreases as the volume fraction of nanorods decreases. The bottom row in Fig. 44 shows the images of dried deposits formed during fast evaporation (about 11 min), accomplished by placing the drop in open environment. In (f) there is a dark ring formed at the edge. As the volume fraction decreases, we observed concentric multiple ring formed in the interior of this ring while the width of the ring also slightly decreased (g, h, and i). Upon decreasing the concentration further, very thin ring was formed without additional rings inside (h).

The higher magnification images of the region near the contact line, taken under cross polarizers, during the evaporation process is shown in Fig. 45. When the evaporation is carried out in a closed environment, the evaporation proceeds such that the color change representative of complete drying of particles does not start till a thick band of deposit already forms close to the edge. In open environment, where the evaporation is faster and the process is completed in nearly one-sixth of the time, the deposit at the edge seems to dry out quicker, and at the same time, a concentric ring develops within the drop. This process is observed till a number of rings form in the system.

Other instances where such concentric rings have been reported include formation of the Liesegang rings [27,69,295–299], multi-rings for latex particles observed by Stone and co-workers [300], concentric rings obtained by Maeda [301] by evaporating collagen solution droplets and multi-rings in polymers and polyelectrolytes [302–309]. In the experimental study by Stone and co-workers [300], it was shown that the formation of multi-rings is more likely for dilute sols of latex particles and for large size drops. They rationalized their observations by stating that the contact line can move inwards till it encounters the next pinning sites. The ability to form multi-rings is therefore controlled by the interplay of depinning and pinning of contact line; due to high evaporation rate at the edge the depinning can take place and the contact line moves till it encounters the next set of pinned particles. This is similar to the observations made by Deegan in his experiments [197].

Starting from initial studies of Liesegang from 1896, Liesegang rings have been seen for more than a hundred years in reaction-diffusion systems [69,296–299], where periodic precipitate form in the wake of a reaction front. In the typical system, one of the reactants is dispersed in a gel, as other reactant is added, it propagates through diffusive flux. The reaction causes a local depletion of reaction, and this leads to concentric rings of

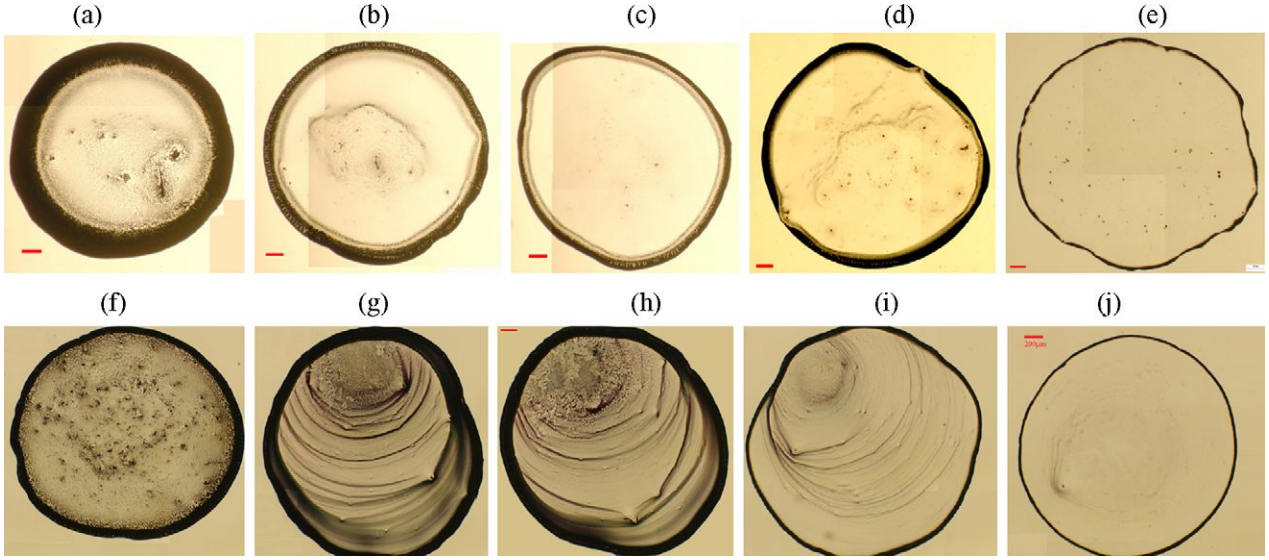

Fig. 44. "Coffee stain" formed by drying drops of gold NR sol. The images in the upper row show the drying drops from slow evaporation. The volume fraction decreases from left to right: (a) 1×10^{-5}, (b) 5×10^{-6}, (c) 3.3×10^{-6}, (d) 2.5×10^{-6} and (f) 1.25×10^{-6}. The images in the middle row are from fast evaporation. The volume fraction of the drops in the same column is identical. The scale bar is 200 μm [125].

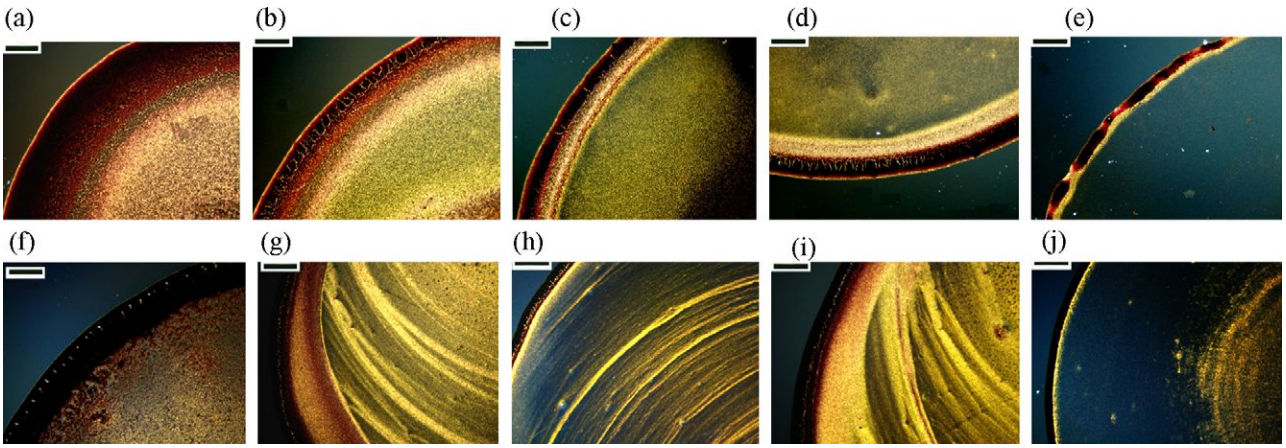

Fig. 45. The patterns formed by various concentrations and different evaporation condition were visualized by polarized optical microscopy. The same number of figure was used for the same sample shown in Fig. 44. The scale bar is 200 μm [125].

precipitates, as shown schematically in Fig. 46. The spacing and width of Liesegang rings follows simple scaling laws (for example the position of nth band x_n scales as $t_n^{0.5}$ and the width w_n increases as x_n) and have been described or modeled quite successfully by various researchers in the past [27,69,295–298].

Unlike Liesegang rings, where diffusive flux competes with propagating reaction front and precipitation, the dominant transport in our system is through convective flow. The transition to the liquid crystal can be thought of like the precipitation reaction, and in close analogy, once the concentration levels reach the metastable regime, spontaneous nucleation and growth of liquid crystalline phase occurs. This locally can lead to depletion zone and allow a similar formation of concentric bands. But from our preliminary data, the spacing between the bands as well as the width of the bands does not seem to follow the scaling behavior observed in the case of the Liesegang rings. In Fig. 47 we show a well-defined concentric multiple ring pattern. The distance between the contact lines as well as the time between pinning and sticking events do not show any periodicity. Therefore the motion of the contact line cannot be described as a simple sinusoidal response [301] or through reaction-diffusion models typically used for Liesegang rings [27,69,295–298]. We believe that with precise control of the drop size, roughness of the substrate and evaporation condition, one might obtain better data to conduct more systematic analysis of the multiple ring patterns.

The question of what really controls the pattern formation, and the kinetics of phase transition requires further experimental study and theoretical analysis. So we offer only a phenomenological explanation. Essentially, the presence of particles can pin the contact line, and the more the number of particles, i.e. higher the concentration, better the pinning. The capillary action is controlled by the packing fraction. Hence one can expect that the higher initial concentration causes a stronger flow, and results in transfer of all the solute to the contact line. On the other hand, at the lower concentration of solute, the velocity reached is not high enough to ensure that all particles reach the edge before drying

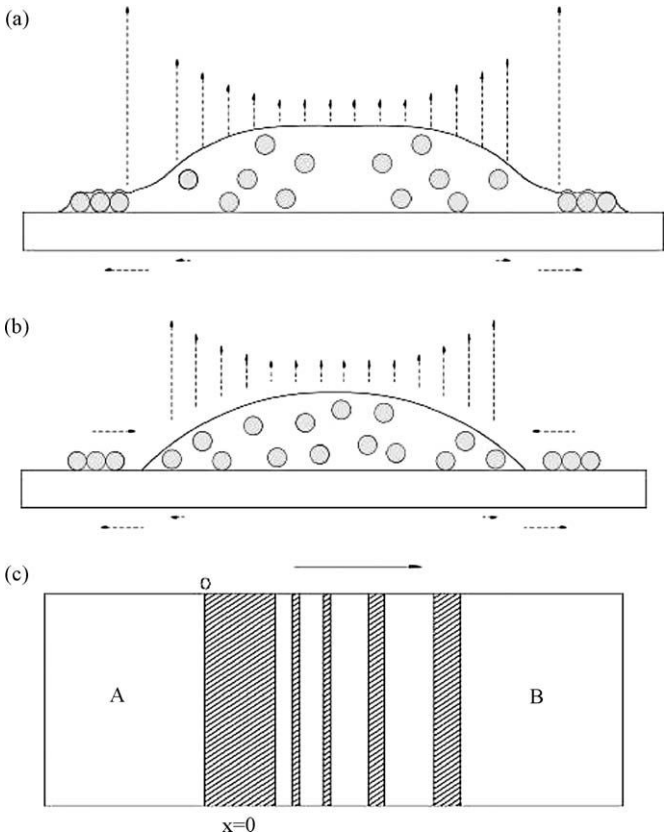

Fig. 46. (a) Schematic illustrating how nanoparticles accumulate at the contact line when the rate of evaporation is slow (akin to coffee ring mechanism). Most of the particles are carried to the edge and form a single dark ring. (b) The case of fast evaporation: contact line recedes, till it encounters next set of pinned particles. (c) Schematic illustrating how Liesegang rings form when two species A moves into initially uniform concentration of B, forming dark precipitates with location and width given by characteristic scaling laws (see text for details).

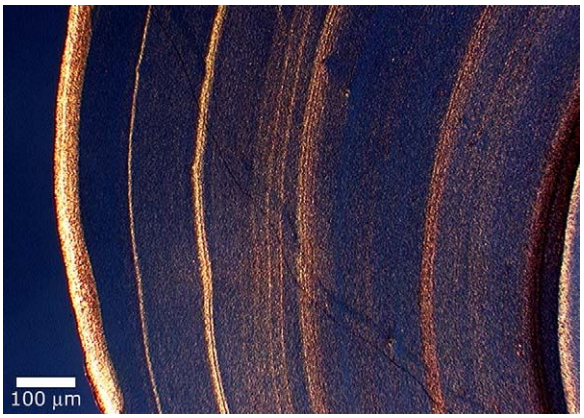

Fig. 47. The well-defined concentric multiple ring pattern formed by evaporation of dilute gold nanorod sol. Image taken under optical microscope with cross polarizers. The scale bar is 100 μm [125].

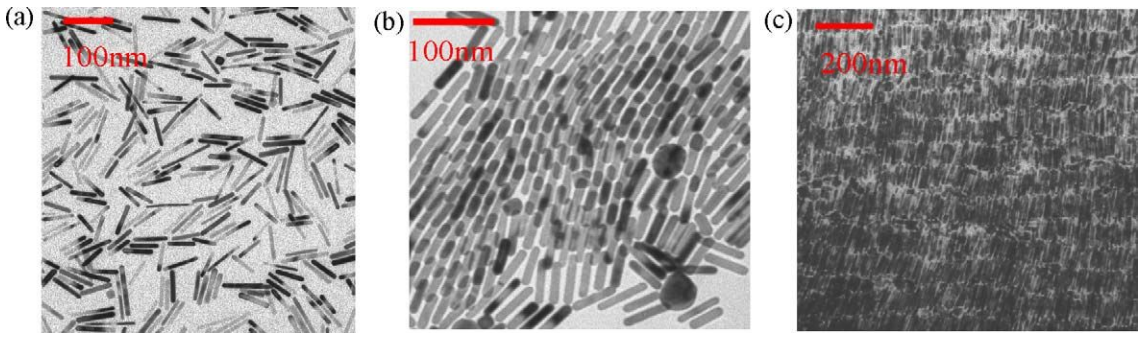

Fig. 48. TEM images of gold NRs assembly. Aspect ratio is 6. (a) Isotropic phase, (b) nematic-like assembly and (c) smectic like assembly [125].

complicates the process. If drying weakens the flow, the particles can get pinned at some distance away from the first band. Thus this interplay of capillary flux, diffusive flux towards emerging domains (due to phase transition) and pinning–depinning cause multiple rings to form. The phenomenon will be described and understood better if an elaborate study of the pattern formation for a range of aspect ratios, drop sizes, evaporation rates and surfactant concentration is carried out. The reason why surfactant concentration can play a role is as (1) it alters the surface tension, changing the contact angles, and (2) presence of surfactant induces Marangoni stresses that can alter the flow terms [310–312].

Several of the unsolved problems for our research are relevant to the coffee ring type assemblies and multi-ring patterns observed in colloids [197–199], polymers and polyelectrolytes [302–309], collagen [313], porphyrin dyes [314] and have received recent attention, though, as far as we know, corresponding pattern formation has not been studied in a quantitative fashion for rod-like particles. We hope that our description of the observations will provide the inspiration for in-depth study of the same.

7.5. Self-assembly on TEM grids

The formation of the ring patterns indicates that this capillary flow driven assembly can self-organize and order the nanorods. While the formation of micron size domains can be observed in an optical microscope, the resolution to the scale of nanorods is not possible. We decided to examine the self-assembled nanorods in TEM. Since the patterns formed over the glass slides cannot be used in TEM studies, we evaporated drops of 1 μl sol of gold nanorods on the carbon coated copper TEM grids. While the self-assembly is still controlled by drying mediated fluxes, the physical properties including surface roughness, contact angle, etc. of the grid are quite different from the surface condition of the glass slide. Yet we can observe the orientational and positional order of the pattern formed on the same TEM grid by characterizing the location and orientation of individual rods. Thus we can contrast the role played by the initial concentration and size of gold nanorods and the influence of different evaporation condition. In the following subsections, we outline some such observations.

7.5.1. Two-dimensional phase transitions observed in self-assembly on a TEM

When an extremely dilute dispersion of gold nanorods is dried over the TEM grid, the nanorods can deposit a monolayer, within which the position and orientation of each rod can be assessed using image analysis. In what follows we summarize the characteristics of observed patterns, and then provide qualitative arguments about how their formation can be explained. For aspect ratio of 6, at low number density, 2–4 NRs form aggregates and are dispersed in an isotropic state, as seen in Fig. 48. As the number density increases, nanorods start to form a monolayer of partially nematic-like phase. With further increase of number density, nanorods form a multilayer of smectic-like phase. For short nanorods (aspect ratio is 3), the smectic-like assembly showing both orientational and positional order was observed (Fig. 49). The ordered assembly was observed for the very long nanorods (aspect ratio is 14), as seen in Fig. 50. In this case, even though the suspension contains some of the spherical byproducts, phase transition from isotropic to nematic and smectic phase can be confirmed by the self-assembly of dried suspension, as seen in Fig. 50.

Several groups have reported such nematic-like and smectic-like assemblies for gold nanorods [315–319] as well as other rod-like nanoparticles [320–326]. When only a layer of nanorods is found on the grid, as observed in Figs. 48–50, the pattern formation, and in this case, possible phase change occurs in a thin region, implying that the assembly process is two-dimensional rather than three-dimensional. The order parameter, as well as phase diagram depends upon the dimensionality of the problem. In this case, the angle between the director and the long axis of each rod can be measured and the formula for two-dimensional order parameter is $S = \langle \cos 2\theta \rangle$.

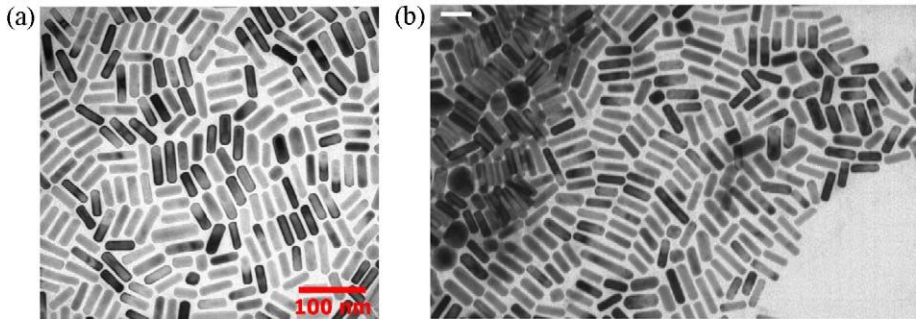

Fig. 49. TEM images of gold NRs assembly. Aspect ratio is 3. a) Isotropic phase and (b) transition from isotropic to smectic like assembly [125].

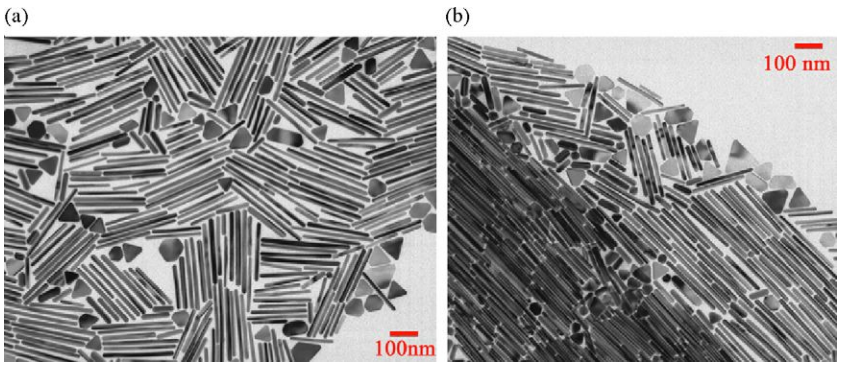

Fig. 50. TEM images of gold NRs assembly. Aspect ratio is 14. (a) Isotropic phase and (b) nematic-like assembly [125].

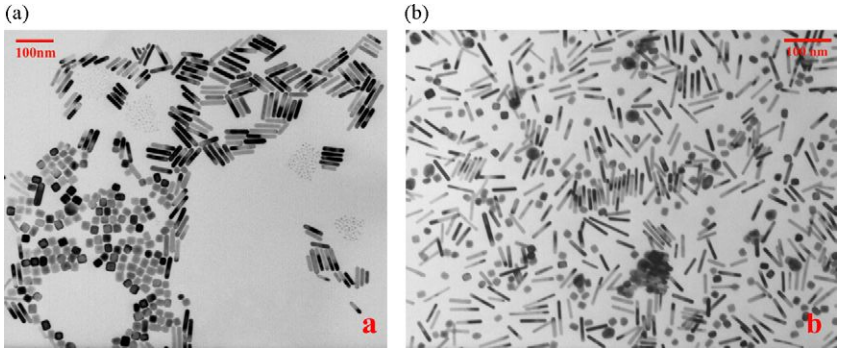

Fig. 51. TEM image of self-assembly of as-made sol: (a) slower evaporation and (b) faster evaporation. The coverage of particle in both images is about 20% [125].

Bates and Frenkel [285] studied two-dimensional hard rod fluids consisting of spherocylinders confined to lie in a plane using Monte Carlo simulations. For long rods, a 2D nematic phase is observed at high density and the transition from this phase to the low density isotropic phase is continuous. For short rods, the nematic phase disappears so that, the solid phase (which is akin to both smectic and crystal phase) undergoes a first order transition directly to an isotropic phase. In this respect, according to Bates and Frenkel [285], the order parameter is dependent on the size of the system, and the characteristic feature of 2D system is absence of a true long range order. The order parameter depends both on density of rods and on the system size. By determining the order parameter as a function of system size, one can compare it with the prediction that $S \sim N^{-k_B T/2\pi K}$, where N is the number of particles and K is the Franck's constant of elasticity [285]. Since a realistic comparison will require a system size with nearly 7000 particles (as was used in simulation), we were not able to compute these statistics, though in future, if extended assembly of nanorods is found, it will be a worthwhile experiment to examine this behavior.

7.5.2. Heterogeneity and polydispersity of the sample

As-made sol is typically a mixture of rod-like and spherical particles. When as-made sol is evaporated 'slowly' on the TEM, shape selective assembly or micro phase separation of different shapes is seen to occur. Nanorods and spherical particles assemblies form separate clusters on the TEM grid, as shown in Fig. 51. In case of faster evaporation, the particles of different shape are kinetically trapped into a mixture as seen in Fig. 51b. Such phenomenon is extensively studied theoretically and has also been confirmed by simulations [327].

Fig. 52 shows another example showing micro phase separation of 3 different shapes of nanoparticles (nanorods, nanospheres and nanocubes). The shape separation not only leads to locally purer, low polydispersity samples, but can provide domains with high amount of order. While it is well known that polydispersity prevents long range positional ordering [108], on a TEM grid, the lack of long range order could be a consequence of 2D liquid crystal phase, as discussed before. Several reports on self-assembly of gold nanorods [318,319,328] focused on patterns formed in a small domain, and concluded that the concentration and pH of the dispersion determine the properties of self-assembly. Given the non-equilibrium nature of assembly on TEM grids, the comparisons with patterns expected from equilibrium cannot explain the range of patterns obtained. For example, even if the dispersion has rods of a given aspect ratio in a known concentration to begin with, factors like whether evaporation is homogeneous and heterogeneous, determine the patterns formed by rods before solvent evaporates away. Nearly a hundred years back, Perrin [89,90] saw two-dimensional packing of spherical colloidal particles and

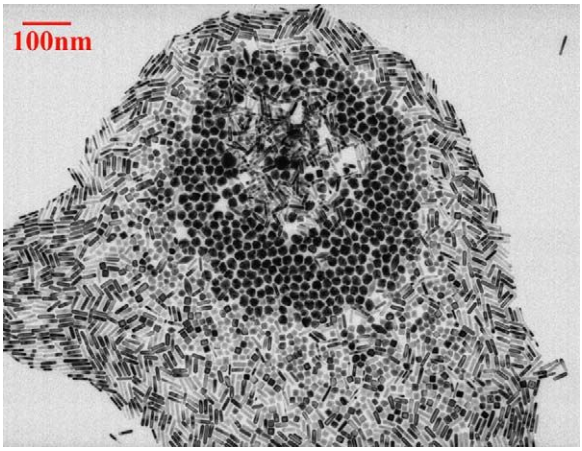

Fig. 52. TEM image of self-assembly of as-made sol showing micro phase separation of 3 different shapes of nanoparticles [125].

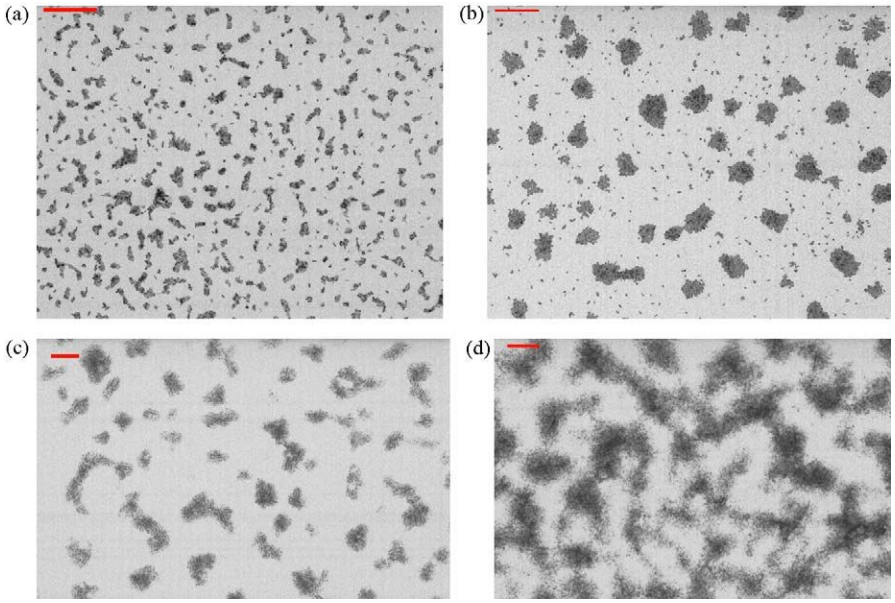

Fig. 53. The TEM images showing different patterns formed at different coverage ratio of (a) 4%, (b) 10%, (c) 15% and (d) 40%. The aspect ratio is 5 and the scale bar is 1 μm [125].

reasoned that capillary forces can make particles organize into a close packed structure. The role of capillary forces [214,329–331], quantified as immersion forces for partially submerged particles, and floatation forces for particles on air–solvent interface, is being actively investigated for spherical systems. In principle, the origin of forces will be similar for rods, but the shape anisotropy will change the directional nature of the forces.

7.5.3. Patterns formed by evaporation

Rabani et al. [200] modeled the drying mediated self-assembly in spherical particles by accounting for pinning, diffusion and solvent assisted aggregation. The equilibrium and non-equilibrium patterns were found to correspond very well to the experimentally observed patterns for spherical CdSe particles. The case of homogeneous evaporation provides patterns expected from coarsening behavior, for example the phase separated domains can exhibit self-similar growth as expected for systems undergoing spinodal decomposition. In heterogeneous evaporation, the local concentration and solvent fluctuations produce patterns that are a consequence of both thermodynamic and kinetic effects. The rate of drying and the timescale for particle diffusion become important parameters in determining the outcome for the drying dispersion. We have observed similar patterns in the assemblies on TEM grids for gold nanorods, though in absence of similar simulations or theory for rod-like particles, our inferences about their thermodynamic or kinetic origin are at best intuitive or speculative.

Fig. 53 shows the patterns taken from the center area of a single TEM grid. The aspect ratio of NRs is 5. At very low coverage (less than 5%) ribbon-like aggregates of nanoparticles dominate the self-assembly (Fig. 53a). As the coverage increases, Fig. 53b, disk-like aggregates of nanoparticles dominate the self-assembly. At still higher coverage or particle density, the clusters are interconnected. We observed similar patterns in the nanorod suspensions with aspect ratio of 3–6. The dynamics of nanoparticle assembly must be modulated here by interparticle attractive forces, phase separation kinetics and by drying induced solvent fluxes, though the role of these factors is unclear for we only see (if we may say so), the fossil and not the beast, on a TEM grid. Further, the aggregates thus formed could simply result from a diffusion-limited aggregation [231,332], where the aggregate structure is rather insensitive to interparticle interactions. For example, such aggregates formed by colloidal gold sols (∼15 nm spherical particles) have been characterized by describing them as fractals [333–335]. The use of similar structure analysis can be applied to patterns formed here, and it is likely to be useful in describing optical and transport properties of such self-assembled structures. The reader can refer to excellent text by Meakin [231] for a detailed discussion on fractals, diffusion-limited aggregation and pattern formation.

The drying of gold nanorod suspensions can sometimes yield interesting ring patterns as shown in Fig. 54. These patterns were observed when the coverage was between 10 and 20% and they occur in the region between the center and the edge of the drop on TEM grid. The ring patterns were formed by various aspect ratio of gold NRs (aspect ratio 4–7). The shape of the ring is very close to perfect circle and the size of the ring is ranged from 200 nm (the diameter of the hole) to 1 μm and does not seem to depend on the

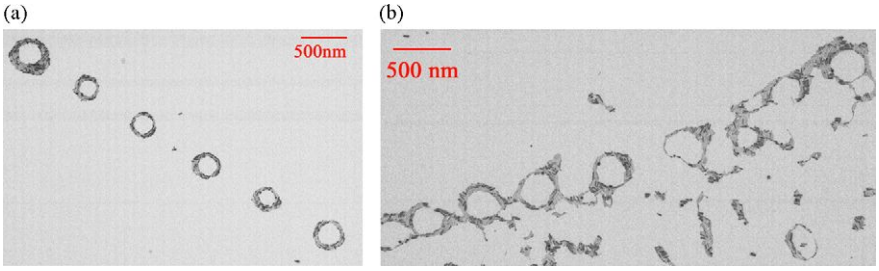

Fig. 54. Ring-like array observed when the coverage is 10–20%: (a) aspect ratio is 4 and (b) aspect ratio is 6 [125].

aspect ratio of gold nanorods. Interestingly many rings were found to lie in a straight line and are not only similar in size, but also in the distance that separates them.

The formation of such rings on TEM grids has been reported before by Ohara et al. [336], for a dispersion of 2.5 nm silver nanoparticles coated with dodecanethiol and dispersed in hexane. The scenario in this case is quite different from the coffee ring mechanism [197–199] that operates in sessile drops, and where capillary driven outward flow is said to drive the particles to the edge, as discussed before. In this case [336], the authors postulated that for a wetting fluid, the solvent evaporates as a thin film, and so the hole that opens up pins the contact line, and as the hole advances outwards, it pushes particles outwards. Unlike the case studied by Deegan and co-workers [197–199], here the pinning is not automatic, and it is dependent on the particle–substrate interaction as well as particle size. The theoretical arguments of Ohara et al. [336] suggest that the ring sizes should be same for a given concentration of nanoparticles, as observed in Fig. 54. We were not able to draw any reliable correlations of ring size with particle size or aspect ratio, and expect that more controlled experiments will be useful in deciphering the role of shape anisotropy and particle–substrate interaction in controlling the pattern formation.

We observed cellular network structures as shown in Fig. 55 when the coverage reaches about 30–50%. If we compare the network structure for different aspect ratio, the cells are better defined for the shorter nanorods. The size of the holes, that ranges from 100 to 700 nm, does not seem to correlate with the aspect ratio of nanorods. The network structure provides a continuous matrix over the substrate, with relatively low amount of material, and this could be useful for fabricating devices.

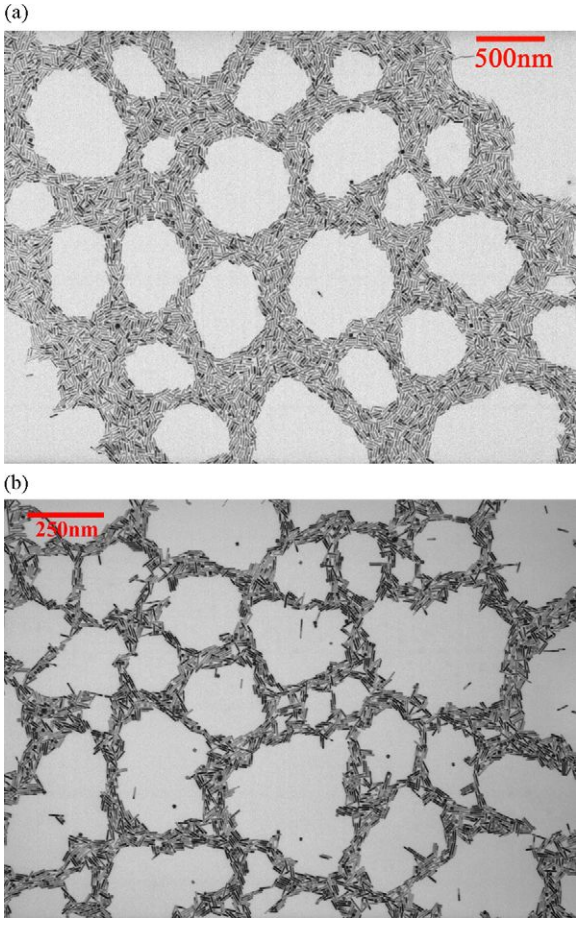

Fig. 55. The cellular network structure formed by gold NRs with different aspect ratios: (a) aspect ratio of 4 and (b) aspect ratio of 6 [125].

8. Synopsis and outlook

The colloidal dispersion of gold particles were the ruby red fluids concocted by alchemists for centuries, before Faraday's keen experimental eye established that they contained dispersed particles of elemental gold. In this article, we started out by looking at the early studies on colloidal gold, as means of introducing key concepts related to colloidal nature of gold sols and for unearthing multiple references to synthesis of nanorods (albeit as byproducts), to seed-mediated methods (called nuclear methods) and to means of characterizing the physical properties of colloidal gold. Thereafter we presented a gist of basic ideas about Brownian motion and interaction forces, to set stage for establishing what determines colloidal stability. We believe that even though a great amount of attention is paid to aspects related to synthesis and applications of gold nanorods, the field will advance much more if colloidal behavior of gold sols was better characterized and better understood. For example, we presented a simple, but effective method for shape separation of particles using centrifugation-assisted sedimentation. Since the separation is affected by Brownian motion in external field, in principle the same hydrodynamic arguments that we advanced for sedimentation, could be used for affecting shape separation using electrophoresis.

The possibility of using gold nanorods for chemical and biological sensing is largely dependent on our ability to understand the size and shape dependent plasmon resonance and electric field enhancements by nanorods. Given the importance of this understanding, we summarized the key concepts necessary to appreciate the optical properties of gold rods and their dispersions. While Mie theory describes the absorption and scattering by spherical particles of any size, the corresponding theories for non-spherical particles are exact only in limits of sizes much larger or much smaller than the wavelength of light interacting with material in question. The computational methods provide useful means of studying the response of nanoparticles and as they get more refined, will provide the requisite information about field enhancements for particles of complex shapes, enabling more quantitative sensing. The rod-like nanoparticles form liquid crystalline phases and a host of patterns mediated by drying induced self-assembly. We expect that these will continue to provide researchers a means of making using patterns with desired amount of order as well as a system that allows us to visualize the thermodynamic and kinetic effects of shape anisotropy. We presented our observation of rings on both glass slides and substrates, and we expect that the experimental protocol will be useful for unraveling interesting dissipative structures. We hope that our research efforts and this review will contribute towards a better understanding of synthesis, optical properties, shape separation and self-assembly of gold nanorods.

Acknowledgements

Mohan Srinivasarao acknowledges financial support from the National Science Foundation (DMR-637233 and DMR-706235). Mohan Srinivasarao also acknowledges support from Nanyang Technological University in Singapore in the form of Tan Chin Tuan Exchange Fellowship, during which time parts of the manuscript was written.

References

[1] M.A. El-Sayed, Accounts of Chemical Research 34 (2001) 257–264.

[2] M.C. Daniel, D. Astruc, Chemical Reviews 104 (2004) 293–346.
[3] C.J. Murphy, T.K. San, A.M. Gole, C.J. Orendorff, J.X. Gao, L. Gou, S.E. Hunyadi, T. Li, Journal of Physical Chemistry B 109 (2005) 13857–13870.
[4] J. Perez-Juste, I. Pastoriza-Santos, L.M. Liz-Marzan, P. Mulvaney, Coordination Chemistry Reviews 249 (2005) 1870–1901.
[5] A.V. Alekseeva, V.A. Bogatyrev, B.N. Khlebtsov, A.G. Mel'nikov, L.A. Dykman, N.G. Khlebtsov, Colloid Journal 68 (2006) 661–678.
[6] L.A. Dykman, V.A. Bogatyrev, Uspekhi Khimii 76 (2007) 199–213.
[7] X.C. Jiang, M.P. Pileni, Colloids and Surfaces A: Physicochemical and Engineering Aspects 295 (2007) 228–232.
[8] S. Eustis, M.A. El-Sayed, Chemical Society Reviews 35 (2006) 209–217.
[9] P.K. Jain, X. Huang, I.H. El-Sayed, M.A. El-Sayad, Plasmonics 2 (2007) 107–118.
[10] X.H. Huang, P.K. Jain, I.H. El-Sayed, M.A. El-Sayed, Nanomedicine 2 (2007) 681–693.
[11] J.H. Song, F. Kim, D. Kim, P.D. Yang, Chemistry—A European Journal 11 (2005) 910–916.
[12] K.L. Kelly, E. Coronado, L.L. Zhao, G.C. Schatz, Journal of Physical Chemistry B 107 (2003) 668–677.
[13] S. Link, M.A. El-Sayed, Journal of Physical Chemistry B 103 (1999) 8410–8426.
[14] S. Link, M.A. El-Sayed, Journal of Physical Chemistry B 103 (1999) 4212–4217.
[15] S. Link, M.A. El-Sayed, International Reviews in Physical Chemistry 19 (2000) 409–453.
[16] C. Burda, X.B. Chen, R. Narayanan, M.A. El-Sayed, Chemical Reviews 105 (2005) 1025–1102.
[17] M.A. El-Sayed, Accounts of Chemical Research 37 (2004) 326–333.
[18] A.P. Alivisatos, Journal of Physical Chemistry 100 (1996) 13226–13239.
[19] M. Faraday, Philosophical Transactions of the Royal Society of London 147 (1857) 36.
[20] R. Zsigmondy, The Chemistry of Colloids, John Wiley & Sons, Inc., New York, 1917.
[21] R. Zsigmondy, Colloids and the Ultramicroscope, John Wiley & Sons, Inc., New York, 1909.
[22] T. Svedberg, The Formation of Colloids, D. Van Nostrand Company, Inc., New York, 1921.
[23] T. Svedberg, A. Tiselius, Colloid Chemistry, The Chemical Catalog Company, Inc., New York, 1928.
[24] T. Svedberg, K.O. Pedersen, The Ultracentrifuge, Oxford University Press, Oxford, 1940.
[25] G. Mie, Annalen Der Physik 25 (1908) 377–445.
[26] R. Gans, Annalen Der Physik 37 (1912) 881–900.
[27] W. Ostwald, An Introduction to Theoretical and Applied Colloid Chemistry, John Wiley & Sons, Inc., New York, 1917.
[28] R. Zsigmondy, E. Huckel, Zeitschrift Fur Physikalische Chemie—Stochiometrie Und Verwandtschaftslehre 116 (1925) 291–303.
[29] W.D. Bancroft, Applied Colloid Chemistry, McGraw-Hill Book Company, Inc., New York, 1921.
[30] S.A. Maier, H.A. Atwater, Journal of Applied Physics 98 (2005).
[31] K.A. Willets, R.P. Van Duyne, Annual Review of Physical Chemistry 58 (2007) 267–297.
[32] E. Hutter, J.H. Fendler, Advanced Materials 16 (2004) 1685–1706.
[33] C.Z. Li, K.B. Male, S. Hrapovic, J.H.T. Luong, Chemical Communications (2005) 3924–3926.
[34] R. Elghanian, J.J. Storhoff, R.C. Mucic, R.L. Letsinger, C.A. Mirkin, Science 277 (1997) 1078–1081.
[35] M. Hu, J.Y. Chen, Z.Y. Li, L. Au, G.V. Hartland, X.D. Li, M. Marquez, Y.N. Xia, Chemical Society Reviews 35 (2006) 1084–1094.
[36] C.X. Yu, J. Irudayaraj, Analytical Chemistry 79 (2007) 572–579.
[37] S.F. Cheng, L.K. Chau, Analytical Chemistry 75 (2003) 16–21.
[38] K. Aslan, J. Zhang, J.R. Lakowicz, C.D. Geddes, Journal of Fluorescence 14 (2004) 391–400.
[39] Z.P. Li, C.H. Liu, Y.S. Fan, X.R. Duan, Analytical and Bioanalytical Chemistry 387 (2007) 613–618.
[40] C. Sonnichsen, A.P. Alivisatos, Biophysical Journal 88 (2005) 364A–365A.
[41] C.J. Orendorff, S.C. Baxter, E.C. Goldsmith, C.J. Murphy, Nanotechnology 16 (2005) 2601–2605.
[42] C.J. Murphy, A.M. Gole, S.E. Hunyadi, J.W. Stone, P.N. Sisco, A. Alkilany, B.E. Kinard, P. Hankins, Chemical Communications (2008) 544–557.
[43] A.J. Haes, S.L. Zou, G.C. Schatz, R.P. Van Duyne, Journal of Physical Chemistry B 108 (2004) 6961–6968.
[44] A.J. Haes, C.L. Haynes, A.D. McFarland, G.C. Schatz, R.R. Van Duyne, S.L. Zou, MRS Bulletin 30 (2005) 368–375.
[45] M.H. Rashid, R.R. Bhattacharjee, T.K. Mandal, Journal of Physical Chemistry C 111 (2007) 9684–9693.
[46] A.C. Templeton, J.J. Pietron, R.W. Murray, P. Mulvaney, Journal of Physical Chemistry B 104 (2000) 564–570.
[47] K. Kneipp, A.S. Haka, H. Kneipp, K. Badizadegan, N. Yoshizawa, C. Boone, K.E. Shafer-Peltier, J.T. Motz, R.R. Dasari, M.S. Feld, Applied Spectroscopy 56 (2002) 150–154.
[48] D.A. Schultz, Current Opinion in Biotechnology 14 (2003) 13–22.
[49] P.K. Jain, K.S. Lee, I.H. El-Sayed, M.A. El-Sayed, Journal of Physical Chemistry B 110 (2006) 7238–7248.
[50] P.K. Jain, M.A. El-Sayed, Nano Letters 7 (2007) 2854–2858.
[51] P.K. Jain, S. Eustis, M.A. El-Sayed, Journal of Physical Chemistry B 110 (2006) 18243–18253.
[52] J.J. Storhoff, A.A. Lazarides, R.C. Mucic, C.A. Mirkin, R.L. Letsinger, G.C. Schatz, Journal of the American Chemical Society 122 (2000) 4640–4650.
[53] A.J. Haes, S.L. Zou, G.C. Schatz, R.P. Van Duyne, Journal of Physical Chemistry B 108 (2004) 109–116.
[54] J.Y. Chen, B. Wiley, Z.Y. Li, D. Campbell, F. Saeki, H. Cang, L. Au, J. Lee, X.D. Li, Y.N. Xia, Advanced Materials 17 (2005) 2255–2261.
[55] W.Y. Huang, W. Qian, M.A. El-Sayed, Y. Ding, Z.L. Wang, Journal of Physical Chemistry C 111 (2007) 10751–10757.
[56] X.H. Huang, I.H. El-Sayed, W. Qian, M.A. El-Sayed, Nano Letters 7 (2007) 1591–1597.
[57] X.H. Huang, I.H. El-Sayed, W. Qian, M.A. El-Sayed, Journal of the American Chemical Society 128 (2006) 2115–2120.
[58] P.K. Jain, I.H. El-Sayed, M.A. El-Sayed, Nano Today 2 (2007) 18–29.
[59] R. Narayanan, M.A. El-Sayed, Chimica Oggi/Chemistry Today 25 (2007) 84–86.
[60] B.I. Ipe, K.G. Thomas, S. Barazzouk, S. Hotchandani, P.V. Kamat, Journal of Physical Chemistry B 106 (2002) 18–21.
[61] M. Horisberger, J. Rosset, Journal of Histochemistry & Cytochemistry 25 (1977) 295–305.
[62] W. Caseri, Macromolecular Rapid Communications 21 (2000) 705–722.
[63] N. Al-Rawashdeh, C.A. Foss, Nanostructured Materials 9 (1997) 383–386.
[64] N.A.F. Al-Rawashdeh, M.L. Sandrock, C.J. Seugling, C.A. Foss, Journal of Physical Chemistry B 102 (1998) 361–371.
[65] S.A. Maier, Current Nanoscience 1 (2005) 17–23.
[66] S.A. Maier, Plasmonics: Fundamentals and Applications, Springer, Bath, 2007.
[67] P.C. Ray, History of Hindu Chemistry, The Bengal Chemical and Pharmaceutical Works, Limited, Calcutta, 1903.
[68] R.D. Tweney, Perspectives on Science 14 (2006) 97–121.
[69] K.H. Stern, Chemical Reviews 54 (1954) 79–99.
[70] X. Michalet, F.F. Pinaud, L.A. Bentolila, J.M. Tsay, S. Doose, J.J. Li, G. Sundaresan, A.M. Wu, S.S. Gambhir, S. Weiss, Science 307 (2005) 538–544.
[71] W.E. Moerner, M. Orrit, Science 283 (1999) 1670.
[72] T. Schmidt, G.J. Schutz, W. Baumgartner, H.J. Gruber, H. Schindler, Proceedings of the National Academy of Sciences of the United States of America 93 (1996) 2926–2929.
[73] R.M. Dickson, D.J. Norris, Y.L. Tzeng, W.E. Moerner, Science 274 (1996) 966–969.
[74] S.M. Nie, S.R. Emery, Science 275 (1997) 1102–1106.
[75] S.M. Nie, R.N. Zare, Annual Review of Biophysics and Biomolecular Structure 26 (1997) 567–596.
[76] A.P. Bartko, R.M. Dickson, Journal of Physical Chemistry B 103 (1999) 11237–11241.
[77] A. Einstein, Annalen Der Physik 17 (1905) 549–560.
[78] A. Einstein, Investigation on the Theory of Brownian Movement, Dover Publications, Inc., New York, 1956.
[79] A. Einstein, Annalen Der Physik 19 (1906) 371–381.
[80] M. von Smoluchowski, Annalen Der Physik 21 (1906) 756–780.
[81] M. von Smoluchowski, Physikalische Zeitschrift 17 (1916) 557–571.
[82] M. von Smoluchowski, Physikalische Zeitschrift 17 (1916) 585–599.
[83] P. Langevin, Comptes Rendus Hebdomadaires des Seances de L Academie des Sciences 146 (1908) 530–533.
[84] S. Chandrasekhar, Reviews of Modern Physics 15 (1943) 1–89.
[85] M.D. Haw, Journal of Physics: Condensed Matter 14 (2002) 7769–7779.
[86] R. Newburgh, J. Peidle, W. Rueckner, American Journal of Physics 74 (2006) 478–481.
[87] J.K.G. Dhont, in: G. Gompper, U.B. Kaupp, J.K.G. Dhont, D. Richter, G. Winkler (Eds.), Physics Meets Biology: From Soft Matter to Cell Biology, 35th Spring School of the Institut fur Festkorperforschung, Forschungszentrum, Julich, 2004.
[88] J.K.G. Dhont, in: J.K.G. Dhont, G. Gompper, D. Richter (Eds.), Soft Matter: Complex Materials on Mesoscopic Scales, 33rd IFF-Ferienschule, Forschungszentrum Julich GmbH, Julich, 2002.
[89] J. Perrin, Annales de Chimie et de Physique 18 (1909) 5–114.
[90] J. Perrin, Atoms, Constable & Company Ltd., London, 1923.
[91] M.J. Nye, The Question of the Atom, Tomash Publishers, Los Angeles, 1984.
[92] M. von Smoluchowski, Annalen Der Physik 25 (1908) 205–226.
[93] M. Doi, S.F. Edwards, The Theory of Polymer Dynamics, Oxford University Press, Oxford, 1986.
[94] W.B. Russel, D.A. Saville, W.R. Schowalter, Colloidal Dispersions, Cambridge University Press, Cambridge, 1989.
[95] M.E. Cates, M.R. Evans, Soft and Fragile Matter, Institute of Physics Publishing, Bristol, 2000.
[96] T.A. Witten, P.A. Pincus, Structured Fluids: Polymers, Colloids, Surfactants, Oxford University Press, New York, 2004.
[97] H.C. Berg, Random Walks in Biology, Princeton University Press, Princeton, 1983
[98] V. Sharma, K. Park, M. Srinivasarao, PNAS (2009), doi:10.1073/pnas.0800599106.
[99] P.C. Hemmer, H. Holden, S.K. Ratkje, The Collected Works of Lars Onsager: With Commentary, World Scientific, Singapore, 1996.
[100] N. Foundation (Ed.), Chemistry 1922–1941 Nobel Lectures, Elsevier Publishing Company, Amsterdam, 1966.
[101] M. von Smoluchowski, Kolloid-Zeitschrift 21 (1917) 98–104.
[102] H.S. Taylor, S. Glasstone (Eds.), A Treatise on Physical Chemistry, vol. II—States of Matter, D. Van Nostrand Company, Inc., New York, 1951.
[103] H. Zocher, Zeitschrift Fur Anorganische Und Allgemeine Chemie 147 (1925), 91-U15.
[104] I. Langmuir, Journal of Chemical Physics 6 (1938) 873–896.
[105] F.C. Bawden, N.W. Pirie, J.D. Bernal, I. Fankuchen, Nature 138 (1936) 1051–1052.
[106] L. Onsager, Annals of the New York Academy of Sciences 51 (1949) 627–659.
[107] J.C.P. Gabriel, P. Davidson, Advanced Materials 12 (2000) 9.
[108] P. Davidson, J.C.P. Gabriel, Current Opinion in Colloid & Interface Science 9 (2005) 377–383.

[109] D.F. Evans, H. Wennerstrom, The Colloidal Domain, Wiley-VCH, New York, 1999.
[110] P.C. Ohara, D.V. Leff, J.R. Heath, W.M. Gelbart, Physical Review Letters 75 (1995) 3466–3469.
[111] C.F. Bohren, D.R. Huffman, Absorption and Scattering of Light by Small Particles, John Wiley & Sons, Inc., New York, 1983.
[112] H.C. van de Hulst, Light Scattering by Small Particles, Dover Publications, Inc., Mineola, 1981.
[113] J.W.L.R. Strutt, Philosophical Magazine 107 (1871) 274–279.
[114] M. Kerker, The Scattering of Light and Other Electromagnetic Radiation, Academic Press, Inc., New York, 1969.
[115] J.D. Jackson, Classical Electrodynamics, John Wiley & Sons, Inc., New York, 1962
[116] S. Link, M.B. Mohamed, M.A. El-Sayed, Journal of Physical Chemistry B 103 (1999) 3073–3077.
[117] E. Hao, R.C. Bailey, G.C. Schatz, J.T. Hupp, S.Y. Li, Nano Letters 4 (2004) 327–330.
[118] E. Hao, S.Y. Li, R.C. Bailey, S.L. Zou, G.C. Schatz, J.T. Hupp, Journal of Physical Chemistry B 108 (2004) 1224–1229.
[119] E. Hao, G.C. Schatz, J.T. Hupp, Journal of Fluorescence 14 (2004) 331–341.
[120] F. Hao, C.L. Nehl, J.H. Hafner, P. Nordlander, Nano Letters 7 (2007) 729–732.
[121] A.A. Lazarides, K.L. Kelly, T.R. Jensen, G.C. Schatz, Journal of Molecular Structure: Theochemistry 529 (2000) 59–63.
[122] A.A. Lazarides, G.C. Schatz, Journal of Physical Chemistry B 104 (2000) 460–467.
[123] C.J. Murphy, Nature Materials 6 (2007) 259–260.
[124] P.B. Johnson, R.W. Christy, Physics Review B 6 (1972) 4370–4380.
[125] K. Park, in: Doctor of Philosophy, School of Polymer, Textile and Fiber Engineering, Georgia Institute of Technology, Atlanta, 2006.
[126] M. Meier, A. Wokaun, Optics Letters 8 (1983) 581–583.
[127] E.K. Payne, K.L. Shuford, S. Park, G.C. Schatz, C.A. Mirkin, Journal of Physical Chemistry B 110 (2006) 2150–2154.
[128] K.L. Kelly, A.A. Lazarides, G.C. Schatz, Computing in Science & Engineering 3 (2001) 67–73.
[129] E.M. Purcell, C.R. Pennypacker, Astrophysical Journal 186 (1973) 705–714.
[130] K.L. Shuford, M.A. Ratner, G.C. Schatz, Journal of Chemical Physics 123 (2005).
[131] S. Underwood, P. Mulvaney, Langmuir 10 (1994) 3427–3430.
[132] A. Campion, P. Kambhampati, Chemical Society Reviews 27 (1998) 241–250.
[133] A. Otto, I. Mrozek, H. Grabhorn, W. Akemann, Journal of Physics: Condensed Matter 4 (1992) 1143–1212.
[134] G.C. Schatz, M.A. Young, R.P. Van Duyne, Surface-Enhanced Raman Scattering: Physics and Applications 103 (2006) 19–45.
[135] K. Kneipp, Y. Wang, H. Kneipp, L.T. Perelman, I. Itzkan, R. Dasari, M.S. Feld, Physical Review Letters 78 (1997) 1667–1670.
[136] R.G. Freeman, K.C. Grabar, K.J. Allison, R.M. Bright, J.A. Davis, A.P. Guthrie, M.B. Hommer, M.A. Jackson, P.C. Smith, D.G. Walter, M.J. Natan, Science 267 (1995) 1629–1632.
[137] W.H. Yang, G.C. Schatz, R.P. Vanduyne, Journal of Chemical Physics 103 (1995) 869–875.
[138] M. Srinivasarao, Chemical Reviews 99 (1999) 1935–1961.
[139] K. Nassau, The Physics and Chemistry of Color, John Wiley & Sons, Inc., New York, 2001.
[140] Y. Dirix, C. Bastiaansen, W. Caseri, P. Smith, Advanced Materials 11 (1999) 223.
[141] Y. Dirix, C. Darribere, W. Heffels, C. Bastiaansen, W. Caseri, P. Smith, Applied Optics 38 (1999) 6581–6586.
[142] B.M.I. van der Zande, L. Pages, R.A.M. Hikmet, A. van Blaaderen, Journal of Physical Chemistry B 103 (1999) 5761–5767.
[143] C.L. Murphy, C.J. Orendorff, Advanced Materials 17 (2005) 2173–2177.
[144] J. Perez-Juste, B. Rodriguez-Gonzalez, P. Mulvaney, L.M. Liz-Marzan, Advanced Functional Materials 15 (2005) 1065–1071.
[145] S. Matsuda, Y. Yasuda, S. Ando, Advanced Materials 17 (2005) 2221–2224.
[146] S.G. Lipson, H. Lipson, D.S. Tannhauser, Optical Physics, Cambridge University Press, Cambridge, 1995.
[147] S. Inoue, K.R. Spring, Video Microscopy: The Fundamentals, Springer, New York, 1997.
[148] M. Srinivasarao, J.O. Park, in: R.F. Brady (Ed.), Comprehensive Desk Reference of Polymer Characterization and Analysis, Oxford University Press, 2003.
[149] M. Born, E. Wolf, Principles of Optics: Electromagnetic Theory of Propagation, Interference and Diffraction of Light, Cambridge University Press, Cambridge, 1999.
[150] D.V. Goia, E. Matijevic, New Journal of Chemistry 22 (1998) 1203–1215.
[151] J. Turkevich, P.C. Stevenson, J. Hillier, Journal of Physical Chemistry 57 (1953) 670–673.
[152] J. Turkevich, P.C. Stevenson, J. Hillier, Discussions of the Faraday Society (1951) 55.
[153] G. Frens, Nature: Physical Science 241 (1973) 20–22.
[154] M.K. Chow, C.F. Zukoski, Journal of Colloid and Interface Science 165 (1994) 97–109.
[155] Y.Y. Yu, S.S. Chang, C.L. Lee, C.R.C. Wang, Journal of Physical Chemistry B 101 (1997) 6661–6664.
[156] N.R. Jana, L. Gearheart, C.J. Murphy, Journal of Physical Chemistry B 105 (2001) 4065–4067.
[157] K.R. Brown, D.G. Walter, M.J. Natan, Chemistry of Materials 12 (2000) 306–313.
[158] P.L. Gai, M.A. Harmer, Nano Letters 2 (2002) 771–774.
[159] M.Z. Liu, P. Guyot-Sionnest, Journal of Physical Chemistry B 109 (2005) 22192–22200.
[160] C.J. Johnson, E. Dujardin, S.A. Davis, C.J. Murphy, S. Mann, Journal of Materials Chemistry 12 (2002) 1765–1770.
[161] J.X. Gao, C.M. Bender, C.J. Murphy, Langmuir 19 (2003) 9065–9070.
[162] B. Nikoobakht, M.A. El-Sayed, Chemistry of Materials 15 (2003) 1957–1962.
[163] B.M.I. van der Zande, M.R. Bohmer, L.G.J. Fokkink, C. Schonenberger, Langmuir 16 (2000) 451–458.
[164] L.Y. Cao, T. Zhu, Z.F. Liu, Journal of Colloid and Interface Science 293 (2006) 69–76.
[165] A. Gole, C.J. Murphy, Chemistry of Materials 16 (2004) 3633–3640.
[166] N.R. Jana, L. Gearheart, C.J. Murphy, Advanced Materials 13 (2001) 1389–1393.
[167] L.F. Gou, C.J. Murphy, Chemistry of Materials 17 (2005) 3668–3672.
[168] N.R. Jana, L. Gearheart, C.J. Murphy, Chemistry of Materials 13 (2001) 2313–2322.
[169] C.J. Murphy, N.R. Jana, Advanced Materials 14 (2002) 80–82.
[170] S. Ross, C.E. Kwartler, J.H. Bailey, Journal of Colloid Science 8 (1953) 385–401.
[171] M.S. Bakshi, I. Kaur, Colloid and Polymer Science 281 (2003) 10–18.
[172] S.B. Velegol, B.D. Fleming, S. Biggs, E.J. Wanless, R.D. Tilton, Langmuir 16 (2000) 2548–2556.
[173] B. Nikoobakht, M.A. El-Sayed, Langmuir 17 (2001) 6368–6374.
[174] B. Veisz, Z. Kiraly, Langmuir 19 (2003) 4817–4824.
[175] K. Torigoe, K. Esumi, Langmuir 8 (1992) 59–63.
[176] R.J. Puddephatt, The Chemistry of Gold, Elsevier, New York, 1978.
[177] A.J. Bard, in: A.J. Bard (Ed.), Encyclopedia of Electrochemistry of the Elements, vol. IV, Marcel Dekker, New York, 1975.
[178] E. Leontidis, K. Kleitou, T. Kyprianidou-Leodidou, V. Bekiari, P. Lianos, Langmuir 18 (2002) 3659–3668.
[179] Y.S. Sedunov, Physics of Drop Formation in the Atmosphere, Wiley, New York, 1974, p. 234.
[180] T.G.M. van de ven, Colloidal Hydrodynamics, Academic Press, Inc., London, 1989
[181] S. Ramaswamy, Advances in Physics 50 (2001) 297–341.
[182] J. Happel, H. Brenner, Low Reynolds Number Hydrodynamics, Noordhoff International Publishing, Leyden, 1973.
[183] H. Fujita, Foundations of Ultracentrifugation Analysis, John Wiley & Sons, Inc., New York, 1975.
[184] Z. Dogic, A.P. Philipse, S. Fraden, J.K.G. Dhont, Journal of Chemical Physics 113 (2000) 8368–8380.
[185] J.M. Peterson, Journal of Chemical Physics 40 (1964) 2680.
[186] M. Doi, S.F. Edwards, The Theory of Polymer Dynamics, Oxford University Press, New York, 1988, p. 406.
[187] N.R. Jana, Chemical Communications (2003) 1950–1951.
[188] M. Rasa, B.H. Erne, B. Zoetekouw, R. van Roij, A.P. Philipse, Journal of Physics: Condensed Matter 17 (2005) 2293–2314.
[189] A.P. Philipse, Journal of Physics: Condensed Matter 16 (2004) S4051–S4062.
[190] M. Rasa, A.P. Philipse, Nature 429 (2004) 857–860.
[191] A.P. Philipse, G.H. Koenderink, Advances in Colloid and Interface Science 100 (2003) 613–639.
[192] G.M. Whitesides, J.P. Mathias, C.T. Seto, Science 254 (1991) 1312–1319.
[193] G.M. Whitesides, B. Grzybowski, Science 295 (2002) 2418–2421.
[194] N. Bowden, A. Terfort, J. Carbeck, G.M. Whitesides, Science 276 (1997) 233–235.
[195] B.A. Parviz, D. Ryan, G.M. Whitesides, IEEE Transactions on Advanced Packaging 26 (2003) 233–241.
[196] P. Ball, The Self-Made Tapestry: Pattern Formation in Nature, Oxford University Press, New York, 1999.
[197] R.D. Deegan, Physical Review E 61 (2000) 475–485.
[198] R.D. Deegan, O. Bakajin, T.F. Dupont, G. Huber, S.R. Nagel, T.A. Witten, Nature 389 (1997) 827–829.
[199] R.D. Deegan, O. Bakajin, T.F. Dupont, G. Huber, S.R. Nagel, T.A. Witten, Physical Review E 62 (2000) 756–765.
[200] E. Rabani, D.R. Reichman, P.L. Geissler, L.E. Brus, Nature 426 (2003) 271–274.
[201] N.D. Denkov, O.D. Velev, P.A. Kralchevsky, I.B. Ivanov, H. Yoshimura, K. Nagayama, Langmuir 8 (1992) 3183–3190.
[202] N.D. Denkov, O.D. Velev, P.A. Kralchevsky, I.B. Ivanov, H. Yoshimura, K. Nagayama, Nature 361 (1993) 26–126.
[203] P. Pieranski, L. Strzelecki, B. Pansu, Physical Review Letters 50 (1983) 900–903.
[204] P. Pieranski, Contemporary Physics 24 (1983) 25–73.
[205] P. Pieranski, Physical Review Letters 45 (1980) 569–572.
[206] C.B. Murray, C.R. Kagan, M.G. Bawendi, Science 270 (1995) 1335–1338.
[207] C.B. Murray, C.R. Kagan, M.G. Bawendi, Annual Review of Materials Science 30 (2000) 545–610.
[208] Y.N. Xia, B. Gates, Y.D. Yin, Y. Lu, Advanced Materials 12 (2000) 693–713.
[209] A. vanBlaaderen, R. Ruel, P. Wiltzius, Nature 385 (1997) 321–324.
[210] S.H. Sun, C.B. Murray, Journal of Applied Physics 85 (1999) 4325–4330.
[211] M.P. Pileni, Langmuir 13 (1997) 3266–3276.
[212] O.D. Velev, E.W. Kaler, Advanced Materials 12 (2000) 531–534.
[213] J. Aizenberg, P.V. Braun, P. Wiltzius, Physical Review Letters 84 (2000) 2997–3000.
[214] P.A. Kralchevsky, K. Nagayama, Particles at Fluid Interfaces and Membranes, Elsevier Science B.V., Amsterdam, 2001.
[215] U. Gasser, E.R. Weeks, A. Schofield, P.N. Pusey, D.A. Weitz, Science 292 (2001) 258–262.
[216] F.S. Bates, G.H. Fredrickson, Physics Today 52 (1999) 32–38.
[217] F.S. Bates, Science 251 (1991) 898–905.
[218] F.S. Bates, G.H. Fredrickson, Annual Review of Physical Chemistry 41 (1990) 525–557.
[219] C.D. Bain, E.B. Troughton, Y.T. Tao, J. Evall, G.M. Whitesides, R.G. Nuzzo, Journal of the American Chemical Society 111 (1989) 321–335.
[220] P.E. Laibinis, G.M. Whitesides, D.L. Allara, Y.T. Tao, A.N. Parikh, R.G. Nuzzo, Journal of the American Chemical Society 113 (1991) 7152–7167.
[221] A. Kumar, H.A. Biebuyck, G.M. Whitesides, Langmuir 10 (1994) 1498–1511.
[222] B.M. Discher, Y.Y. Won, D.S. Ege, J.C.M. Lee, F.S. Bates, D.E. Discher, D.A. Hammer, Science 284 (1999) 1143–1146.

[223] S. Jain, F.S. Bates, Science 300 (2003) 460–464.
[224] M.W. Matsen, F.S. Bates, Macromolecules 29 (1996) 1091–1098.
[225] M.S. Barrow, R.L. Jones, J.O. Park, M. Srinivasarao, P.R. Williams, C.J. Wright, Spectroscopy—An International Journal 18 (2004) 577–585.
[226] L. Song, R.K. Bly, J.N. Wilson, S. Bakbak, J.O. Park, M. Srinivasarao, U.H.F. Bunz, Advanced Materials 16 (2004) 115.
[227] M. Srinivasarao, D. Collings, A. Philips, S. Patel, Science 292 (2001) 79–83.
[228] G. Widawski, M. Rawiso, B. Francois, Nature 369 (1994) 387–389.
[229] M.C. Cross, P.C. Hohenberg, Reviews of Modern Physics 65 (1993) 851–1112.
[230] P.S. Stevens, Patterns in Nature, Little, Brown and Company, Boston, 1974.
[231] P. Meakin, Fractals, Scaling and Growth Far from Equilibrium, Cambridge University Press, Cambridge, 1998.
[232] V.F. Puntes, K.M. Krishnan, A.P. Alivisatos, Science 291 (2001) 2115–2117.
[233] M.A. Horsch, Z. Zhang, S.C. Glotzer, Nano Letters 6 (2006) 2406–2413.
[234] Z.Y. Tang, Z.L. Zhang, Y. Wang, S.C. Glotzer, N.A. Kotov, Science 314 (2006) 274–278.
[235] S.C. Glotzer, M.A. Horsch, C.R. Iacovella, Z.L. Zhang, E.R. Chan, X. Zhang, Current Opinion in Colloid & Interface Science 10 (2005) 287–295.
[236] S.C. Glotzer, M.J. Solomon, N.A. Kotov, AIChE Journal 50 (2004) 2978–2985.
[237] D.J. Norris, E.G. Arlinghaus, L.L. Meng, R. Heiny, L.E. Scriven, Advanced Materials 16 (2004) 1393–1399.
[238] D. Frenkel, Science 296 (2002) 65–66.
[239] V.J. Anderson, H.N.W. Lekkerkerker, Nature 416 (2002) 811–815.
[240] D. Frenkel, Journal of Physical Chemistry 91 (1987) 4912–4916.
[241] D. Frenkel, Molecular Physics 60 (1987) 1–20.
[242] D. Frenkel, Journal of Physical Chemistry 92 (1988) 3280–3284.
[243] S. Chandrasekhar, Liquid Crystals, Cambridge University Press, Cambridge, 1977
[244] M. Kleman, O.D. Lavrentovich, Soft Matter Physics: An Introduction, Springer-Verlag Inc., New York, 2003.
[245] P.G. de Gennes, J. Prost, The Physics of Liquid Crystals, Oxford University Press, USA, 1995.
[246] H.N.W. Lekkerkerker, G.J. Vroege, Philosophical Transactions of the Royal Society of London Series A: Mathematical, Physical and Engineering Sciences 344 (1993) 419–440.
[247] G.J. Vroege, H.N.W. Lekkerkerker, Reports on Progress in Physics 55 (1992) 1241–1309.
[248] P. Davidson, A. Garreau, J. Livage, Liquid Crystals 16 (1994) 905–910.
[249] B.J. Lemaire, P. Davidson, J. Ferre, J.P. Jamet, P. Panine, I. Dozov, J.P. Jolivet, Physical Review Letters 88 (2002).
[250] B.J. Lemaire, P. Davidson, J. Ferre, J.P. Jamet, D. Petermann, P. Panine, I. Dozov, J.P. Jolivet, European Physical Journal E 13 (2004) 291–308.
[251] B.J. Lemaire, P. Davidson, J. Ferre, J.P. Jamet, D. Petermann, P. Panine, I. Dozov, D. Stoenescu, J.P. Jolivet, Faraday Discussions 128 (2005) 271–283.
[252] B.J. Lemaire, P. Davidson, P. Panine, J.P. Jolivet, Physical Review Letters 93 (2004).
[253] B.J. Lemaire, P. Davidson, D. Petermann, P. Panine, I. Dozov, D. Stoenescu, J.P. Jolivet, European Physical Journal E 13 (2004) 309–319.
[254] P. Davidson, P. Batail, J.C.P. Gabriel, J. Livage, C. Sanchez, C. Bourgaux, Progress in Polymer Science 22 (1997) 913–936.
[255] S. Lamarque-Forget, O. Pelletier, I. Dozov, P. Davidson, P. Martinot-Lagarde, J. Livage, Advanced Materials 12 (2000) 1267.
[256] O. Pelletier, P. Davidson, C. Bourgaux, C. Coulon, S. Regnault, J. Livage, Langmuir 16 (2000) 5295–5303.
[257] O. Pelletier, C. Bourgaux, O. Diat, P. Davidson, J. Livage, European Physical Journal B 12 (1999) 541–546.
[258] O. Pelletier, P. Davidson, C. Bourgaux, J. Livage, Europhysics Letters 48 (1999) 53–59.
[259] F.M. van der Kooij, K. Kassapidou, H.N.W. Lekkerkerker, Nature 406 (2000) 868–871.
[260] F.M. van der Kooij, H.N.W. Lekkerkerker, Journal of Physical Chemistry B 102 (1998) 7829–7832.
[261] F.M. van der Kooij, H.N.W. Lekkerkerker, Langmuir 16 (2000) 10144–10149.
[262] F.M. van der Kooij, H.N.W. Lekkerkerker, Physical Review Letters 84 (2000) 781–784.
[263] F.M. van der Kooij, H.N.W. Lekkerkerker, Philosophical Transactions of the Royal Society of London Series A: Mathematical, Physical and Engineering Sciences 359 (2001) 985–995.
[264] F.M. van der Kooij, D. van der Beek, H.N.W. Lekkerkerker, Journal of Physical Chemistry B 105 (2001) 1696–1700.
[265] F.M. van der Kooij, M. Vogel, H.N.W. Lekkerkerker, Physical Review E 62 (2000) 5397–5402.
[266] D. van der Beek, H.N.W. Lekkerkerker, Europhysics Letters 61 (2003) 702–707.
[267] D. van der Beek, H.N.W. Lekkerkerker, Langmuir 20 (2004) 8582–8586.
[268] D. van der Beek, A.V. Petukhov, S.M. Oversteegen, G.J. Vroege, H.N.W. Lekkerkerker, European Physical Journal E 16 (2005) 253–258.
[269] D. van der Beek, T. Schilling, H.N.W. Lekkerkerker, Journal of Chemical Physics 121 (2004) 5423–5426.
[270] P.A. Buining, H.N.W. Lekkerkerker, Journal of Physical Chemistry 97 (1993) 11510–11516.
[271] P.A. Buining, A.P. Philipse, H.N.W. Lekkerkerker, Langmuir 10 (1994) 2106–2114.
[272] Z. Dogic, D. Frenkel, S. Fraden, Physical Review E 62 (2000) 3925–3933.
[273] M. Adams, Z. Dogic, S.L. Keller, S. Fraden, Nature 393 (1998) 349–352.
[274] M. Adams, S. Fraden, Biophysical Journal 74 (1998) 669–677.
[275] S. Varga, K. Purdy, A. Galindo, S. Fraden, G. Jackson, Physical Review E 72 (2005).
[276] K.R. Purdy, S. Varga, A. Galindo, G. Jackson, S. Fraden, Physical Review Letters 94 (2005).
[277] Z. Dogic, S. Fraden, Current Opinion in Colloid & Interface Science 11 (2006) 47–55.
[278] Z. Dogic, S. Fraden, Physical Review Letters 78 (1997) 2417–2420.
[279] Z. Dogic, S. Fraden, Philosophical Transactions of the Royal Society of London Series A: Mathematical, Physical and Engineering Sciences 359 (2001) 997–1014.
[280] S.D. Lee, R.B. Meyer, Journal of Chemical Physics 84 (1986) 3443–3448.
[281] S.D. Lee, R.B. Meyer, Physical Review Letters 61 (1988) 2217–2220.
[282] D. Frenkel, H.N.W. Lekkerkerker, A. Stroobants, Nature 332 (1988) 822–823.
[283] D. Frenkel, J.F. Maguire, Physical Review Letters 47 (1981) 1025–1028.
[284] D. Frenkel, B.M. Mulder, J.P. McTague, Physical Review Letters 52 (1984) 287–290.
[285] M.A. Bates, D. Frenkel, Journal of Chemical Physics 112 (2000) 10034–10041.
[286] M.A. Bates, D. Frenkel, Journal of Chemical Physics 109 (1998) 6193–6199.
[287] P. Bolhuis, D. Frenkel, Journal of Chemical Physics 101 (1994) 9869–9875.
[288] P. Bolhuis, D. Frenkel, Journal of Chemical Physics 106 (1997) 666–687.
[289] P. Bolhuis, M. Hagen, D. Frenkel, Physical Review E 50 (1994) 4880–4890.
[290] P.G. Bolhuis, A. Stroobants, D. Frenkel, H.N.W. Lekkerkerker, Journal of Chemical Physics 107 (1997) 1551–1564.
[291] D. Frenkel, B.M. Mulder, J.P. McTague, Molecular Crystals and Liquid Crystals 123 (1985) 119–128.
[292] Y.O. Popov, T.A. Witten, European Physical Journal E 6 (2001) 211–220.
[293] Y.O. Popov, Physical Review E 71 (2005).
[294] S.D. Lee, Physical Review A 39 (1989) 3631–3639.
[295] G.T. Dee, Physical Review Letters 57 (1986) 275–278.
[296] D.A. Smith, Journal of Chemical Physics 81 (1984) 3102–3115.
[297] G. Venzl, J. Ross, Journal of Chemical Physics 77 (1982) 1302–1307.
[298] S. Prager, Journal of Chemical Physics 25 (1956) 279–283.
[299] H.K. Henisch, Periodic Precipitation, Permagon Press, New York, 1991.
[300] L. Shmuylovich, A.Q. Shen, H.A. Stone, Langmuir 18 (2002) 3441–3445.
[301] H. Maeda, Langmuir 16 (2000) 9977–9982.
[302] S.W. Hong, J.F. Xia, Z.Q. Lin, Advanced Materials 19 (2007) 1413.
[303] S.W. Hong, J.F. Xia, M. Byun, Q.Z. Zou, Z.Q. Lin, Macromolecules 40 (2007) 2831–2836.
[304] Z.Q. Lin, S. Granick, Journal of the American Chemical Society 127 (2005) 2816–2817.
[305] M. Byun, S.W. Hong, L. Zhu, Z.Q. Lin, Langmuir 24 (2008) 3525–3531.
[306] S. Maheshwari, L. Zhang, Y.X. Zhu, H.C. Chang, Physical Review Letters 1 (2008).
[307] J. Xu, J.F. Xia, Z.Q. Lin, Angewandte Chemie-International Edition in English 46 (2007) 1860–1863.
[308] J. Xu, J.F. Xia, S.W. Hong, Z.Q. Lin, F. Qiu, Y.L. Yang, Physical Review Letters 96 (2006).
[309] L. Zhang, S. Maheshwari, H.C. Chang, Y.X. Zhu, Langmuir 24 (2008) 3911–3917.
[310] H. Hu, R.G. Larson, Journal of Physical Chemistry B 110 (2006) 7090–7094.
[311] H. Hu, R.G. Larson, Langmuir 21 (2005) 3963–3971.
[312] H. Hu, R.G. Larson, Langmuir 21 (2005) 3972–3980.
[313] H. Maeda, Langmuir 15 (1999) 8505–8513.
[314] R. van Hameren, P. Schon, A.M. van Buul, J. Hoogboom, S.V. Lazarenko, J.W. Gerritsen, H. Engelkamp, P.C.M. Christianen, H.A. Heus, J.C. Maan, T. Rasing, S. Speller, A.E. Rowan, J. Elemans, R.J.M. Nolte, Science 314 (2006) 1433–1436.
[315] B. Nikoobakht, Z.L. Wang, M.A. El-Sayed, Journal of Physical Chemistry B 104 (2000) 8635–8640.
[316] K. Mitamura, T. Imae, N. Saito, O. Takai, Journal of Physical Chemistry B 111 (2007) 8891–8898.
[317] N.R. Jana, Angewandte Chemie-International Edition in English 43 (2004) 1536–1540.
[318] N.R. Jana, L.A. Gearheart, S.O. Obare, C.J. Johnson, K.J. Edler, S. Mann, C.J. Murphy, Journal of Materials Chemistry 12 (2002) 2909–2912.
[319] T.K. Sau, C.J. Murphy, Langmuir 21 (2005) 2923–2929.
[320] P.D. Yang, F. Kim, Chemphyschem 3 (2002) 503.
[321] D. Zimnitsky, J. Xu, Z.Q. Lin, V.V. Tsukruk, Nanotechnology 19 (2008).
[322] H. Maeda, Y. Maeda, Langmuir 12 (1996) 1446–1452.
[323] F. Kim, S. Kwan, J. Akana, P.D. Yang, Journal of the American Chemical Society 123 (2001) 4360–4361.
[324] L.S. Li, A.P. Alivisatos, Advanced Materials 15 (2003) 408.
[325] L.S. Li, M. Marjanska, G.H.J. Park, A. Pines, A.P. Alivisatos, Journal of Chemical Physics 120 (2004) 1149–1152.
[326] H. Maeda, Y. Maeda, Physical Review Letters 90 (2003).
[327] G.H. Koenderink, G.A. Vliegenthart, S. Kluijtmans, A. van Blaaderen, A.P. Philipse, H.N.W. Lekkerkerker, Langmuir 15 (1999) 4693–4696.
[328] C.J. Orendorff, P.L. Hankins, C.J. Murphy, Langmuir 21 (2005) 2022–2026.
[329] P.A. Kralchevsky, N.D. Denkov, Current Opinion in Colloid & Interface Science 6 (2001) 383–401.
[330] P.A. Kralchevsky, K. Nagayama, Langmuir 10 (1994) 23–36.
[331] P.A. Kralchevsky, K. Nagayama, Advances in Colloid and Interface Science 85 (2000) 145–192.
[332] T.A. Witten, L.M. Sander, Physical Review Letters 47 (1981) 1400–1403.
[333] D.A. Weitz, M. Oliveria, Physical Review Letters 52 (1984) 1433–1436.
[334] M.Y. Lin, H.M. Lindsay, D.A. Weitz, R.C. Ball, R. Klein, P. Meakin, Nature 339 (1989) 360–362.
[335] P. Dimon, S.K. Sinha, D.A. Weitz, C.R. Safinya, G.S. Smith, W.A. Varady, H.M. Lindsay, Physical Review Letters 57 (1986) 595–598.
[336] P.C. Ohara, J.R. Heath, W.M. Gelbart, Angewandte Chemie-International Edition in English 36 (1997) 1078.